Strathclyde Institute for Pharmaceutical and Biomedical Sciences

Exploiting the Potential of Foam Nests produced by *Engystomops pustulosus*

Sarah Brozio

Thesis presented in fulfilment of the requirement for the degree of Doctor of Philosophy

2018

Declaration

This thesis is the result of the author's original research. It has been composed by the author and has not been previously submitted for examination which has led to the award of a degree.

Signed: 

Date: 08/2018

To Mum,

Most people live their lives watching their role models from a distance. I got lucky, I had mine by my side every single day.

Acknowledgments

I would like to thank every person who was a part of, or who made this thesis possible. Firstly, thank you so much to my incredible supervisor Dr Paul Hoskisson for his support, guidance and for providing me with so many opportunities throughout this research. Thank you for every cool bit of research that I got to carry out, especially in Trinidad.

Thank you to EPSRC for funding this PhD, as well as The Biochemical Society, Microbiology Society and Pauline Fitzpatrick Research Award for providing the travel grants which made each Trinidad trip possible.

Thank you to the University of Glasgow Trinidad Expedition for each field trip over the last four years. A special thank you to Ellie, Mark and Tom, for getting up at 5am to collect foam, helping remove so many eggs and showing me everything Trinidad had to offer.

A massive thank you to the members of HW601 for making the lab so much fun. Thank you to Kirsty and Stuart for the coffee and the hikes, you kept me sane. Thank you to Jana for your friendship through the years. Thank you to Abbey King for all your help, you were the best masters student I could have asked for.

Thank you to my parents, Heather and Cornel, for your unwavering support and always answering the phone. None of this would have been possible without you. To my sister and best friend, Liesl, thank you for being my cheerleader every step of the way. Thank you for making me laugh, always.

To the best roommates I could have asked for, Lauren and Ailidh, thank you for always being there through everything the last few years have thrown at us. Thank you to Jenn and Becca, for every cup of coffee and listening to every rant.

Finally, thank you to my husband, Iain, for always being on my team. Thank you for every stupid video we watched. Thank you for supporting me every step of the way. I could not have done it without you.

Abstract

Foams are formed of air trapped in a solid or liquid creating cell-like structures. They are attracting attention in the pharmaceutical industry as potential drug delivery systems. The Tungara frog, *Engystomops pustulosus*, constructs foam nests which act as incubation chambers protecting the developing eggs and tadpoles from predation and environmental damage. This foam is highly stable and does not harm the eggs, sperm or tadpoles. Amphibians produce a range of proteins and peptides that may have pharmaceutical utility, and this is a growing area of research.

This work investigated the potential of the foam-nest produced by *E. pustulosus* as a novel drug release system. Bioinformatics were used to gain insight in to the six proteins that comprise the foam, the Ranaspumins (RSN), highlighting that many of the proteins have homology to uncharacterised amphibian proteins and that one protein, RSN-2, remains a unique surfactant protein. The foam was characterised as pharmaceutical foam revealing that it is low density, resistant to shear and is non-toxic to HaCaT cells. The foams drug release capabilities were tested by loading the foam with model hydrophilic and hydrophobic dyes and measuring their release profiles. The foam delivery potential was then tested with an antibiotic, rifampicin, demonstrating that the foam could successfully release an active drug with a release profile that shows promise for drug delivery. This work developed methodology to produce a synthetic foam using recombinant RSNs. A universal method was developed to clone each *rsn* gene into a plasmid vector which could be induced to overexpress each RSN in the bacterium *Escherichia coli* and subsequent purification. All six RSNs were cloned and overexpressed, but only RSN-2 could be purified successfully. The recombinant RSN-2 was investigated for its effect on mammalian and bacterial cells and was used to produce a stable foam, with release experiments showing that RSN-2 can be used to create a foam drug delivery system as the first step towards a completely synthetic foam. Overall, this work demonstrates that *E. pustulosus* foam has great potential as a drug release system.

Table of Contents

1.0 Introduction

Foams are defined as air trapped within a solid or a liquid forming a cell like structure (Weaire and Hutzler., 2001). They are useful in nature, food production, firefighting and the cosmetics industry (Hill *et al*., 2017). They have become integral to our everyday lives, appearing on the top of a beer, when cleaning dishes, as antiseptic for cleaning cuts and as shaving foam. Further, research into foams is rapidly growing in the cosmetics and pharmaceutical industry, where foams have been designed to aid makeup removal and foam drug formulations are used to deliver active agents like ibuprofen or antimicrobials through the skin. Over the last 10 years, hundreds of patents have been filed for novel foams and their potential uses (Zhao *et al.,* 2009).

Foam drug delivery is gaining traction within drug release research. Many drug delivery systems, including nanoparticles, hydrogels and loaded polymers have been investigated and produced as a novel way to deliver drugs. They are highly useful as they can directly deliver agents to a specific target or reduce toxicity of a drug to prevent unwanted side effects and provide prolonged drug release reducing the need for oral medication. However, many drug delivery systems are held back by issues with toxicity, expense or inadequate release. Many novel drug delivery systems, including foam-based systems, are being researched in order to gain the benefits of current release systems while reducing the negatives (Zhao *et al*., 2010).

Nature often provides solutions to problems in indirect ways. A small frog called *Engystomops pustulosus* or the Tungara frog produces foam nests in which it lays eggs during reproduction. These foam nests act as protective incubators for tadpoles during their development, prevent predation and environmental degradations. Interestingly, the foam produced is highly stable and appears to be non-toxic (Cooper *et al.,* 2010). The foam can also take-up dyes or active agents and release them much like a drug release system.

To investigate if the foam produced by *E. pustulosus* could be used as a novel drug delivery system an in-depth characterization of the foam including its toxicity, stability and drug release potential must be examined. To fully exploit the properties of the *E. pustulosus* foam a method to synthetically reproduce a viable foam must be produced and the properties of its protein components must be completely understood.

1.1 Foam Dynamics:

Foams have important roles in the food industry, cosmetic industry, alcohol production and firefighting (Arzhavitina *et* al., 2010, Hill *et al*., 2017). Market reports indicate that the food foaming agent industry is worth $5.3 billion, global fire prevention is valued at $16 billion and the medical foam industry is predicted to be worth $30 billion by 2026. Research and patent filings for pharmaceutical foams have steadily increased, demonstrating a need for novel foams and foaming agents (Zhao *et al* 2010). However, foams have been the subject of in depth study for years with foams having been initially outlined in 1873 by Joseph Plateau (Plateau., 1873). As a result, their physical and chemical properties have been well defined (Weaire., 2002). Foams have vast variety in appearance and be transparent or opaque, solid-like, gel-like or liquid-like (Saint-Jalmes, 2006). Foams are highly variable, have large surface areas, are low density and often demonstrate both solid and liquid like behaviours making them interesting to study (Hill *et al*., 2017).

There are two main categories of foams, solid foams and liquid foams (Weaire and Hutzler., 2001). Solid foams occur when gas is dispersed in a solid, such as a baked cake, foam insulation for buildings or foam mattresses. Liquid foams are gas encapsulated in liquid, such as coffee foam, foam made with laundry detergent and foams used in drug delivery. For the purpose of this research, only liquid foams will be focused on any further. Liquid foams are relatively unstable, usually collapsing within minutes or hours of production. They are often described as metastable as their stability and structure are heavily impacted

by pressure, gravity and external environmental factors. This results in bubble coalescence and foam coarsening, as well as structural collapse (Hill *et al*., 2017).

The basic foam structure is described as a bubble of gas contained in a continuous film of liquid (Zhao *et al*., 2010). These bubbles are named cells and are generally between 0.1mm and 3mm in size (Wilson., 1989). Cells can vary in size, shape and heterogeneity. While some foams contain homogenous polyhedral shaped cells, others may contain heterogenous circular cells, or a mix of both (Zhao *et al.,* 2010). Temperature, pressure and pH impact the shape of cells formed. The thin films of liquid separating cells are called lamella, and plateau borders are formed where three lamella merge (**Fig 1.1**) (Hansen and Derderian, 1976). Lamella can be between 10nm and 1um in thickness (Zhao *et al*., 2010). Foams can be described as wet or dry (Weaire., 2002), and this is determined by the volume fraction (φ) of the foam:

$$\varphi = V^{liquid} / V^{foam}$$

φ is calculated by dividing the liquid fraction volume by the total volume of foam, and foams with a volume fraction of < 0.05 are considered dry foams (Hill *et al*., 2017), this often reflects that the liquid volume of the foam is less than 1% (Weaire and Hutzler, 2001). Further wet foams with high liquid volumes can undergo drainage and coarsening turning them into a dry foam (Hill *et al*., 2017).

Foams do not occur spontaneously, they always require an energy input for foam formation. Further, a reduction in tension at the air-water interface is required for a foam to be made, and the resulting foam must be stabilized otherwise it will collapse almost immediately (Hill

et al., 2017). This reduction and stability is usually carried out by one of two agents; small molecule surfactants or proteins. Most foams are produced using a small molecule surfactant, such as sodium dodecyl sulfate (SDS). Surfactants or detergents are amphipathic molecules, and this feature is key. During foam formation the surfactant accumulates at the air-water interface, exposing its hydrophobic regions to the air, and the hydrophilic regions to the water. This allows the reduction of the interface, allowing the transformation of the liquids' bulk state to a foam (Weaire and Hutzler, 2001).

Foams stabilized with proteins most often occur when a high concentration of protein is degraded in some manner, usually through mechanical means, exposing hydrophobic regions in the protein structure. This exposure of hydrophobic regions acts similarly to a surfactant molecule and facilitates the change in air-water interface (Hill *et al*., 2017). An example of this type of foam formation is the beating of egg whites into a foam. In some much rarer examples, surfactant proteins allow for the change in surface tensions. These surfactants have evolved in functions specifically requiring a reduction in the tension of the air water interface. Bacteria such as *Streptomyces coelicolor* and *Bacillus subtilis* produce surfactant proteins like SapB (Willey *et al.,* 1991) and Surfactin (Arima *et al.,* 1968) which are required for aerial development but also have antagonistic properties against other bacteria providing a competitive advantage (Straight *et al.,* 2006). Protein surfactants also occur in filamentous fungi to aid hyphae growth and are produced by many fish and frogs to produce foams during reproduction (Cooper *et al*., 2004).

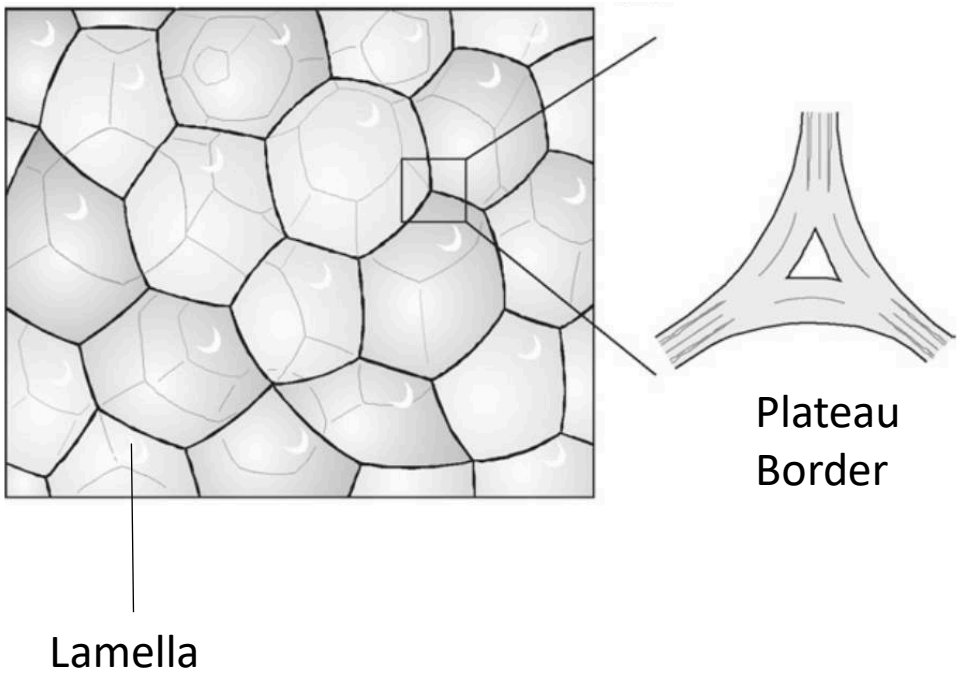

Figure 1.1: Diagram of foam cell structure. Lamella form the outer boarders of vesicles, and plateau boarders are formed when three lamellae meet (Arzhavitina *et* al., 2010).

1.2 Dermal Drug Delivery Systems:

Treatment of major diseases is often limited by the properties of the drugs approved to treat them. Many conventional "free" drugs have problems with solubility, toxicity, exceedingly rapid breakdown, poor pharmacokinetics or targeting issues (Torchilin., 2014). This can mean traditional drug treatments do not adequately reach their target organ or the high concentration needed for successful uptake results in unwanted effects. The properties and capabilities of these drugs can be improved by the use of drug release systems. Drug delivery systems cover a broad range of drug carriers with the number of systems available and being researched growing rapidly (Allen *et al*., 2004). Nanoparticles have been manufactured using liposomes, silica, gold, silver, solid lipids and many more (Torchulin, 2014). Other researched systems involve the use of nanotubes, polymer-drug conjugates, protein-drug conjugates and hydrogels (Zhao *et al*., 2010). Many of these drug release systems have been engineered to release anticancer drugs, antimicrobials and antivirals. Examples of these are listed in **Table 1.1**.

An area of drug delivery being focused on is topical drug release. Generally, drugs delivered through the skin are delivered with creams or gels and are often require multiple applications over several days for appropriate treatment. These creams treat conditions such as eczema, acne, muscle pain. Delivering drugs through the skin is important for treating multiple conditions. These include delivering antiseptics such as Silver sulfadiazine to wounds (Barillo., 2014), Dithranol to treat Psoriasis (Rodgers *et* al., 2011) and Sodium hypochlorite to treat burns (Gallagher *et al.,* 2012). Dermal delivery is often used as an

alternative to oral medicines instead treating the target area (Djekic *et al.,* 2016). However, creams are often painful to apply and can have difficulty releasing adequate concentrations (Zhao *et al.,* 2009). The skin has evolved as an effective barrier often limiting drug permeability (Alvarez-Roman *et al.,* 2004), and the ultimate goal of any topical treatment is to safely deliver an appropriate concentration of drug through this barrier without causing any detrimental effects (Roberts *et al*., 2017). Due to these limitations many topical drug release systems have been investigated in search of novel ways of delivering drugs to the skin. These include topical nanoparticles loaded with zinc oxide to be used as sun cream (Silva *et al.,* 2016), lipid vesicles as a treatment for fungal infections with hydrophobic antifungal Ketoconazole (Guo *et al.,* 2015) and hydrogels that enhance ibuprofen uptake through epidermis (Djekic *et al*., 2016). However, the benefits of these systems may come with issues that have yet to be fully resolved. There is growing evidence that many nanoparticles cause damage to the skin and their toxicity may be a limiting factor (Yah *et al*., 2016). There is a high chance of skin irritation (Roberts *et al.,*2017), often caused by the high concentration of surfactants used during nanoparticle assembly (Silva *et al,* 2016). Hydrogels such as Nu-Gel and Purilon are frequently used to treat major wounds as a result of foot ulcers or surgery, and loaded hydrogels are being developed to help deliver drugs at the site of release. However, many of these have yet to reach clinical trials and no market impact data is available (Boateng *et* al., 2008). Some hydrogel data demonstrates issues with low concentration release (Djekic *et al*., 2016), and these issues are also evident in nanoparticle and liposome concentration release (Zhao *et al.,* 2010). Pharmaceutical foams

may provide a solution to some of the problems encountered with nanoparticle-based drug delivery systems, while still having more benefits than creams or oral dosage treatments (Zhao *et al*., 2010).

Pharmaceutical foams are not a novel concept and have been researched for over 30 years (Zhao *et al,* 2010). They have been used to deliver a variety of drugs including antifungals, antimicrobials, steroids and painkillers to treat infections, psoriasis and muscle pain. Foams have also been used as antiseptic wound and skin cleaners (Purdon *et al*., 2003). A detailed list of foam delivery systems is displayed in **Table 1.2**. There are multiple benefits to using foam delivery for topical treatments. Studies have shown that consumers and patients prefer applying a foam comparted to gels or creams (Bureiko *et al.,* 2015, Cutis *et al.,* 2002). Foams are less dense, easier to apply as they do not require harsh rubbing and spread easily. This means when treating painful conditions, they're often deemed more soothing (Purdon *et al.,* 2003). Further, foams used to treat psoriasis with corticosteroids allowed for higher concentrations to be applied compared to available lotions without causing increased toxicity (Feldman *et al*., 2000, Feldman *et al.,* 2001). Another foam containing Clobetasol propionate that is used to treat psoriasis also displayed improved treatment compared to the equivalent lotion (Purdon *et al.,* 2003). Foams often come in pressurised canisters, this production is expensive and considered the biggest negative of their use (Purdon *et al*., 2003). The current foam delivery systems are generally short-lived foams which coalesce and collapse quickly, delivering their drug load almost immediately. Many of these systems have aqueous bases and this can result in problems with drug solubility (Zhao *et al,* 2009).

As well as a range of problems with both current and novel drug release systems, the cost of many current skin treatments is expensive. The NHS spends £80 per Psoriasis patient every 6 months for Dithranol treatments alone, and there are over a million estimated sufferers in the UK (Rodgers *et al.,* 2011). Minor burns have an average cost of £1,850 per patient (Griffiths *et al.,* 2006), and major burns can cost around £75,000 to treat. Around £3,200 is the cost of dressings alone, and £1,400 is used on the medication required for treatment (Pellatt *et al.,* 2010). Treatments involving IV antibiotics require hospital stays increasing their expense, constantly having to change wound dressings to prevent infection and reapply creams for wound treats further increase NHS cost, and ineffective drug release is not cost effective either. This has left an obvious gap in the research where highly stable foams which can facilitate long-term release of a variety of drugs molecules, that require reduced applications compared to creams or other skin treatments while would be a useful treatment approach and much more cost effective. The stable biologically compatible foam nests produced by the Tungara frog may provide a potential solution to this problem.

Table 1.1: Examples of commercially available nanoparticles:

(Allen *et al.,* 2004, Weissig *et al.,* 2014)

Name (Year approved)	**Active Agent**	**Application**
AmBisome (1997)	Liposomal amphotericin B	Leishmaniasis Fungal infections
Bexxar (2003)	Anti-CD-20 I-tositumomab	Non-Hodgkin's lymphoma
Doxil (1995)	Liposomal doxorubicin	Kaposi's sarcoma Refractory breast and ovarian cancer
Inflexal V (1997)	Influenza virus antigens	Influenza vaccine
Kadcyla (2013)	Monoclonal antibody	Metastatic breast cancer
Mircera (2012)	PEGylated epoetine beta	Anaemia in renal failure adult patients
Peg-Intron (2001)	PEG-Interferon α-2b	Hepatitis C

Table 1.2: Examples of pharmaceutical foams commercially available:

(Purdon *et al.,* 2003, Tamarkin *et al.,* 2016, Zhao *et al.,* 2010)

Name	**Active Agent**	**Application**
Anestafoam	4% Lidocaine	Temporary pain relief
Bactoshield	4% Chlorohexidine gluconate	Surgical and wound cleaner
Delfen	12.5% Nonoxynol-9	Vaginal contraceptive
Epifoam	1% Hydrocortisone acetate	Reduces skin swelling and itching
Fabior	0.1% Tazarolene	Acne treatment
Ibuleve	5% Ibuprofen	Inflammation and pain relief for muscles or arthritic pain
Luxiq	0.12% Betamethasone valerate	Reduces irritation and swelling of the scalp
Olux-E	0.05% Clobetasol propionate	Eczema treatment
Septisol	0.23% Hexachlorophene	Bacteriostatic wound cleanser
Sorilux	0.005% Calcipotriene	Psoriasis
Verdeso	0.05% Desonide	Dermatitis

1.3 The Tungara Frog - *Engystomops pustulosus*

Anuran amphibians (Frogs and Toads) exhibit a remarkable diversity of reproduction modes which is characterised by multiple examples of parallel evolution of similar strategies in phylogenetically diverse species (Duellman and Trueb., 1986). Modes of reproduction range from large numbers of unprotected eggs through to small numbers of eggs with remarkable degrees of parental care and even tadpole feeding strategies (Duellman and Trueb., 1986). Between these extremes, there is a huge diversity of intermediate forms of reproductive behaviour. Many frogs produce foam nests to protect their eggs during tadpole development, which may include cryptic behaviour (hiding nests between leaves or in burrows) or nests which are exposed and open (Cooper *et al.,* 2010; Duellman and Trueb., 1986). Foam-nesting behaviours is known in phylogenetically diverse anurans such as the Rhacophorine frogs *Polypedates leucomystax* (The common Asian tree frog) found in South Asia (Yorke., 1983) and *Chiromantis rufescens* (The African foam nest tree frog) found across central Africa (Coe., 1967), the leptodactylid, *Leptodactylus fuscus* (The whistling frog) found in South American and the Caribbean (Downie., 1984) and the microhylids *Chiasmocleis leuciosticta* (Haddad and Hodl 1997). The number of frog species which adopt this reproductive strategy is not currently understood. Despite belonging to phylogenetically diverse families (**Fig 1.2**), these frogs have all evolved similar mechanisms for protecting their tadpoles during development. One particularly well-studied member of the foam-nesting frogs is the neotropical leptodactylid *Engystomops pustulosus*, which is

commonly known as the Tungara frog (**Fig 1.3**). It has a wide distribution and can be found across Central and South America and on the Caribbean islands of Trinidad and Tobago. *E. pustulosus* is an adaptable species found in a variety of habitats including grasslands, savannas, forest and almost any pool of water (Leigh *et al* 1999). These pools could be ponds and natural puddles or temporary water collected in man-made holes such as drainage ditches and potholes (Cooper *et al.,* 2010).

E. pustulosus has an interesting call comprised of a whine combined with chucks which is used to attract female mates (Ryan *et al.,* 1990). Some evidence suggests that their calls escalate depending on the number of other males present, and the presence of one of their main predators, fringe-lipped bats (Akre *et al*., 2010). The male frogs use their call to attract a female mate, and once they're paired they build a foam nest during amplexus (**Fig 1.3C**). These foam nests are often produced in groups, with multiple mating pairs producing nests at the same time to create rafts of nests in one pool (**Fig 1.4**) (Fleming *et al.,* 2009).

After a female has selected a calling male for a mate, the female begins producing fluid from her cloaca that contains the foam precursors - a cocktail of carbohydrates and six proteins named Ranaspumins (Fleming *et al*., 2009) The male clings to the female's back and uses his back legs to rapidly whip the liquid into a foam. At the same time the female will begin to release clutches of eggs (Heyer and Rand., 1997). A three-step nest building process then occurs. Firstly, an eggless raft layer is built as the base of the foam nest. Then the main building phase occurs, where fertilized eggs are incorporated into the foam and the majority of the nest is produced. Finally, the termination phase occurs where egg release is slowed

and eventually stops, while the foam whipping action becomes more sporadic and also stops (Dalgetty and Kennedy., 2010). The whole process takes around an hour (Heyer and Rand., 1997) and results in a small white spherical foam nest approximately 2-8cm in size (**Fig 1.4**). Tadpole development occurs over the next 2-3 days, and after this time the tadpoles will exit the nest facilitating its collapse (Downie *et al.,* 1993). It is unknown if the tadpoles facilitate the nest collapse through the production of enzymes during the hatching process.

The foam nests created in this process essentially acts as an incubation chamber for the eggs while they develop into tadpoles. It provides protection from predation, from micro-organisms and insects which could damage, infect or eat the developing eggs. Further the foam prevents damage from environmental factors by preventing dehydration caused by water loss and aiding temperature regulation in a tropical environment (Cooper *et al.,* 2010). Stable natural foams are rare, and the foam produced by the Tungara frog has some interesting properties. The foam is highly stable, holding its structure for up to 10 days in tropical environments (Fleming *et al.,* 2009). Most foams collapse within minutes to hours, so this length of stability is unusual. Further, the foam is biocompatible, it does not damage the eggs, sperm or tadpoles despite having significant surfactant properties (Mackenzie *et al*., 2009). Most surfactants damage cells walls, and this quality of surfactant non-toxicity could have great potential for exploitation in biotechnology and medicine.

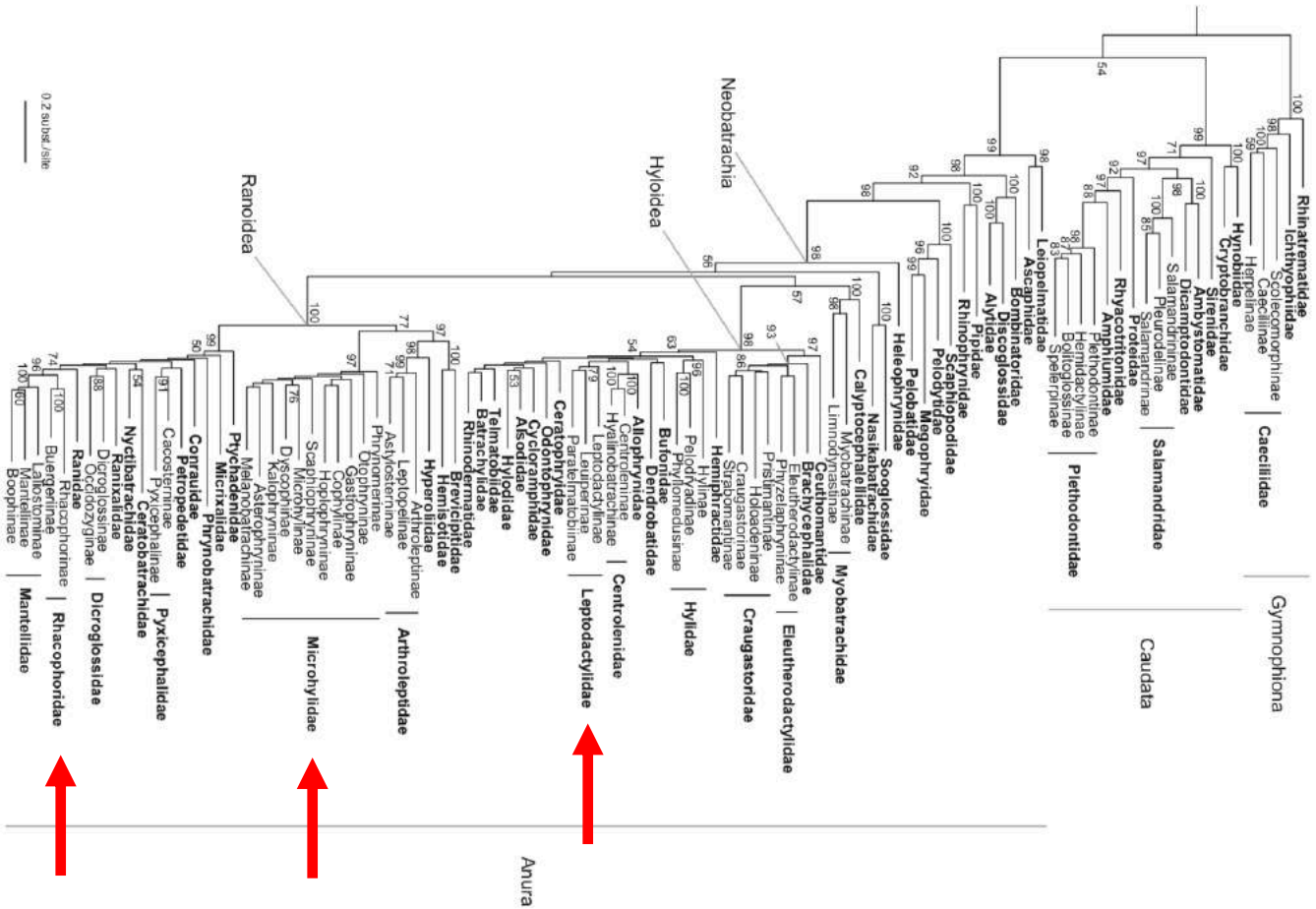

Figure 1.2: Phylogenetic tree of Anuran families (Pyron and Weins., 2011). Red arrows highlight families with foam-nesting species.

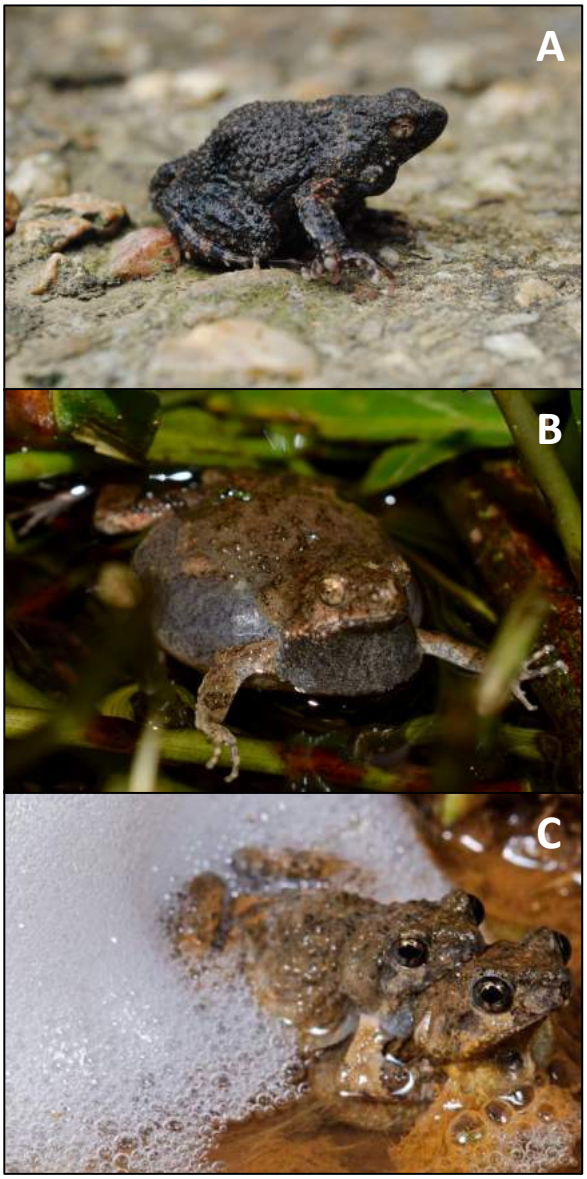

Figure 1.3: Photographs of the Tungara Frog. **A:** *Engystomops pustulosus* **B:** A calling *E. pustulosus* male. **C:** A foam nesting pair. Images: Sarah Brozio.

Figure 1.4: *Engystomops pustulosus* foam nests. **A:** Communally produced foam nest mass collected from a pond. **B:** Fresh nest produced under lab conditions over in fresh water. **C:** Fresh foam nest in a puddle. Images: Sarah Brozio.

1.4 Ranaspumins

Proteins and peptides from anuran amphibians have been shown to have massive potential for a wide variety of applications. Most notably, peptides isolated from frogs have demonstrated all manner of medically important functions. This research field has grown rapidly with the number of peptides published increasing from 500 in 2002 (Rinaldi*., 2002*) to 2000 in 2013 (Xu *et al*., 2013). These peptides include the Dermaseptins isolated from *Phyllomedusa* species which have activity against Gram-positive bacteria, Gram-Negative bacteria, HIV and HPV (Zairi *et al.,* 2009). Fallaxin discovered from *Leptodactylus fallax* has inhibitory activity against *Escherichia coli*, *Klebsiella pneumoniae* and *Pseudomonas aeruginosa* (Neilsen *et al.,* 2007). Hylaerleasins produced by *Hyla simplex* aid wound healing (Wu *et al*., 2011), and a Temporin peptide from *Rana chensinensis* has antitumor effects (Wang *et al*., 2012). Very few proteins have been isolated and characterised from Frog foam nests, but these proteins display unusual properties. They include *Lv*- RSN-1 which exhibits rare protein surfactant activity (Cavalcante-Hissa *et al*., 2016) and Ranasmurfin from *Polypedates leucomystax* which is a rare blue coloured copper-protein (McMahon *et al*., 2006). Amphibians are undoubtedly a source of unusual and useful proteins or peptides, and this area should be researched further.

The *Engystomops pustulosus* nest is built using a protein-carbohydrate precursor liquid which contains 1-2mg/ml of protein (Fleming *et al*., 2009). The carbohydrate component of this mixture is yet to be elucidated. The protein component of the foam consists of six proteins called Ranaspumin (RSN) 1-6, which are all in the range of 10-40kDa (Cooper *et al*.,

2005). Mass spectrometry data indicates that RSN-1 and RSN-6 are the dominant proteins in the foam, however the ratio of concentrations they are present in is unknown (Fleming *et al.,* 2009).

The RSN proteins were isolated by collecting foam samples, carrying out SDS-Page on the soluble foam liquid and excising the six prominent bands present. The bands were submitted for amino acid sequencing via Edman degradation. The resulting peptide sequences where used to design primers for DNA sequencing. Three female frogs where euthanised, their oviducts harvested and the RNA from the oviducts was isolated. The mRNA was then reverse transcribed into cDNA, and PCR carried out with the designed primers. The PCR products were sequenced elucidating the DNA sequence of each RSN (Fleming *et al.,* 2009), the DNA sequences and accession numbers are displayed in **Table 1.3**. The sequences collected allowed for bioinformatic comparisons to other proteins, and for function predictions to be carried out. Recombinant proteins for RSN-1, RSN-2, RSN-4 and RSN-6 were produced by overexpression in *E. coli* and used for further protein characterisation (Fleming *et al.,* 2009). RSN-1 demonstrated sequence similarities to cystatins but does not demonstrate any cystatin activity. RSN-3, RSN-4 and RSN-5 displayed similarities to fucose binding lectins which often display antimicrobial activity (Pistole., 1981). RSN-6 is homologous to a C-Type lectin, associated with galactose binding, with recombinant RSN-4 exhibiting crosslinking activity when used to agglutinate blood cells. However, this was not inhibited by the addition of fucose, suggesting it is not be a fucose binding lectin. However, this activity could be inhibited by lactose and galactose. Despite

predictions of carbohydrate binding function, no erythrocyte agglutination occurred with recombinant RSN-3 or RSN-6.

RSN-2 is the most well defined Ranaspumin. RSN-2 showed no homology to other known protein sequences in any database. The RSN-2 amino acid sequence is amphipathic indicating it had potential as a surfactant. This was proven correct, and RSN-2 is a protein surfactant (Fleming *et al*., 2009). RSN-2 is an 11kDa protein, whose structure was solved by NMR (Mackenzie *et al*., 2009). It has a mixed α/β structure, made up of a kinked α-helix and a four stranded antiparallel β-sheet (**Fig 1.5**). Despite appearing relatively polar when folded, RSN-2 absorbs well at the air-water interface. It is believed that RSN-2 undergoes a conformational change which causes the protein to unhinge exposing a hydrophobic pocket. This conformational change exposes RSN-2's amphipathic nature, allowing it to behave as a surfactant and reduce surface tension required for foam formation (Mackenzie *et al.,* 2009, Morris *et al.,* 2016). RSN-2 has significant surfactant activity and appears to be the main surfactant protein in *E. pustulosus* foam (Cooper *et al.,* 2010). Surfactant activity of proteins is rare in biology, as its can have damaging impacts on other proteins, and the structures of cell walls, membranes and viability (Mackenzie *et al*., 2009). RSN-2 does not appear to harm biological membranes, as its presence in the foam does not damage the sperm, eggs or tadpoles. Further, overexpression of recombinant RSN-2 in *E. coli* is not toxic to the cells (Cooper *et al*., 2010). Its role as a surfactant protein has been exploited in other processes including magnetic nanoparticle production. This research utilised RSN-2 to produce cost effective and potentially recyclable microemulsions for the synthesis of 8–10

nm super-paramagnetic iron oxide nanoparticles (Choi *et al* 2012). Further, RSN-2 was used in combination with Calvin cycle enzymes to produce a photosynthetic foam which could be utilised for carbon fixation and sugar synthesis (Wendell *et al.,* 2010). This quality of surfactant activity combined with no clear toxicity is an unusual quality and may be highly useful in the pharmaceutical industry, but this has not been previously explored.

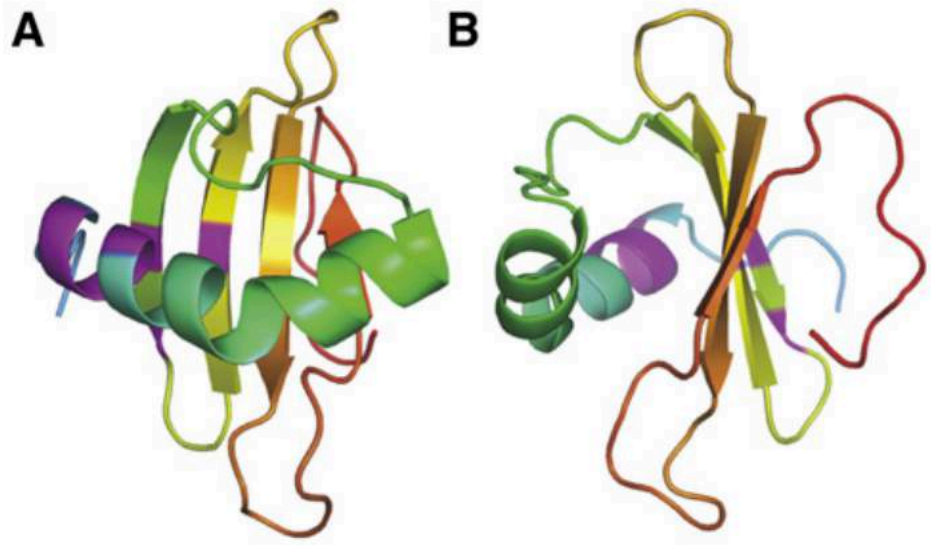

Figure 1.5: Structure of Ranaspumin-2 as solved using NMR. **A:** Demonstrating RSN-2 in its folded conformation. **B:** Folded conformation rotated 90°. Both highlight the single kinked α-helix and four β-sheet structures.

Table 1.3: Ranaspumin Summary

(Fleming *et al*., 2009)

Protein	Accession Number	Predicted Size (kDa)	Sequence Similarity
Ranaspumin-1 (RSN-1)	AY226146	14	Cysteinyl proteinase inhibitors
Ranaspumin-2 (RSN-2)	AY226147	11	None
Ranaspumin-3 (RSN-3)	AY226148	18	Fucolectins from teleosts
Ranaspumin-4 (RSN-4)	AY226149	21	Fucolectins from teleosts
Ranaspumin-5 (RSN-5)	AY226150	18	Fucolectins from teleosts
Ranaspumin-6 (RSN-6)	AY226151	27	C-Type galactose binding lectin

1.5 Project aims and objectives

The foam produced by the Tungara frog has many interesting qualities which warrants further investigation. The foam's stability, compatibility with eggs and antimicrobial characteristics indicates it may have value as a biocompatible material in medicine. Further, RSN-2's ability to act as a surfactant protein while not harming biological membranes and its previous use in other industrial processes suggests it may itself have value in drug delivery. Many of the proteins required for producing the foam remain uncharacterised with no defined function, and elucidating these functions is important in understanding the foam's qualities. To analyse *E. pustulosus* foam potential as a drug delivery system, four aims and objectives were defined for this research:

1. Foam characterisation:

The foam produced by *E. pustulosus* has potential in the context of a pharmaceutical foam. The structure, stability and toxicity need to be fully characterised to be better understand the overall properties of whole foam as produced by frogs. Techniques such as microscopy, rheology, circular dichroism, mammalian and bacterial cell assays will be used for foam characterisation.

2. Defining the drug release potential of *E. pustulosus* foam:

The ability of foam to be loaded and release drug molecules has not been previously investigated. A range of model dyes and authentic drug molecules will be tested, and their

release profiles assessed and defined. Understanding the basic release profile of the foam will allow its potential as a drug release system to be elucidated.

3. Recombinant protein cloning and overexpression:

To produce recombinant foam proteins and characterise them, a cloning strategy will be developed to insert codon optimised *rsn* genes into a plasmid vector system and overexpress each RSN in an efficient manner in *E. coli* and to develop a purification procedure.

4. Synthetic foam production:

The final goal of this research was to produce a synthetic version of the *E. pustulosus* foam from recombinant RSN proteins and evaluate if the synthetic foam could be used as a drug delivery system with the goal of utilising this as a treatment for burns and wound infections.

2.0 Materials and Methods

2.1 Collection of *Engystomops pustulosus* foam:

The *E. pustulosus* foam used throughout this research was collected from multiple sites and frogs in Northern Trinidad. Foam collections were carried out during the wet season (May-August) in 2014, 2015, 2016 and 2017. The sites these samples were taken from are displayed in **Figure 2.1**. Foam samples were gathered using two methods.

2.1.1 Foam collected directly from sites:

When rain occurred, sites where checked between 6am-8am (to ensure freshness) to see if new foam nests had been laid the previous night. If a fresh nest was located, it was stored in a plastic container and taken to a laboratory to be processed. Each nest had as many eggs removed as possible using tweezers, ensuring that the eggs were not burst open, yielding egg proteins in to the foam. The egg free portion of the foam nest was then placed a storage tube and frozen at -20°C. All eggs removed from nests were placed in aerated dechlorinated water and allowed to develop into tadpoles. The tadpoles were returned to the original sites of collection. All foam samples were transported back to the UK on ice and immediately stored at -80°C.

2.1.2 Foam collected in laboratory:

Sites with a frequent *E.s pustulosus* population were checked each evening for amplexing pairs. Pairs were gathered and placed into a plastic container in clean aerated water. The couples were left overnight to allow them time to settle and nest. The nest produced was

taken, each egg was removed, and the foam samples stored in the same manner as above. All eggs removed from nests were placed in aerated dechlorinated water and allowed to develop into tadpoles. The tadpoles were returned to the original sites of collection. Any pairs of frogs collected were returned to their site of collection after nesting was complete.

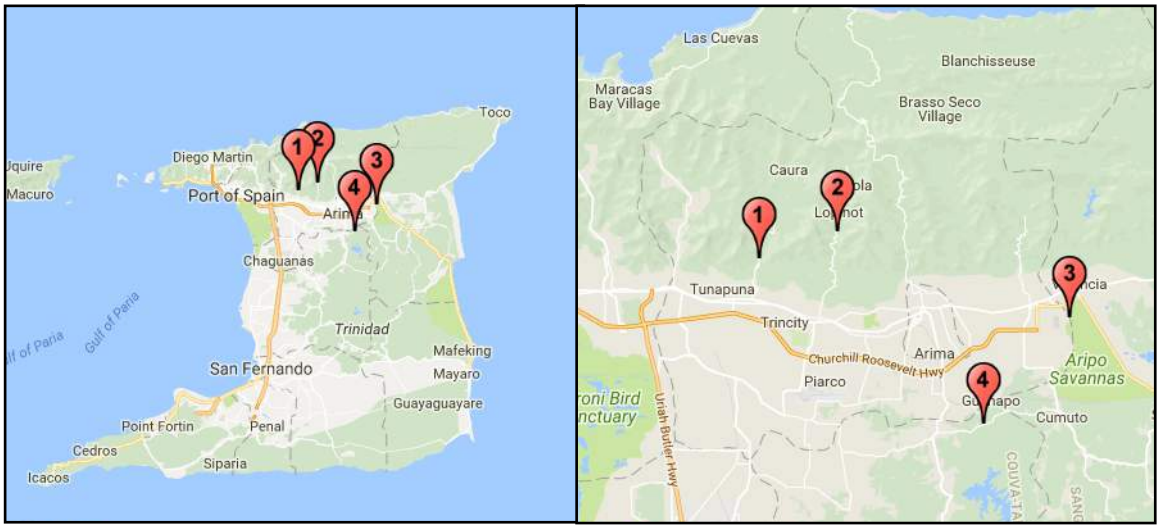

Figure 2.1: Map of foam collection sites in Northern Trinidad. Markers display the sites where foam and frogs were collected. **1:** Caura Valley. **2:** Lopinot Road. **3:** Aripo Savanas. **4:** Tunapuna Road, Arena Forest. Map Data: Google 2018.

2.2 Foam Characterisation Techniques:

2.2.3 Foam Density:

The method for determining foam density was adapted from Arzhavitina *et al*., 2010. Foam samples were defrosted at room temperature. Three aliquots (5 ml) of foam were measured into 15 ml falcon tubes and each foam sample was weighed. Three falcon tubes were filled with 5ml of distilled water and each tube was weighed. The average weight of an empty falcon tube was subtracted from all the other measurements. The mean of water weights and the foam weights were determined. All measurements were determined in triplicate. The foam density was the calculated as below:

Foam Density = Average Foam Weight/Average Water Weight

2.2.4 Microscopy:

Foam was defrosted to room temperature before use. Foam was unloaded or loaded with either Nile Red (Sigma) or Calcein (Sigma). All foam images were taken with brightfield settings under 4x magnification using NIS-Elements AR.3.2. software. Fiji software was used for image analysis.

2.2.5 Rheology:

To evaluate the viscosity, elasticity and plasticity of the foam rheology experiments were employed. Foam samples were defrosted to room temperature. Aliquots (400µg) of foam were weighed to ensure a constant sample size. All rheology measurements were determined using a Haake Mars Rotational Rheometer (Thermo Scientific). All experiments

were programmed and carried out using Thermo Scientific HAAKE RheoWin software. All experiments were carried out using P20 upper plate and TM20 lower plate. Protocols carried out were adapted from Kealy., 2008, Marze *et al*., 2009 and Piazza *et al*., 2008.

2.2.6 Amplitude Sweep:

An aliquot of defrosted foam was placed on the lower TM20 plate. The upper plate was then lowered onto the foam sample, until the gap between the upper and lower plates reached 1mm. Sheer stress (τ) was then applied to the foam. This occurs in a range from 0.1–200Pa, over 20 increments, where the stress increases by around x1.5 each increment. Measurements representing the elastic (G') and viscosity (G'') responses were collected in triplicate and automatically averaged by the software. This data was then exported in XML format and further analysis carried out using Origin Software.

2.2.7 Oscillation Time Sweep:

An aliquot of foam was placed on the lower TM20 plate. The upper plate was lowered onto the foam sample until the gap was set at 0.5mm. The sheer stress was then applied at a constant 100Pa, with a frequency of 3Hz. The temperature of the lower plate was maintained at 37°C throughout the experiment. Viscoelasticity (G' and G'') were measured every 15 secs for 1h. Each time point was gathered in triplicate and automatically averaged. The data was then exported in XML format and the graphs produced using Origin software.

Samples of foam were subjected to oscillation sweeps and time sweeps. The oscillation sweeps were completed with a 1mm gap, and a 0.1Pa to 200Pa range. Time sweep

experiments were run for 1h, at 100Pa and 3 Hz using a 0.5mm gap. Data points were collected in triplicate and averaged before graphs were plotted.

2.3 Bacterial Strain Cultivation:

2.3.1 Media:

All bacterial strains in this study were grown on lysogny broth (LB) (Bertani, 1951) containing:

10g/L Tryptone

5g/L Yeast Extract

10g/L NaCl

20g/L Agar was added for solid medium

All media components were dissolved in distilled water, and autoclaved at 121°C, 15psi for 15mins. If antibiotics were required, they were added to the media after autoclaving.

2.3.2 Strains:

All the strains used throughout this work are shown in **Table 2.1**. All microbiology work was carried out using aseptic techniques. Strains were grown by streaking on solid LB media, at 37°C overnight, and a single colony picked from the plate to inoculate 5ml of liquid LB. All media contained the appropriate antibiotic for strain growth. Glycerol stocks were made for strain storage. These were produced by adding 500µl of 50% sterile glycerol to 500µl of overnight culture. All stocks were stored at -80°C.

2.3.3 Plasmids:

rsn genes were codon optimised using the Integrated DNA Technologies (IDT) codon optimization tool (https://www.idtdna.com/CodonOpt). Restriction enzyme sites were

added to the flanking regions. *NdeI* and *NcoI* sites were added to the 5' flank. *BamHI* and *XhoI* sites were added to the 3' using IDTs tools before plasmids containing codon optimised Ranaspumin (*rsn*) genes were synthesised by either Integrated DNA Technologies (IDT) or Eurofins (detailed in **Table** 2.2). All plasmids used in this research are displayed in **Table 2.2**. All plasmids were checked by sequencing following Eurofins requirements.

Table 2.1: Bacterial strains

Strain	Genotype	Description	Source
Escherichia coli			
Escherichia coli DH5α	F⁻ Φ80*lac*ZΔM15 Δ(*lac*ZYA-*arg*F) U169 *rec*A1 *end*A1 *hsd*R17(r_k^-, m_k^+) *pho*A *sup*E44 *thi*-1 *gyr*A96 *rel*A1 λ⁻	Strain used for general plasmid propagation.	Invitrogen
Escherichia coli BL21 (DE3)	*fhuA2 [lon] ompT gal (λ DE3) [dcm] ΔhsdS λ DE3 = λ sBamHIo ΔEcoRI-B int::(lacI::PlacUV5::T7 gene1) i21 Δnin5*	Strain for routine T7 promotor protein overexpression.	New England Biolabs
Escherichia coli One Shot BL21*	F⁻*ompT hsd*S_B (r_B^-, m_B^-) *galdcmrne*131 (DE3)	Strain for over expression of low copy T7 promotor plasmids.	Invitrogen
Escherichia coli Rosetta (DE3)	F⁻ *ompT hsdS*$_B$(r_B^- m_B^-) *gal dcm* (DE3) pRARE (Cam^R)	Strain for over expression of proteins using rare *E. coli* codons.	Novagen
Escherichia coli ATCC 8739		Fecal strain used to test antimicrobial agents	ThermoFisher
Staphylococcus aureus ATCC 29213		Wound isolate used to test antimicrobial agents	ThermoFisher

Table 2.2: Plasmids

Plasmid	Description	Antibiotic Resistance	Source
pET28a	PT7 Expression vector, N-term and C-term HisTags. N-term thrombin site.	Kanamycin	Novagen
pUCIDT RSN-1	Contains synthesised Ranaspumin-1 gene	Ampicillin	Integrated DNA Technologies
pEXA2 RSN-2	Contains synthesised Ranaspumin-2 gene	Ampicillin	Eurofins
pEXA2 RSN-3	Contains synthesised Ranaspumin-3 gene	Ampicillin	Eurofins
pUCIDT RSN-4	Contains synthesised Ranaspumin-4 gene	Ampicillin	Integrated DNA Technologies
pUCIDT RSN-5	Contains synthesised Ranaspumin-5 gene	Ampicillin	Integrated DNA Technologies
pUCIDT RSN-6	Contains synthesised Ranaspumin-6 gene	Ampicillin	Integrated DNA Technologies
pRSN-1	Ranaspumin-1 inserted into pET28a vector with N-term HisTag	Kanamycin	This work
pRSN-2	Ranaspumin-2 inserted into pET28a vector with N-term HisTag	Kanamycin	This work
pRSN-3	Ranaspumin-3 inserted into pET28a vector with N-term HisTag	Kanamycin	This work
pRSN-4	Ranaspumin-4 inserted into pET28a	Kanamycin	This work

	vector with N-term HisTag		
pRSN-5	Ranaspumin-5 inserted into pET28a vector with N-term HisTag	Kanamycin	This work
pRSN-6	Ranaspumin-6 inserted into pET28a vector with N-term HisTag	Kanamycin	This work

2.3.4 Bacterial Growth Curves:

Bacterial growth curves were carried out in 96 well plates (Sigma) using a BioTek Synergy HT microplate reader. Single colonies of *S. aureus* or *E. coli* were used to inoculate 5ml of LB media which was gown overnight, shaking at 37^{o}C. Overnight cultures were diluted 1 in 100 to inoculate each well. Liquid foam proteins or purified RSN- 2 protein was added to treatment wells. Liquid foam was filtered with a Millex 33mm 0.22µm filter before use. All wells had a final volume of 100µl to fit the working volume of 96 well plates. Plates were incubated, shaking, at 37^{o}C with OD600 measurements taken every 10 minutes for 10 hours. Each treatment or control was conducted with 12 replicates. Positive control was treated with media alone. Negative control contained Kanamycin.

2.3.5 Mammalian Cell Viability Assay:

Mammalian cell viability was tested using the MTT Assay (Mosmann., 1983). HaCaT cells were grown in Dulbecco's modified Eagle's medium (DMEM) with 4.5 g/l glucose (SLS) supplemented with 10 % (v/v) fetal bovine serum, 2 mM L-glutamine and 50 units/ml penicillin/streptomycin. Foam proteins were prepared by centrifugation for 10 min at 16,000xG. The supernatant was then filtered using a Millex 33mm 0.22µm filter and concentrated to 2mg/ml using Amicon 10kDa spin filter. The protein concentration was determined by Bradford assay (2.5.7). The cells were grown in 96 well plates and were treated with 200µl of DMEM media and 200µl of varying foam protein concentrations prior to incubation at 37°C for 24 hours. After 24 hours, the media was removed from the cells

and replaced with fresh media and 50µl of 3-(4,5-dimethylthiazol-2-yl)-2,5-diphenyltetrazolium bromide (MTT). This was incubated for 1 h at 37°C, followed by a 30 min incubation in the dark. The absorption measured in a spectrophotometer at 570nm (Riss *et al*., 2013).

2.4 Molecular Biology:

2.4.1 Transformation:

Competent cells were thawed on ice, before adding 1-5µl of plasmid DNA. The cells were incubated for 30 mins on ice, then heat shocked at 42°C for 2 mins. 1ml of LB media was added to mix and incubated at 37°C for 1 hour. Cells were centrifuged, using a Beckman Coulter Microfuge 16, at 10,000 x G for 1 min. The LB media was removed, and the cell pellet re-suspended in 200µl of fresh LB. The 200µl was spread on LB agar plates containing the appropriate antibiotic and incubated at 37°C overnight.

2.4.2 Plasmid Isolation:

All plasmids were isolated using Bioline Isolate II Plasmid Mini Kit. 5ml overnight cultures were used, and plasmid DNA was isolated following the manufacturers protocol. A ThermoScientific NanoDrop 2000 Spectrophotometer was used to measure final DNA concentration. Purity was estimated by calculating the samples A260/A280 ratio. Samples with ratios of approximately 1.8 were used for further steps.

2.4.3 Restriction Digests:

All plasmids were digested with *NdeI* (NEB) and *BamHI* (Promega) in CutSmart buffer (NEB) unless stated otherwise following NEB recommended protocol. 5µl of buffer was mixed with 3µl of BSA, before adding 10µg of DNA. 1µl of each enzyme was added, and then nuclease free water was used to make the final volume to 30µl. Single temperature double digests were performed by incubating at 37°C for one hour.

2.4.4 Agarose Gel Electrophoresis:

Gel electrophoresis was used to check plasmids and PCR products. 2% agarose was dissolved in 1 x TAE buffer (diluted from 50X stock solution) and was boiled in the microwave. 50X TAE stock solution contained 2M Tris acetate and 50mM EDTA. Samples were mixed and loaded with Bioline 5X Loading Buffer Blue. Bioline Hyperlader was used to estimate band sizes. 10µl of sample was added to each well. Gels were run in 1x TAE buffer at 100V for 30-45 mins depending on product sizes. These were then stained in Gel Red solution for 30 mins, shaking at room temperature before being visualised under UV light (300nm).

2.4.5 Gel Extraction:

Digested plasmid bands were extracted from gels to be utilised in ligation steps. Correct bands were located under UV transillumination (300nm). The required bands were cut out the gel using a sterile scalpel and extracted using Bioline Gel Extraction kit, following the manufacturers protocol.

2.4.6 Ligation:

Digested *rsn* gene fragments were ligated into pre-digested pET28a plasmid using T4 ligase (NEB). Reactions were mixed using 2µl of supplied buffer, a 1:5 vector: insert ratio of DNA, 1µl of ligase and made up to the final volume of 20µl with nuclease free water. Ligations were carried out at 4°C overnight.

2.4.7 Polymerase Chain Reaction (PCR):

Colony PCRs (cPCR) were carried out to check inserts had been ligated into vectors due to the small size of some of the fragments being difficult to visualise on gels. The primers used in this work were designed using GenScript and are detailed in **Table 2.3**. Bioline MyTaq DNA Polymerase kit was used for all cPCR experiments. Multiple single colonies from each transformation plate were selected for cPCR screening. Each colony was added to a PCR tube with a sterile pipette tip, and then used to inoculate 1ml of LB. Each reaction contained 1µl of each 10µM primer (Forward and Reverse), 5µl of Bioline MyTaq reaction buffer which contains dNTPs, 1µl of DNA polyermase (Bioline MyTaq) and 11µl of nuclease free water to make a final volume of 20µl. All products were checked with agarose gel electrophoresis.

Table 2.3: Primers

Primer	Forward Primer (5'- 3')	Reverse Primer (5'- 3')	Product size (bp)
RSN-1	GCTGTGATCAGCCAGCATT	TCTGCTTGACGTGGCAATAC	262
RSN-2	GCTGATTCTGGATGGAGACC	CATCATCGTCTTTGCGACAC	275
RSN-3	TGCAGTCATACCGGTGGTAA	ACCTCAACCTCGCACAGACT	293
RSN-4	GTGTTTCCACACCGGGTTAG	ATATTGACGTAGCGGCCAAC	251
RSN-5	TAACCCGACTTGGTGGAAAG	CTGTTCTTTCCGAGGGACTG	247
RSN-6	TTGTGGGGTGTCAACAAAGA	AAGAGCCATATCCCCCACTT	238

2.5 Protein Techniques

2.5.1 Polyacrylamide Gel Electrophoresis (PAGE):

Native PAGE gels were run on precast Invitrogen Novex NativePAGE 4-16% Bis-Tris gels. Native samples were mixed with 6 X Purple loading dye (NEB) in a 1:1 ratio. Native gels were run at 120V for 45 mins.

Sodium dodecyl sulfate (SDS) PAGE gels were run using either precast Invitrogen WedgeWell 4-20% Tris-Glycine Gels or NuPAGE 4-12% Bis-Tris Protein Gels. Samples were mixed with 6 X SDS loading dye and heated to 75°C for 7 mins before being loaded onto a gel. A 10-200kDa broad range protein ladder (NEB) was added to all SDS PAGE gels.

All gels were stained in Instant Blue solution (Expedeon) for 30 mins and then stored in distilled water. Buffers used in these experiments are detailed in **Table 2.4**.

2.5.2 Glycostain:

Thermo Fisher Pierce glycostaining kit was used to identify glycosylated proteins. SDS-Page was carried out on precast 4-20% Tris Glycine WedgeWell gel and glycostain was performed according to the manufacturer's instructions.

Table 2.4: Reagents for PAGE

Buffer	**Contents**
20 X Native Running Buffer	Tris 50 mM, MOPS 50 mM, EDTA 1 Mm 1L Dissolved in water
10 Tris Glycine SDS Running Buffer	250 mM Tris 1.9M Glycine 1% SDS 1L Dissolved in water
10 X MES Running Buffer	500 mM MES 500 mM Tris base 1% SDS
6 X SDS Loading Dye	0.5g Tris HCl 1.2g SDS 6ml Glycerol 900µl β-Mercaptoethanol Make up to 10ml with distilled water

2.5.3 Circular Dichromism (CD):

Circular Dichromism measurements were taken using Chirascan Plus (Applied Photophysics) with a 0.1mm quartz cuvette (Hellma), at 20°C. All samples were measured in the far-UV in a wavelength range of 180-280nm (Kelly *et al.,* 2005). A step size of 1 nm, bandwidth of 1 nm and reading time of 1 s per point were chosen. Baseline and buffer spectra were measured and subtracted from the sample spectra before further analysis. Baseline measurements were taken with an empty cuvette. Buffer measurements were taken using PBS as samples were stored in PBS. All samples were measured in triplicate. All data analysis was performed using Global3 software and Excel.

2.5.4 Fourier transform infrared spectroscopy (FTIR):

Fourier transform infrared spectroscopy (FTIR) was carried out using a Nicolet iS10 Smart iTR spectrophotometer (Thermo Scientific). Solid and liquid foam spectra were recorded in the range on 4000cm^{-1} and 500cm^{-1}, over 128 scans at a resolution of 4cm^{-1} and an interval of 1cm^{-1}. This range provides suitable spectra for estimating protein secondary structure (Griffiths and Haseth., 2007). Background measurements were taken and removed from results before analysis using Excel.

2.5.5 Protein Overexpression:

Optimal conditions for protein overexpression were tested for all six Ranaspumin proteins. The conditions tested are detailed in **Table 2.5**. Growth temperature, IPTG concentration and expression cell type were assessed to identify the combination which produced the

highest protein concentration. Once ideal conditions had been picked, cultures were scaled up to 50ml or 1L. Media was inoculated with fresh overnight culture and cells were grown at 37°C to OD600 0.4-0.6. Isopropyl β-D-1-thiogalactopyranoside (IPTG) was then added to the culture to induce protein overexpression to the appropriate final concentration. The temperature was dropped to 25°C and cultures incubated overnight. Cells were harvested by centrifugation at 4000xG for 30 mins.

Table 2.5: Overexpression Conditions

Condition	
Cell Type	BL21, BL21*, Rosetta
IPTG Concentration	0.2mM, 0.5mM, 1mM
Temperature	15°C, 25°C, 30°C, 37°C

2.3.1 Protein Purification:

E. coli cells used for protein overexpression were lysed using BugBuster Master Mix (Millipore). Cultures were grown and induced according to each RSNs optimum conditions, then centrifuged for 30 mins at 15,000rpm to harvest the cells. Cell pellets were re-suspended with 5ml BugBuster per g of cell pellet. Complete protease inhibitor cocktail (Roche) was also added to the suspension. This was incubated, shaking, at room temperature for 1 hour. Lysate was clarified by centrifugation at 15,000rmp for 30 mins at 4°C.

Proteins were purified with nickel affinity chromatography using an AKTA Purifier system using Unicorn 5.11 software (GE Healthcare). Protocols were programmed using the GE Healthcare AKTA manual. Lysate was loaded on to pre-equilibrated HisTrap columns (GE Healthcare). The unbound protein was washed away with 10 column volumes of buffer A (**Table 2.6**) before applying a gradient of buffer B (**Table 2.6**) to elute the bound protein. The buffers used for purification are detailed in **Table 2.6**. All protein fractions were checked for proper lysis, purified bands, contamination and purity with SDS Page before further use.

2.3.2 Bradford Assay:

Bradford assays were carried out using BioRad Bradford reagents, following the BioRad protocol. Standards were prepared by diluting 1mg/ml BSA to a range of concentrations in order to produce a standard curve. Samples were mixed with Bradford reagent and

incubated for 5mins at room temperature. Absorbance was measured at 595nm and protein concentrations calculated using the standard curve produced.

Table 2.6: Purification Buffers

Buffer	
Tris HisTrap A	20 mM Tris-HCl at pH 7.5 500 mM NaCl 20 mM Imidazole 10% glycerol
Tris HisTrap B	20 mM Tris-HCl at pH 7.5 500 mM NaCl 1 M Imidazole 10% Glycerol
Sodium HisTrap A	20mM Sodium Phosphate 0.5M Sodium Chloride 20mM Imidazole
Sodium HisTrap B	20mM Sodium Phosphate 0.5M Sodium Chloride 500mM Imidazole

2.4 Drug Release Techniques:

2.4.1 Dye Molecules Release:

Aliquots (400mg) of foam were prepared by mixing with either 400µl of 1mg/ml Nile Red (Sigma) or 1mg/ml Calcein (Sigma) solution in Ethanol (100%). This was then placed inside dialysis tubing and sealed by knotting each end before being submerged in 10 ml of Phosphate buffered saline (PBS) which was preheated to 37°C. For experiments carried out with Nile Red 50% ethanol was also added to the medium to ensure the Nile Red remained soluble. The release experiments were carried out at 37°C, over 168 hours. To maintain the volume of the assay, 1 ml of pre-heated PBS was added to the medium sink following sampling. The concentration of each sample was determined spectrophotometrically at 495nm (Calcein) or 590nm (Nile Red) and the concentration calculated using calibration curves of the pure dyes (Litvinchuk *et al*., 2009, Dutta *et al*., 1996). All release experiments were carried out in triplicate.

2.4.2 Antibiotic Release Dialysis Method:

Aliquots (400mg) of foam were mixed with Rifampicin (25mg/ml). The loaded foam was placed into dialysis tubing (Sigma), sealed and submerged in 10 ml of PBS. This was incubated at 37°C for 48 h. Samples (1ml) were taken a various time points (e.g. 0hr, 1hr, 2hrs, 4hrs, 6hrs,24hrs, 48hrs) and fresh media added to maintain sink conditions. Samples where measured spectrophotometrically at 475nm (Benetton *et al.,* 1998). Concentration was the calculated using a calibration curve. All release experiments carried out in triplicate.

2.4.3 Antibiotic Release Transwell Method:

Aliquots (100mg) of foam were loaded with Rifampicin (25 mg/ml). Loaded foam was the placed into a Transwell permeable support (Corning) containing a collagen coated 1µm polyester membrane. Each support was inserted into 24 well plate containing 600µl of PBS with the membrane sitting level with the PBS. The plate was then incubated for 48 hours at 37°C. 600µl of PBS was collected from a well for each time point, and the absorbance measured at 475 nm. Each time point was taken in triplicate.

2.5 Statistics:

Standard Error bars for all data sets were produced by calculating the standard deviation of all points using Excel, and all points displayed on graphs represent the mean of the data. One-Way ANOVAs were applied to data sets using Excel to demonstrate statistical significance. P-Values were considered significant if their value was less than 0.05.

3.0 Bioinformatic Analysis of Ranaspumins:

The use of computers in the analysis of biological macromolecules has revolutionised how we carry-out and develop hypotheses in modern biology. A wide range of bioinformatics tools have been developed to analyse the sequences and structures of proteins. These exploit databases of hypothetical proteins, known protein domains, structures and functions to predict these qualities for unknown protein sequences derived from the burgeoning amounts of data from sequencing projects. Programs such as BLAST (Altschul *et al*., 1990), Jalview (Waterhouse *et al.,* 2009) and I-TASSER (Roy *et al.,* 2010) utilise databases including Protein Data Bank (Berman *et* al., 2000), UniProt (Uniprot Consortium., 2017) and Protein Information Resource (Barker *et al.,* 2000) to provide functional predictions on input sequences. These examples are not an exhaustive list and a multitude of programs and scripts are available for protein analysis. Previous bioinformatic investigations of the Ranaspumin (RSN) amino acid (AA) sequences indicated no direct matches or very few close matches from BLAST. Moreover, apart from some limited sequence similarity between RSN-3 and RSN-5, the Ranaspumins do not have conserved sequence motifs when aligned against each other. The RSN-1 sequence exhibits some sequence similarity to potential cystatin-like proteins. Cystatins are a family of cysteine protease inhibitors; however, protease inhibitory activity was not observed when recombinant RSN-1 was assayed (Fleming *et al.,* 2009). RSN-2 returns no hits in BlastP and only its amphipathic sequence provided any

indication of its function. The structure of RSN-2 was solved by NMR and its function as a surfactant elucidated (Mackenzie *et al*., 2009).

RSN-3, RSN-4, RSN-5 and RSN-6 results all suggested they could have carbohydrate-binding lectin-like function. RSN-3, RSN-4 and RSN-5 were all classed as fucolectins with predicted fucose binding. These RSNs where predicted to have structural similarities based on secondary structural predictions. RSN-6 also has lectin homology and was classed as a C-type lectin with potential galactose binding. Only RSN-4 was clearly shown to have any carbohydrate binding properties when tested with red blood cell agglutination. However, the predicted fucose binding activity was absent, but lactose and galactose binding could be demonstrated (Fleming *et al.,* 2009).

Most of the bioinformatic analysis carried out on the RSN sequences occurred 10 years ago. The emergence of cheap whole genome sequences has resulted in a massive increase in sequences available in the databases in the intervening time and many of the databases have been significantly expanded and updated. This includes the addition of genomes from multiple amphibian species such as several clawed frogs, *Xenopus sp*. (Buisine *et al.,* 2015., Session *et al.,* 2016), the Bullfrog, *Rana catesbiana* (Hammond *et al*., 2017), and the Axolotl, *Ambystoma mexicanum* (Nowoshilow *et al.,* 2018). Furthermore, many new bioinformatics programs and algorithms are available for secondary structure prediction enhancing the utility of raw nucleotide sequence. Here bioinformatic analysis using BlastP and I-TASSER was carried out to provide an update on the phylogenomic distribution of RSNs amino acid sequences.

3.1 RSN-1 Analysis

A protein-protein Blast query of the RSN-1 AA sequence returned 69 hits, the top five are displayed in **Table 3.1** and the alignments are shown in **Fig 3.1**. The Blast query indicated no putative conserved domains, through the Blastp algorithm in the NCBI non-redundant blast server. Across the five sequences, there are 17 conserved residues, including a PATP motif. In line with previous results, many of the returned homology matches with cystatins, including a match with a cystatin protein from the Asian common toad (*Duttaphrynus melanostictus*). However, even with the highest-ranking matches, RSN-1 only shared 37% identity with these proteins with relatively low E-values. The E-value indicates the likeliness of a match occurring by random chance.

I-TASSER was used to generate a model for the structure of RSN-1 (**Fig 3.2**) The model C score was calculated at -1.22. This C score is on a range of -2 – 5, where the higher the score the more confidence assigned to the structural model. The C score assigned to the RSN-1 model indicates that its most likely inaccurate. I-TASSER uses COFACTOR to predict any potential ligand binding sites and the possible ligand from the model produced. COFACTOR predicted a Ca^{2+} binding site at the K52 and L55 residues (**Fig 3.2**) with a C score of 0.07. The COFACTOR C score is reported on a scale of 0-1, where the closer to 1 indicates higher confidence in the prediction. As well as a low structural confidence, the results also indicate a low confidence in the ligand binding prediction. I-TASSER also provides structural analogues of the predicted structure, the first five analogues are listed in **Table 3.2**. All five results are cystatins, but they all share 20% or less identity

with the predicted RSN-1 structure. The bioinformatic analysis of RSN-1 suggests that the protein may have cystatin activity, however previous research has demonstrated that this is not the case. This indicates that the updated bioinformatic analysis offers no new insight into RSN-1's potential function.

Table 3.1: Top 5 RSN-1 Blast Hits

Name	**Organism**	**Identity**	**E-value**	**Accession**
Cysteine protease inhibitor	Asian Common Toad (*Duttaphrynus melanostictus*)	31%	0.004	AGX85322.1
Cystatin-A	Baiji (*Lipotes vexillifer*)	33%	$3x10^{-4}$	XP_007449770.1
Cystatin-A	Sperm Whale (*Physeter catodon*)	33%	$9x10^{-4}$	XP_007112234.1
Cystatin-A	Mongolian Gerbil (*Meriones unguiculatus*)	37%	0.002	XP_021490320.1
Cystatin-A	Common Bottle Nose Dolphin (*Tursiops truncates*)	32%	0.011	XP_019778427.1

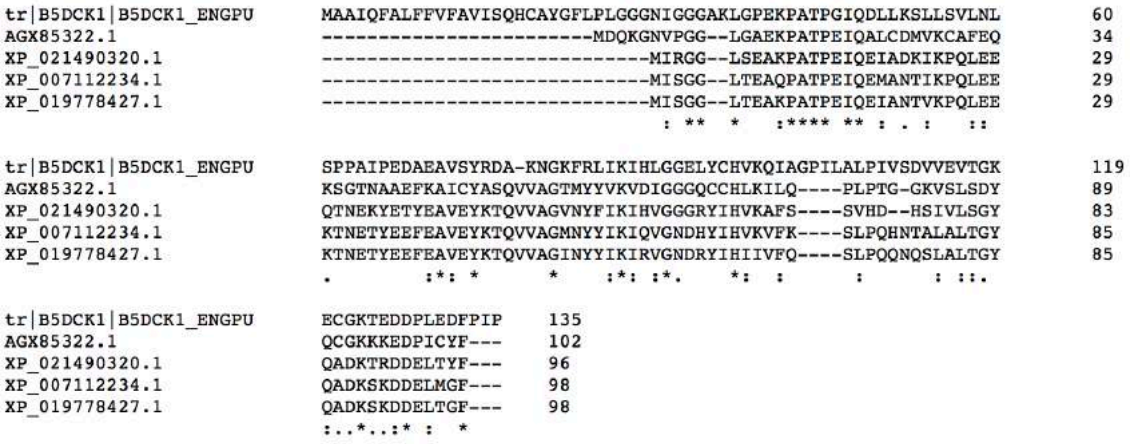

Figure 3.1: BlastP alignments for top five results against RSN-1 AA sequence produced in Clustal Omega. Conserved residues are marked with a *.

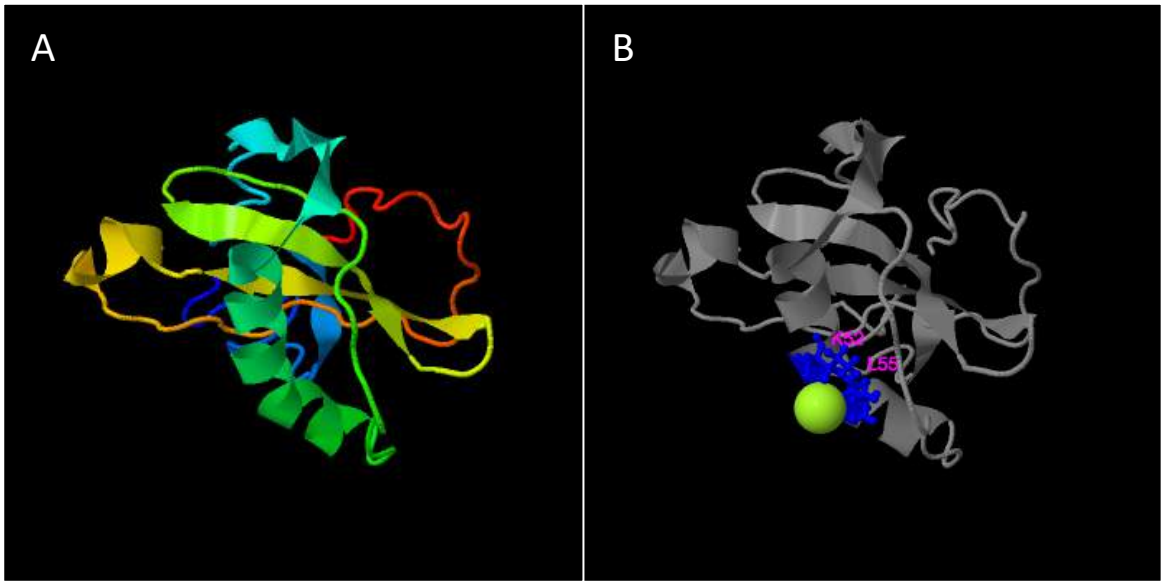

Figure 3.2: A: Structural prediction of RSN-1 produced using I-TASSER. C score = -1.22. **B:** Predicted ligand binding site of RSN-1 constructed using COFACTOR through I-TASSER.

Table 3.2: I-TASSER RSN-1 Structural analogues

PBD Hit	Description	TM-Score	Identity
1stfI	Structure of recombinant human stefin b in complex with the cysteine proteinase Papain	0.674	0.206
3k9mc	Cathepsin B in complex with stefin A	0.659	0.278
4lziA	*Solanum tuberosum* Multicystatin	0.570	0.093
1iv9A	Crystal Structure of Single Chain Monellin	0.538	0.083
3lh4A	Crystal Structure of Sialostatin L2	0.531	0.103

3.2 RSN-2 Analysis

A Blast query of the RSN-2 AA sequence returned no hits and indicated no conserved putative domains. These results are the same as previous investigations. RSN-2 is the main surfactant protein in the foam, and its structure (**Fig 3.4**) and mechanism of action has previously been solved (Mackenzie *et al.,* 2009). There is only one other frog foam protein surfactant identified, Lv-RSN-1, and the two proteins have less than 15% sequence similarity (**Fig. 3.3**) indicating these proteins evolved similar functions seperately. I-TASSER compared RSN-2's known structure to other protein structures, and the top five analogues are highlighted in **Table 3.3**. The structural analogues listed include a variety of proteins such as cystatins, lipoproteins and uncharacterised functions. However, all these structures only shared around 10% identity with RSN-2. These results highlight that RSN-2 remains a unique protein. Protein surfactants are rare in nature and RSN-2 doesn't appear to share sequence similarity with any known proteins or have any true protein analogues. It is unlikely that no protein similar to RSN-2 exists and much more probable that any protein analogues have not been isolated yet. mRNA coding for RSN-2 can be found in multiple organs of the Tungara frog (Ref) indicating it may have functions out with foam formations. This may mean RSN-2 has functions that have not been identified yet, belong to a novel class of proteins which has not been identified yet.

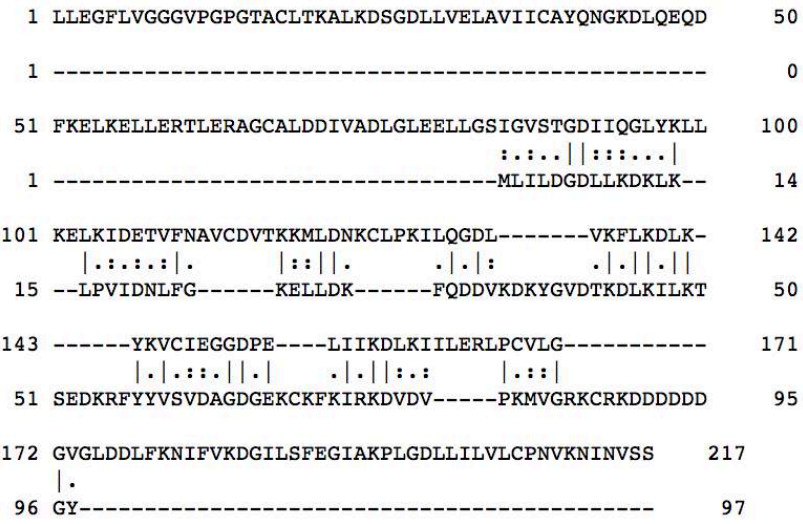

Figure 3.3: Alignment of RSN-2 AA sequence with Lv-RSN-1, created using EMBOSS.

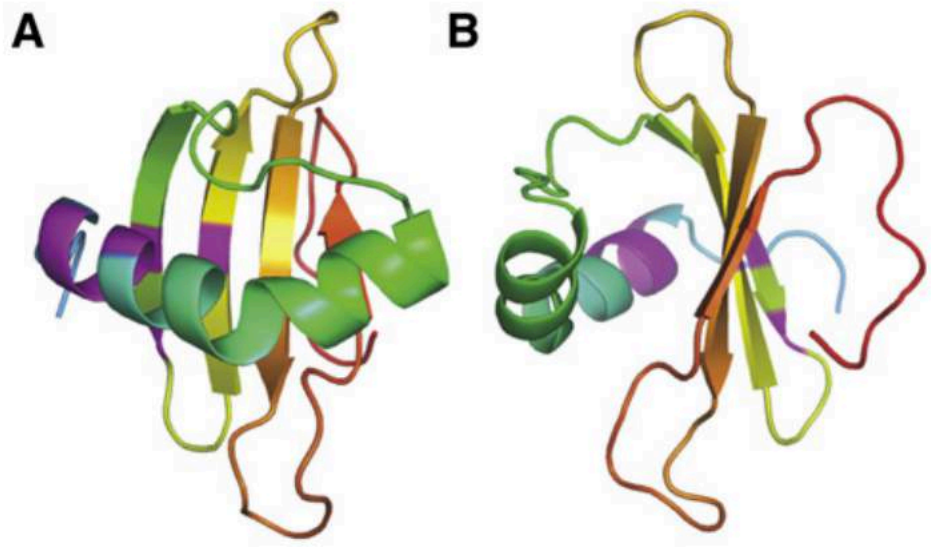

Figure 3.4: Structure of Ranaspumin-2 as solved using NMR. **A:** Demonstrating RSN-2 in its folded conformation. **B:** Folded conformation rotated 90°. Both highlight the single kinked α-helix and four β-sheet structures (Mackenzie *et al*., 2009).

Table 3.3: I-TASSER RSN-2 Structural analogues

PBD Hit	Description	TM-Score	Identity
2mzvA	Secondary structure of a Phytocystatin	0.609	0.124
3k9mC	Cathepsin B in complex with stefin A	0.580	0.191
2y3aA	Crystal structure of p110beta in complex with icSH2 of p85beta	0.574	0.069
4qa8A	Crystal structure of LprF from *Mycobacterium bovis*	0.570	0.101
4z48A	Crystal structure of a DUF1329 family protein (DESPIG_00262)	0.564	0.132

3.3 RSN-3 Analysis

A Blast query of the RSN-3 AA sequence returned 315 hits, the top five are displayed in **Table 3.4** and the alignments are shown in **Fig 3.5**. The results showed that RSN-3 shared approximately 50% similarity with matches of unknown or uncharacterised proteins (**Table 3.4**) from a variety of amphibians from multiple continents, indicating that other frogs may produce similar proteins. The alignments of the top results have 33 conserved residues. mRNA analysis has highlighted the RSN-3 is transcribed in other organs of *E. pustulosus* and not just during foam production suggesting it may have other roles out with the foam nest (Fleming *et al.,* 2009). These functions may potentially be comparable to similar proteins produced in other frogs. It is also notable that RSN-3 and RSN-5 share sequence similarity. A pair-wise alignment using EMBOSS shows that RSN-3 and RSN-5 share 60% amino acid similarity, indicating that they may have complementary functions. Blast also predicts a fucolectin domain or a F5/8 C Type domain which both suggest carbohydrate binding functionality. Further, most of the conserved residues are in this predicted domain. Both RSN-3 and RSN-5 share sequence similarities with proteins from *Xenopus* and *Rana sp* that are all currently uncharacterised and the conserved residues across these unknown proteins indicate they may be part of a wider multi-protein family within the anuran amphibians.

The RSN-3 AA sequence was submitted to I-TASSER and a structure model created (**Fig 3.6**). The model C score was calculated as -1.28, indicating that confidence in the model is low. COFACTOR also predicted ligand binding of Ca^{2+} with a C score of 0.58. Despite

the Blast results indicating fucose binding, this model returned low predictions of fucose binding. However, the structural analogues identified using the structure model (**Fig 3.6**) were fucose binding lectins (**Table 3.5**). Previous research has highlighted that RSN-3 does not have fucose binding properties (Fleming *et al.,* 2009), so the predicted structures do not provide any new information on RSN-3s function but the similarity to other amphibian proteins is a novel insight.

Table 3.4: Top five RSN-3 Blast Hits

Name	**Organism**	**Identity**	**E-value**	**Accession**
Hypothetical protein AB205_0100950	American Bull Frog (*Rana catesbeiana*)	51%	$1x10^{-46}$	PIO27843.1
Ranaspumin-5	Tungara Frog (*Engystomops pustulosus*)	51%	$3x10^{-43}$	AAP48834.1
Uncharacterized protein LOC100144955	Western Clawed Frog (*Xenopus tropicalis*)	49%	$5x10^{-42}$	NP_001119999.1
Hypothetical protein XENTR_v90017256mg	Western Clawed Frog (*Xenopus tropicalis*)	49%	$5x10^{-42}$	OCA32771.1
Hypothetical protein AB205_0024640	American Bull Frog (*Rana catesbeiana*)	51%	$8x10^{-41}$	PIO40589.1

Figure 3.5: BlastP alignments for top five results against RSN-3 AA sequence produced in Clustal Omega. Conserved residues are marked with a *. Predicted C5/8 F Type domain highlighted with red brackets.

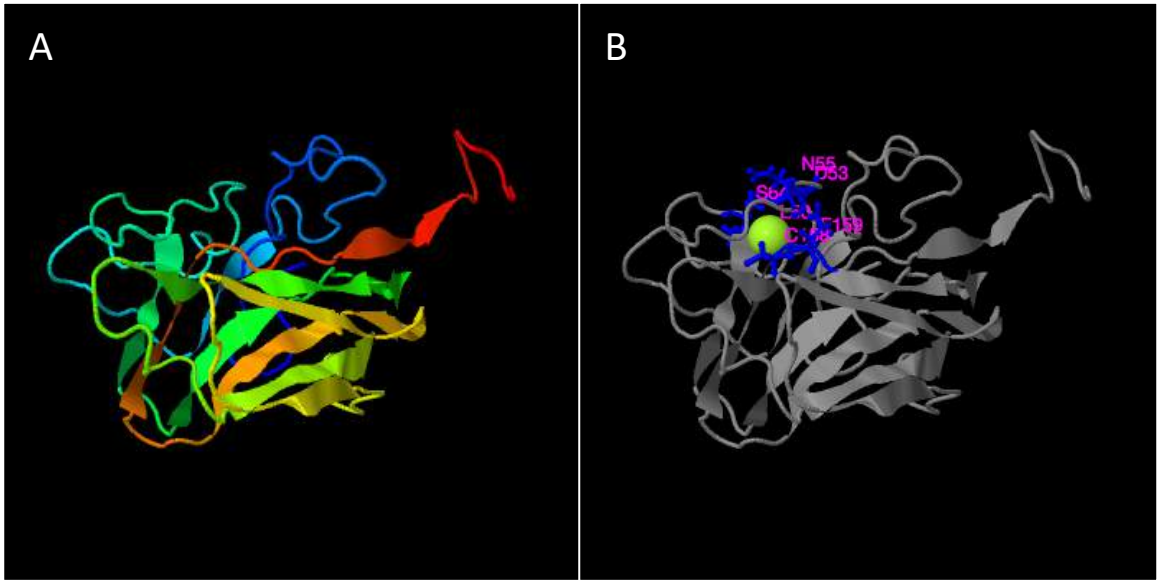

Figure 3.5: A: Structural prediction of RSN-3 produced using I-TASSER. C score = -1.28.

B: Predicted ligand binding site of RSN-3 constructed using COFACTOR through I-TASSER.

Table 3.6: I-TASSER RSN-3 Structural analogues

PBD Hit	Description	TM-Score	Identity
2j1rA	Structure of a *Streptococcus pneumoniae* fucose binding module	0.787	0.298
3le0A	Lectin Domain of Lectinolysin	0.767	0.250
2j22A	Structure of a *Streptococcus pneumoniae* fucose binding module, SpX-3	0.765	0.285
3cqoA	Crystal structure of a f-lectin	0.763	0.360
1k12A	Fucose Binding lectin	0.763	0.382

3.4 RSN-4 Analysis

A Blast query of the RSN-4 AA sequence returned 180 Blast hits, and the first five are displayed in **Table 3.6** and the alignments are shown in **Fig 3.7**. Similar to RSN-3, many of the Blast matches were proteins from a variety of amphibian species and a number of matches were fucolectin like proteins. The alignments indicated that there are 57 conserved residues in the top hits, spread across the entire protein sequence. The Blast query also identified a putative F5/8 C Type domain, which is found on coagulation factors. RSN-4 has previously demonstrated blood agglutination properties, which can be inhibited with galactose and lactose. Previous work has shown that RSN-4 does not bind fucose, so the fucolectin predictions are likely incorrect. The Blast search indicates that RSN-4 has over 50% identity with multiple proteins from other amphibians, which suggests RSN-4 like proteins exist in other frog species. mRNA experiments have shown that RSN-4 is transcribed in multiple organs in *E. pustulosus*, demonstrating that it may have multiple functions unrelated to foam nest formations (Fleming *et al*., 2009).

I-TASSER was used to produce a structural model for RSN-4 (**Fig 3.8**), which was assigned a C score of -0.150. A potential Ca^{2+} ligand binding site was also predicted with a C score of 0.56 (**Fig 3.8**). The model produced shared structural similarities with fucose binding lectins (**Table 3.7**). The C scores calculated indicate the model predicated is not accurate, and previous work has clarified that RSN-4 is not a fucolectin (Fleming *et al.,* 2009).

Table 3.6: Top five Blast Hits for RSN-4

Name	**Organism**	**Identity**	**E-value**	**Accession**
Fucolectin-like protein	High Himalaya Frog (*Nanorana parkeri*)	57%	$3x10^{-57}$	XP_018431282.1
Fucolectin-1-like protein	High Himalaya Frog (*Nanorana parkeri*)	61%	$1x10^{-54}$	XP_018429794.1
Hypothetical protein AB205_0063510	American Bull Frog (*Rana catesbeiana*)	56%	$2x10^{-53}$	PIO23490.1
Fucolectin-1-like protein	High Himalaya Frog (*Nanorana parkeri*)	55%	$2x10^{-52}$	XP_018429925.1
Hypothetical protein XELAEV_18028365mg	African Clawed Frog (*Xenopus laevis*)	50%	$41x10^{-51}$	OCT81542.1

Figure 3.7: BlastP alignments for top five results against RSN-4 AA sequence produced in Clustal Omega. Conserved residues are marked with a *. Predicted C5/8 F Type domain highlighted with red brackets.

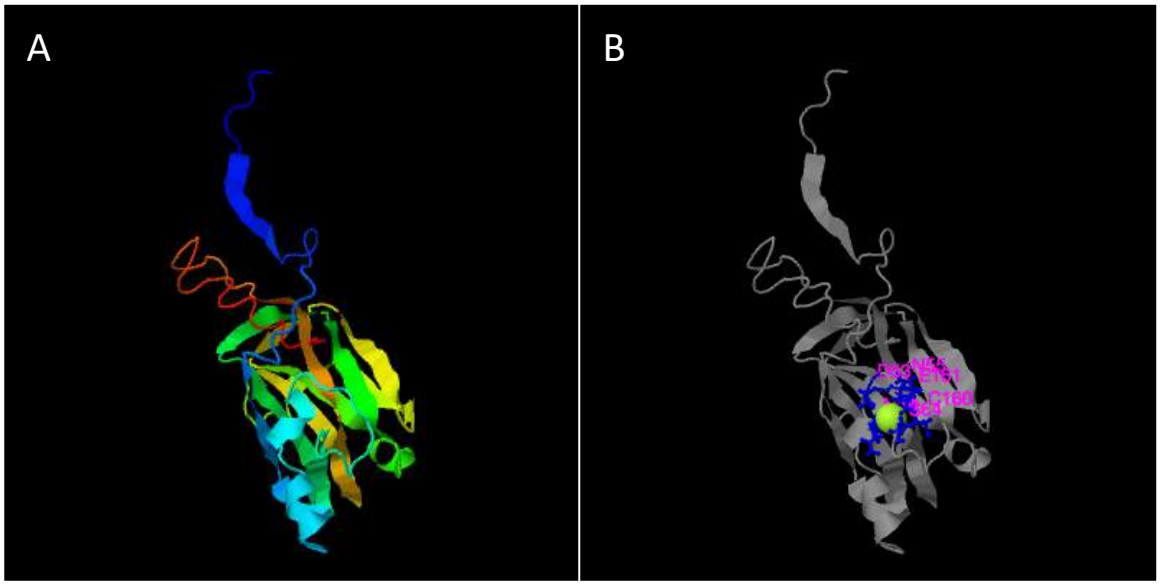

Figure 3.8: A: Structural prediction of RSN-4 produced using I-TASSER. C score = -0.158.

B: Predicted ligand binding site of RSN-4 constructed using COFACTOR through I-TASSER.

Table 3.7: I-TASSER RSN-4 Structural analogues

PBD Hit	Description	TM-Score	Identity
3cqoA	Crystal structure of a f-lectin	0.799	0.506
1k12A	Fucose Binding lectin	0.751	0.455
4bxsV	Crystal Structure of the Prothrombinase Complex from the Venom of *Pseudonaja textilis*	0.670	0.110
3leiA	Lectin Domain of Lectinolysin complexed with Fucose	0.665	0.271
4plmA	Crystal Structure of Chicken Netrin-1	0.662	0.084

3.5 RSN-5 Analysis

A Blast query of the RSN-5 AA sequence returned 286 hits, and the highest five are displayed in **Table 3.8** and the alignments are shown in **Fig 3.9**. Similar to RSN-3, the results display approximately 50% identity of RSN-5 with uncharacterised amphibian proteins from multiple species and these sequences have 42 conserved amino acids. These results along with RSN-5s transcription in other *E. pustulosus* organs may indicate that these proteins have other functions out with the foam and that proteins similar to RSN-5 may be present in other frog species.

Further, the results highlight the sequence similarity of RSN-3 and RSN-5 (**Table 3.4**). The Blast results also suggest a putative F5/8 C Type domain, similar to both RSN-4 and RSN-5. Previous work has suggested that RSN-3, RSN-4 and RSN-5 may bind the carbohydrates present in the foam mixture and the resulting crosslinking stabilises the foam structure. ITASSER was used to predict the structure of RSN-5 from its AA sequence (**Fig 3.10**). The model was given a low C score of -0.86. The structure predicted for RSN-5 is similar to the structure generated for RSN-3, however the low confidence scores for both models make it difficult to draw any real comparisons. A fucose ligand binding site was predicted with a C score of 0.32 (**Fig 3.10**). I-TASSER identified analogues of the predicted structure, **Table 3.9**, and found that the structure shared similarities with fucose binding lectins. Previous work indicated that RSN-5 may be a fucose binding lectin, but no recombinant protein has been produced to test its carbohydrate binding properties (Fleming *et al.,* 2009).

Table 3.8: Top five Blast Hits for RSN-5

Name	**Organism**	**Identity**	**E-value**	**Accession**
Ranaspumin-3	Tungara Frog (*Engystomops pustulosus*)	51%	$4x10^{-43}$	AAP48832.
Hypothetical protein AB205_0100950	American Bull Frog (*Rana catesbeiana*)	48%	$1x10^{-43}$	PIO27843.1
Hypothetical protein XENTR_v90017256mg	Western Clawed Frog (*Xenopus tropicalis*)	46%	$5x10^{-38}$	OCA32771.1
Uncharacterized protein LOC100144955	Western Clawed Frog (*Xenopus tropicalis*)	46%	$6X10^{-38}$	NP_001119999.1
Uncharacterized protein LOC379107	African Clawed Frog (*Xenopus laevis*)	46%	$1x10^{-36}$	NP_001079420.1

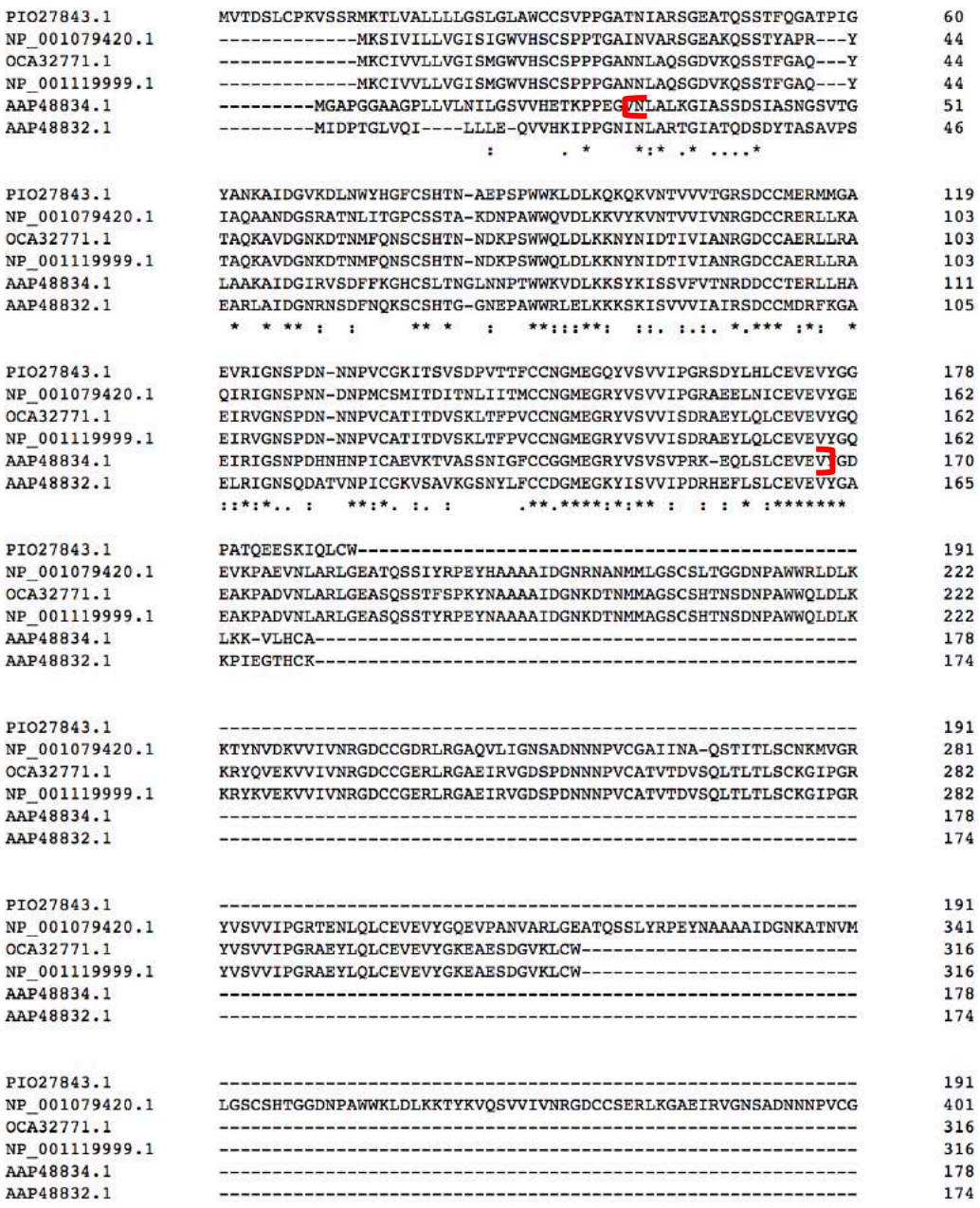

Figure 3.9: BlastP alignments for top five results against RSN-5 AA sequence produced in Clustal Omega. Conserved residues are marked with a *. Predicted C5/8 F Type domain highlighted with red brackets.

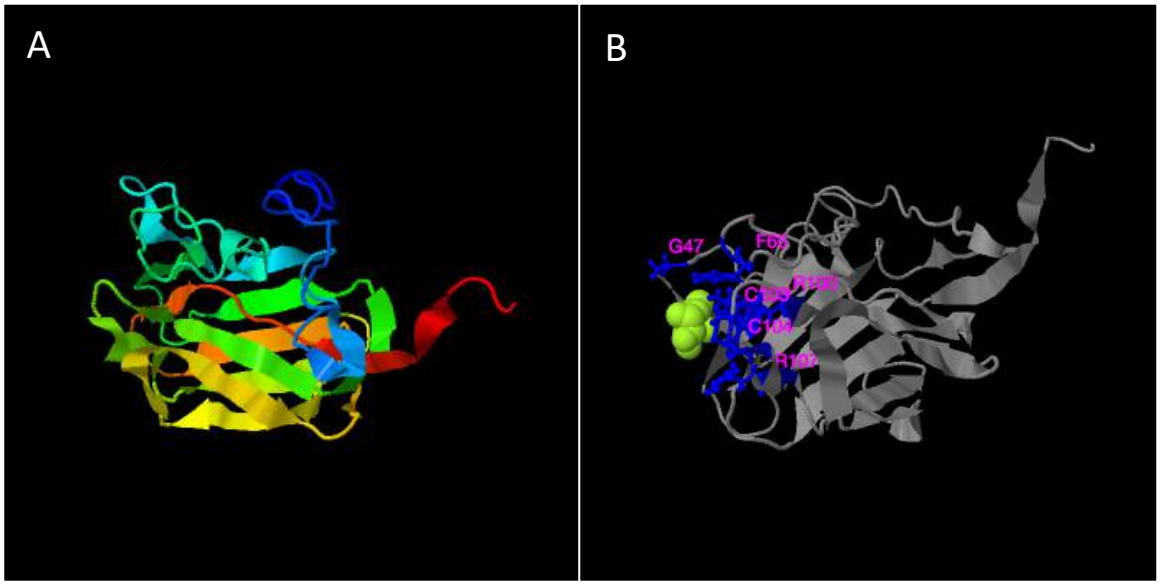

Figure 3.10: A: Structural prediction of RSN-5 produced using I-TASSER. C score = -0.86

B: Predicted ligand binding site of RSN-5 constructed using COFACTOR through I-TASSER.

Table 3.9: I-TASSER RSN-5 Structural analogues

PBD Hit	Description	TM-Score	Identity
1k12A	Fucose Binding lectin	0.788	0.382
3cqoA	Crystal structure of a f-lectin	0.759	0.372
2j1rA	Structure of a *Streptococcus pneumoniae* fucose binding module	0.750	0.286
3leiA	Lectin Domain of Lectinolysin complexed with Fucose	0.740	0.293
2j22A	Structure of a *Streptococcus pneumoniae* fucose binding module, SpX-3	0.728	0.265

3.6 RSN-6 Analysis

A BlastP query of the RSN-6 AA sequence returned 102 hits and the top five are displayed in **Table 3.10** and the alignments are shown in **Fig 3.11**. The results show that RSN-6 shares over 50% sequence similarity with a range of amphibian proteins, and the alignments display 101 conserved residues. The proteins are either uncharacterised or fish egg-like lectins, which have been shown to bind lipopolysaccharides and interact with Gram-positive and Gram-negative bacteria (Pistole., 1981). RSN-6 has previously been predicted to have different lectin function to RSN-3, RSN-4 and RSN-5 (Fleming *et al.,* 2009). The Blast results support this theory, and lectin activity may indicate RSN-6 has a role in foam stabilisation. Similar to some of the other RSNs, RSN-6 is present in a variety of *E. pustulosus* organs, suggesting it has functions not associated solely with foam nesting. The Blast query also predicted a β-propeller domain within the AA sequence, which indicates the structure should be dominated by β-sheet formation that is arranged around a central cleft which often forms an active site (Murzin *et al.,* 1992). A large number of the conserved amino acids fall within this potential β-propeller domain, indicating that this type of characterised protein may be present in multiple frog species as part of a larger protein family.

I-TASSER analysis calculated a model of the RSN-6 structure with a C score of 0.39 (**Fig 3.12**). This was the most confidently produced model of all the RSN proteins. The model supports the β-propeller domain prediction from the Blast results. A Ca^{2+} ligand binding site was predicted within the cleft but with a low C score of 0.11, providing little

information on the function of RSN-6. I-TASSER also identified multiple structural analogues (**Table 3.11**) which display lectin like functions. However, no lectin activity has currently been elucidated for RSN-6 (Fleming *et al.,* 2009).

Table 3.10: Top 5 Blast Hits for RSN-6

Name	**Organism**	**Identity**	**E-value**	**Accession**
hypothetical protein AB205_0174880	American Bull Frog (*Rana catesbeiana*)	53%	$5x10^{-91}$	PIO15068.1
fish-egg lectin-like	High Himalaya Frog (*Nanorana parkeri*)	51%	$1x10^{-89}$	XP_018430883.1
fish-egg lectin-like	African Clawed Frog (*Xenopus laevis*)	52%	$6x10^{-88}$	XP_018098061.1
LOC100126637 protein	African Clawed Frog (*Xenopus laevis*)	52%	$2x10^{-87}$	AAI53784.1
hypothetical protein XELAEV_18003428mg	African Clawed Frog (*Xenopus laevis*)	54%	$3x10^{-85}$	OCT56019.1

Figure 3.11: BlastP alignments for top five results against RSN-6 AA sequence produced in Clustal Omega. Conserved residues are marked with a *. Predicted β-propeller domain highlighted with red brackets.

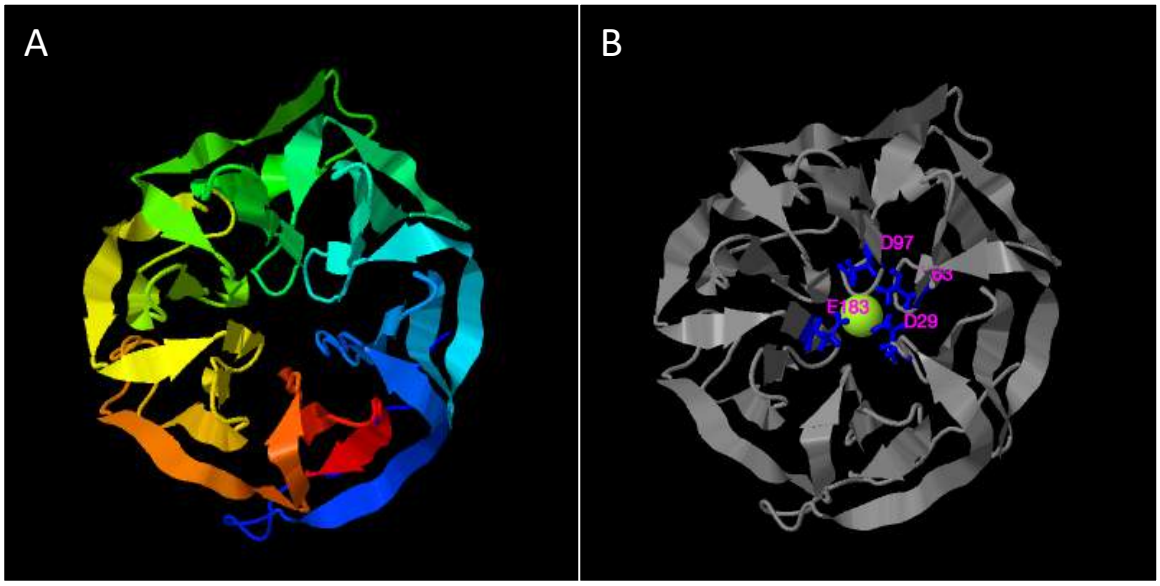

Figure 3.12: A: Structural prediction of RSN-6 produced using I-TASSER. C score =0.39.

B: Predicted ligand binding site of RSN-6 constructed using COFACTOR through I-TASSER.

Table 3.11: I-TASSER RSN-6 Structural analogues

PBD Hit	Description	TM-Score	Identity
4ruqA	Carp Fishelectin	0.934	0.429
5fsbA	Structure of tectonin 2	0.803	0.285
1vcuB	Structure of the human cytosolic sialidase Neu2	0.794	0.047
2vk7A1	The structure of *Clostridium perfringens* nani sialidase and its catalytic intermediates	0.792	0.086
2vk6A	The structure of *Clostridium perfringens* nani sialidase and its catalytic intermediates	0.790	0.086

3.7 Summary:

The amino acid sequences for each of the RSN proteins were queried in BlastP to identify proteins with sequence similarities. I-TASSER was used to generate a structural model for all six of the RSNs and to find potential structural analogues in comparison to the models created. The models generated in I-TASSER all received low confidence scores, with the exception of RSN-6. RSN-1 returned multiple Blast hits for Cystatins, however no cystatin activity has been observed with recombinant RSN-1. RSN-2 returned no Blast hits, highlighting its uniqueness as a surfactant protein which has no amphibian analogues. RSN-3, RSN-4 and RSN-5 all returned Blast hits matching amphibian fucolectins or uncharacterised proteins and were all predicted to have F5/8 C type domains. Blast hits querying RSN-6 displayed matches for fish-egg like lectins or uncharacterised proteins from multiple amphibian species. RSN-6 was predicted to have a putative β-propeller domain. These data make it difficult to formulate hypotheses relating to functionality to test with any potential recombinant proteins produced during the work.

4.0 Characterisation of *Engystomops pustulosus* foam

The foam nests of *E. pustulosus* have been partially characterised in terms of their wider biological role, however the biophysical properties of whole nests are poorly understood. The foam nests are highly stable, maintaining structure for up to 10 days in tropical conditions of around 30°C and 90% humidity, in the absence of tadpoles. The foam resists compression well, demonstrates elasticity and withstands shear. Under a microscope it displays classic wet-dry foam characteristics of a liquid foam and is estimated to be 90% air. The foam does not damage the eggs, sperm or tadpoles despite having significant surfactant activity (Cooper *et al*., 2005). The foam nests are made from a protein rich fluid which also contains a mixture of unidentified carbohydrates. There is around 1-2mg/ml of protein within a foam nest and SDS-PAGE analysis revealed the presence of six proteins, called Ranaspumins (RSN 1-6). The Ranaspumins range from 10-40kDa in size and include a surfactant protein (RSN-2), as well as multiple predicted lectin like proteins (RSN 3-6; Fleming *et al.,* 2009). Research conducted with human erythrocytes showed that RSN-4 can be used to cause blood cell agglutination, however no analysis of the foam protein mixture's impact on mammalian cells had been carried out. Further, the foam prevents predation from insects and protects the developing eggs from microbial degradation (Cooper *et al.,* 2010), but the mechanism of this antimicrobial activity remains unclear. Its potential as a pharmaceutical foam has not been previously investigated. A variety of experiments were carried out to elucidate the foam's structure, stability, impact on bacterial and mammalian cells within the context of a pharmaceutical foam.

4.1 Gel Electrophoresis:

Previous work using SDS-PAGE identified six proteins, called Ranaspumins, in the *E. pustulosus* foam nest. These Ranaspumins were in the range of 10-40kDa (Fleming *et al.,* 2009). The RSN proteins sizes have been predicted by amino acid sequence as the following; RSN-1: 14kDa, RSN-2: 11kDa, RSN-3: 18kDa, RSN-4: 21kDa, RSN-5: 18kDa and RSN-6: 27kDa. However, these predictions do not match published SDS-Page results (Fleming *et al.,* 2009). A range of electrophoresis methods were carried out to confirm that the foam samples collected displayed similar properties to previous work. Gel electrophoresis utilises an electrical current to separate molecules, such as proteins, by size. SDS-PAGE utilises a surfactant, sodium dodecyl sulphate (SDS), to denature the secondary structure of the proteins and coats them in a negative charge allowing them to be separated by size in a linear form. The gel is then stained with Coomassie blue to visualise the bands. SDS-PAGE carried out using solubilised foam proteins highlighted the six RSN proteins in the 10 – 30kDa range as previously highlighted by Fleming *et al.,* 2009. (**Fig 4.1**). Some contamination from the frog eggs was unavoidable, but the Ranaspumin bands match previously produced data (Fleming *et al*., 2009). However, to completely understand which bands are RSN proteins an egg protein control should be added in future to aid in eliminating contamination bands.

Native gel electrophoresis separates proteins by their native charge and folded molecular weight, as no surfactant is used to denature the proteins. Similar to SDS-PAGE, the native gel was also stained with Coomassie blue. Native-PAGE was carried out to identify how the

Ranaspumin proteins behave under non-denaturing conditions (**Fig 4.2)**. The native gel displays multiple large bands, with a few faint bands in the 10-30kDa range that denatured RSNs occur in. It is difficult to speculate on the clearer larger sized bands which occur. These bands are likely complexes formed by multiple RSN proteins, but they may also display egg proteins which have contaminated the foam. A egg protein control could be added to understand any contamination, by eliminating bands caused by these proteins. Further, this would allow the Native-PAGE to be used to identify complexes that may be formed by the RSN proteins.

Glyco-staining can be utilised to identify any glycosylated proteins in a sample. SDS-PAGE is carried out and instead of staining with Coomassie blue, a colorimetric assay can be carried out to elucidate any glycosylated proteins. Identifying glycosylated proteins is important for planning protein overexpression, as *E. coli* cannot glycosylate proteins making protein overexpression of glycosylated proteins in this organism inappropriate. SDS-PAGE was conducted using solubilised foam proteins and stained with a glycosylation staining kit (Pierce). This highlighted that none of the six RSN proteins in the *E. pustulosus* foam were glycosylated (**Fig 4.3**), meaning that the RSN proteins could later be overexpressed and purified using *E. coli.*

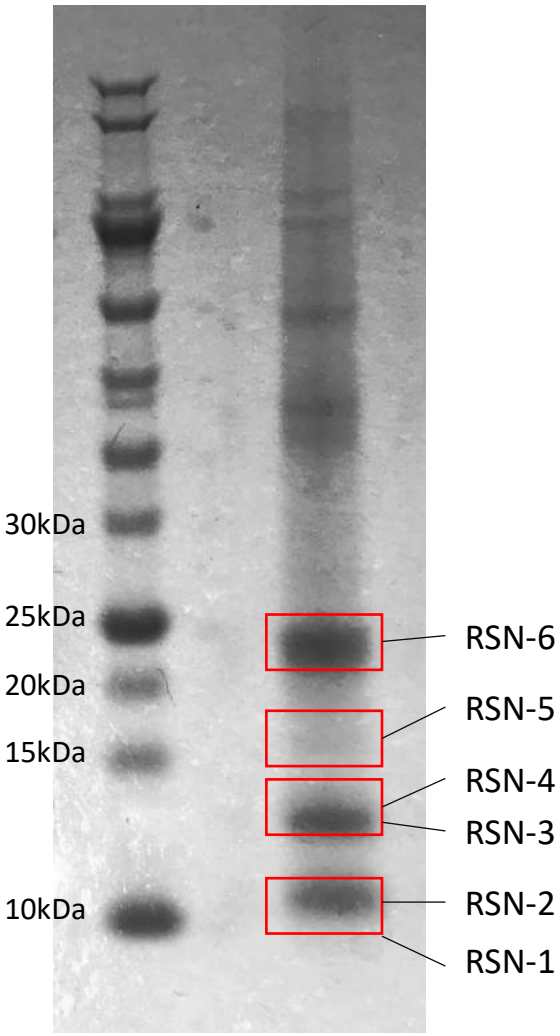

Figure 4.1: SDS Page of *E. pustulosus* foam, carried out using 4-20% Tris-Glycine NuPage precast gel, run in 1 X SDS running buffer. **Marker**: NEB 10-200kDa Broad Range marker. RSN proteins are highlighted in red. Bands align with previous data produced by Fleming *et al.,* 2009. Only RSN-2 molecular weight has previously been published at 11kDa.

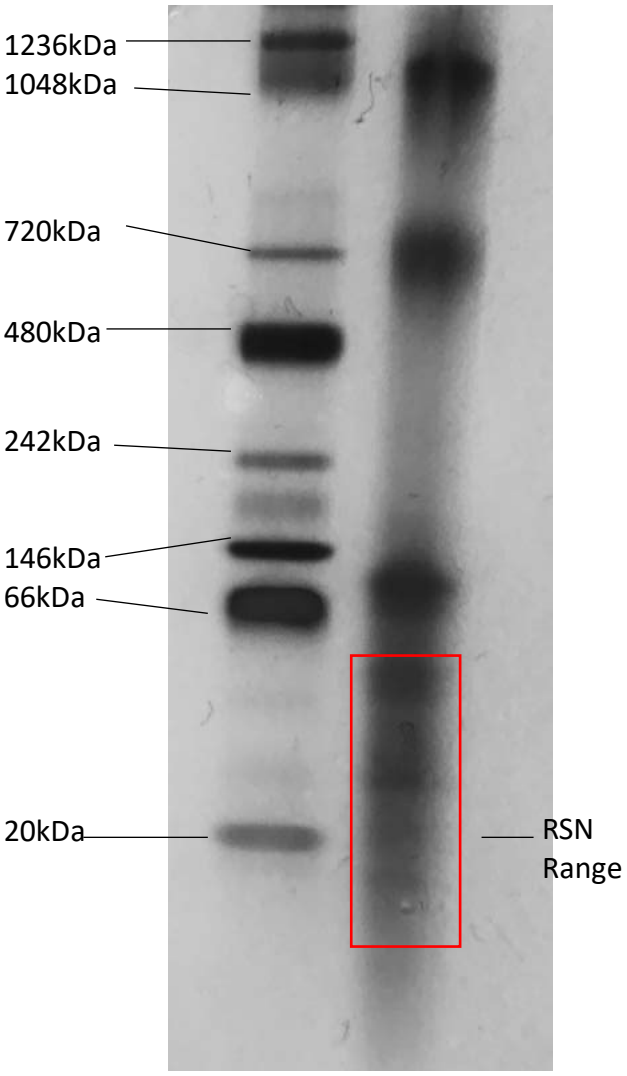

Figure 4.2: Native-PAGE of *E. pustulosus* foam, carried out with NativePAGE Bis-Tris Gel run in 1x Native buffer. **Marker:** NativeMark Unstained Protein Standard (Thermo-Fisher). Red box highlights the size range RSNs appear on SDS-PAGE.

Figure 4.3: Glycosylation-stain of *E. pustulosus* foam, carried out using 4-20% Tris-Glycine NuPage precast gel, run in 1 X SDS running buffer. Gel was stained using Pierce Glycostain kit. **Positive:** Horseradish Peroxidase which is glycosylated **Negative:** Soybean Trypsin Inhibitor is not glycosylated. Controls were provided with the Glycostain kit.

4.2 Secondary Structure:

Understanding the overall secondary structure of *E. pustulosus* foam was required as there remains limited information available on the structures of the Ranaspumins present in the foam mixture. Only the structure of one RSN protein, RSN-2, has been solved and information on the structures of the other RSN proteins is purely from predicted secondary structures. Further, analysis of any difference between the whole foam and solubilised foam were necessary to understand if soluble foam could reasonably be utilised in other experiments and still be representative of the Ranaspumin protein mixture.

Fourier transform infrared spectroscopy (FTIR) and Circular Dichroism (CD) were carried out to identify the gross secondary structure of the foam protein mixture. No FTIR spectra have previously been presented for the foam samples.

FTIR involves using a laser to measure the infrared absorbance of a protein sample, which is then processed through the Fourier transform algorithm to produce spectra for analysis (Girffiths *et al*., 2007). The spectra produced can be compared to well understood protein spectra as peptide groups give characteristic bands which can be used to provide insight into the protein secondary structure (Girffiths *et al*., 2007). The method is non-destructive, simple and can be carried out in a wide variety of conditions. This allows for secondary structure to be assessed across a range of states, temperatures and pH (Kong *et al*., 2007). FTIR has been employed to identify secondary protein structure in a dried state and in aqueous solution, allowing for secondary structure to be studied regardless of whether the protein is in solution or not and compare any differences which may be caused by drying

(Susi *et al.,* 1986). CD is a well-established method for rapid detection of protein secondary structure. CD is the measurement of unequal absorption of left handed and right handed circularly polarised light. Asymmetric molecules absorb polarised light differently, so different secondary structures have distinct CD spectra (Greenfield., 2006). Spectra collected can be run through a multitude of algorithms which cross compare known protein CD spectra and compute the predicted percentage of key secondary structures present (Sreerama and Woody., 2000).

FTIR allowed for the protein secondary structure of the foam to be compared in both a natural foam state and the solubilised foam protein solution. A buffer baseline (PBS) was calculated and subtracted from the overall spectra eliminating any impact the buffer may have had on the overall absorbance. FTIR spectra indicates two peaks in the 500cm^{-1} and 4000cm^{-1} range (**Fig 4.4**) and can be compared to model protein spectra for secondary structure predictions. The peak calculated at 3300cm^{-1} indicates an Amide A Band which is the result of N-H stretch due to the secondary structure. The peak at approximately 1600cm^{-1} implies an Amide I Band which is caused by C=O vibrations of the peptide bond mediated by secondary structure. As these peaks are highest at 1630cm^{-1} it can be concluded that there is β-sheet structure present in the foam proteins (Kong et al 2007). The peaks produced for whole foam and the soluble foam solution are identical, indicating that centrifuging the foam into a liquid solution does not impact the overall secondary structure.

CD has previously been carried out on *E. pustulosus* foam in 2005 indicating the following structures: 8.5% α -helix, 42.7% antiparallel β -sheet, 2.7% parallel β-sheet, 19.7% β-turn, and 23.4% other (Cooper *et at.,* 2005). However, the protein datasets used for running CD algorithms have been updated, providing reasoning for a revision of the CD spectra analysis. The CD spectra collected using solubilised foam displays a positive band at 195nm and a negative band at 218nm (**Fig 4.5**). A buffer (PBS) baseline measurement was collected and subtracted from protein spectra to eliminate any impact of the buffer on absorbance. These bands strongly indicate the presence of β secondary structures when compared to model protein CD spectra (Kelly *et al.,* 2005). Further, calculations carried out by using protein CD algorithm SELCON 3 (Sreerama and Woody., 2000) estimated the structure as: α-helix 9.2%, β-sheet 46%, β-turn 10.9% and unordered 34%. These results are similar to previous CD analysis (Cooper *et al.,* 2005), and the small differences can be explained by the use of an updated protein reference set. The CD data confirms the FTIR results, showing β-sheet structures dominating overall secondary structure. Both data sets reinforce previously presented CD data on *E. pustulosus*, and the FTIR data indicated that the process of producing a soluble foam solution does not affect the overall protein secondary structure. This indicated that experiments carried out using soluble foam can still be representative of the Ranaspumin's collective secondary structures. Unfortunately, the results of both FTIR and CD are limited by the foams multiple protein mixture. As there are multiple proteins present in the samples used, the secondary structure predictions cannot be assigned to a single protein but to the protein mixture as a whole. While this is useful for understanding

more about the foam, and aids understanding of the effect of centrifuging on the foam proteins' secondary structure, it would be useful to carry out both CD and FTIR on each RSN protein to elucidate their secondary structures and how this may play a role in the over foam mixture.

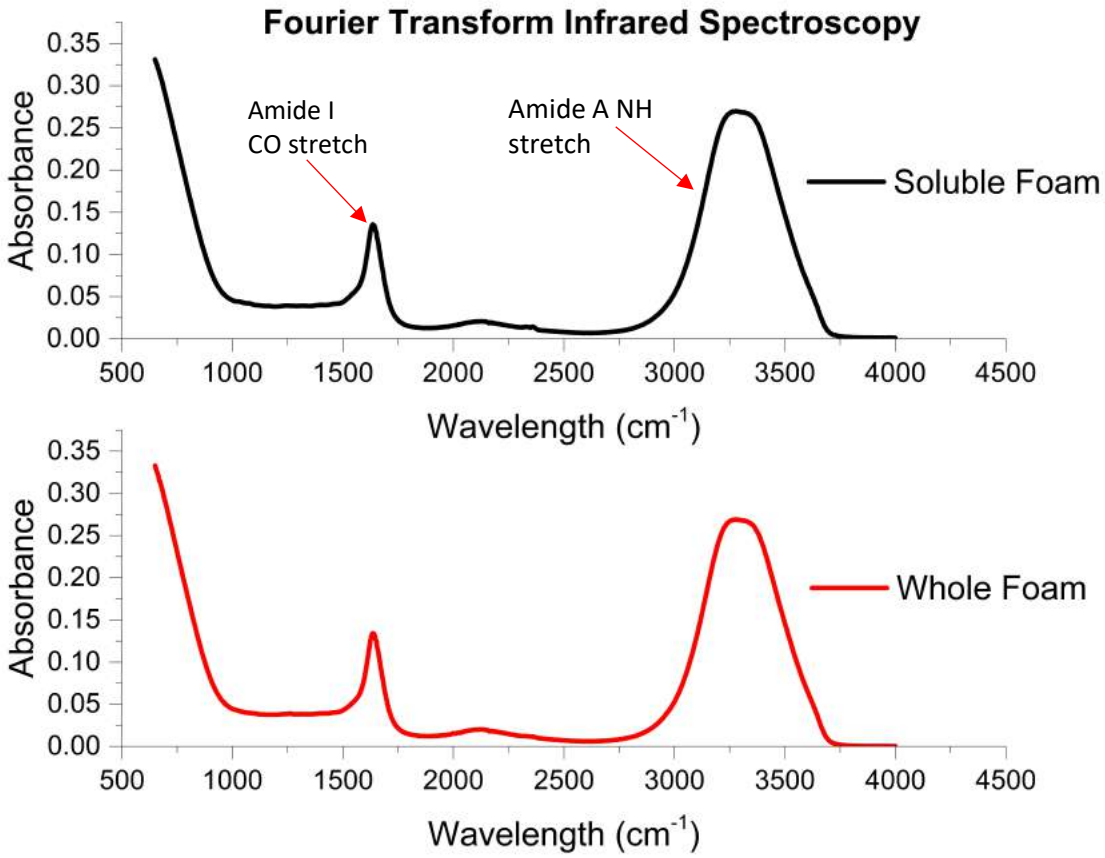

Figure 4.4: FTIR spectra comparing soluble foam (top) and whole foam (bottom). Spectra was collected in the 500 cm^{-1} to 4000 cm^{-1} range. Soluble foam was centrifuged before measurement, whole foam was tested in its natural state. All measurements were carried out in triplicate, and the baseline reading subtracted before processing data. Bands which are indicative of structure produced at 1600 cm^{-1} and 3300cm^{-1} are highlighted with red arrows.

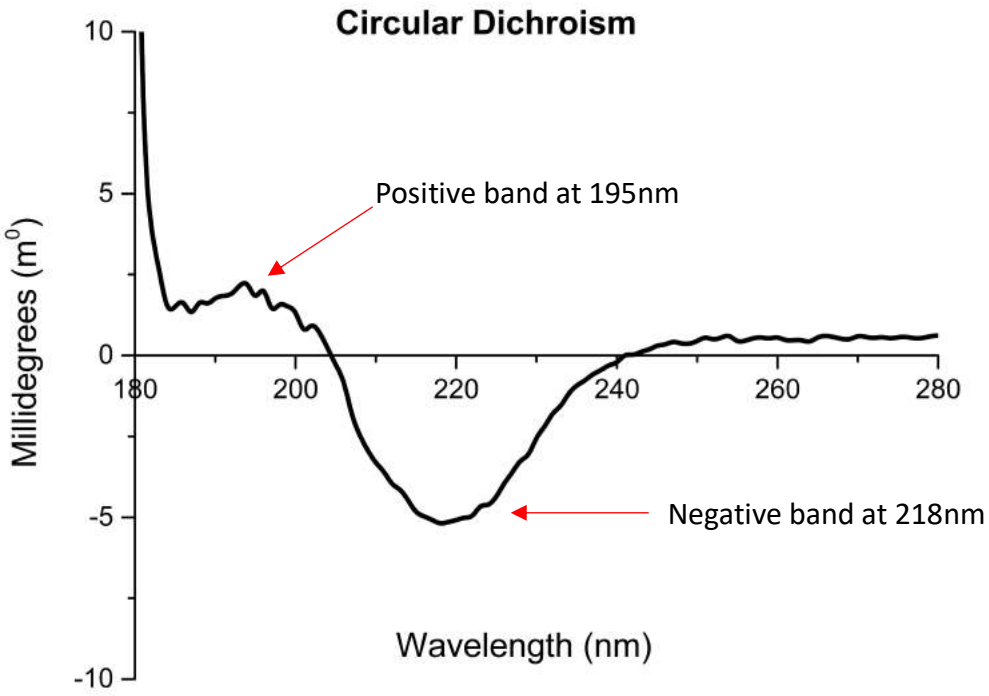

Figure 4.5: CD spectra of soluble foam in PBS buffer in 180 – 280nm range. All measurements were taken in triplicate. Baseline (No sample) and buffer (PBS) readings were subtracted using GlobalX software. Positive and negative bands which are indicative of secondary structure are highlighted with red arrows.

4.3 Whole foam analysis:

E. pustulosus foam has not previously been characterised in the context of a pharmaceutical foam. There are a variety of ways to characterise foams for pharmaceutical use. Macroscopic analysis is used to define a foams appearance and stability. The foam's density must be calculated, as it has implications for firmness and comfort (Arzhavitina *et al.,* 2009, Zhao *et al.,* 2010) The foam vesicle structure can be defined under a microscope, to analyse cell size, shape and heterogeneity. These characterisations were carried out, in order to understand the foam in a pharmaceutical context. *E. pustulosus* foam can be described as viscous and finely porous when observed macroscopically. Previous research has shown that the foam remains stable for 10 days in tropical conditions in the absence of tadpoles (Cooper *et al*., 2010), indicating that the foam is highly stable compared to most pharmaceutical foams which collapse within minutes (Zhao *et al.,* 2010).

Lower density foams are considered better for topical treatment, as they are more comfortable than heavier foams (Zhao *et al.,* 2010). The foam density was calculated by dividing the average weight of 5ml of foam, by the weight of 5ml of water. The density of the foam was estimated to be approximately 0.25g/ml. In comparison shaving foam (Gilette) has a density of 0.98g/ml. The combination of low density and high stability is unusual and could be useful in topical delivery.

A single foam cell or vesicle is defined as a bubble of gas enclosed in a liquid film. Cells can be polyhedral or circular, heterogeneous or homogeneous and usually range between 0.1 and 3mm in size (Wilson., 2013). Foam cell structure was evaluated microscopically, and

the foam vesicle sizes analysed (**Fig 4.6**). In order to evaluate if loading the foam with dyes would impact the foam vesicle structure, microscope analysis was carried out using unloaded foam, and foam loaded with either Nile Red or Calcein. The foam bubbles in all the samples area mixture of spherical and polyhedral, uneven and heterogeneous in size. Foam cell sizes were measured by calculating the ferret diameter of each individual bubble and these revealed that vesicle diameters range from 10-800um (**Fig 4.7**), falling in the normal range of foam vesicle size (Arzhavitina *et al.,* 2009). One-way ANOVAs were used to compare the loaded vesicle sizes to the unloaded vesicle sizes. This calculated P values of 0.715 and 0.811 for Nile Red and Calcein respectively, showing there was no significant difference between average bubble sizes in loaded and unloaded foam images. This indicates that loading dye or potentially a drug does not have an impact on foam vesicle structure.

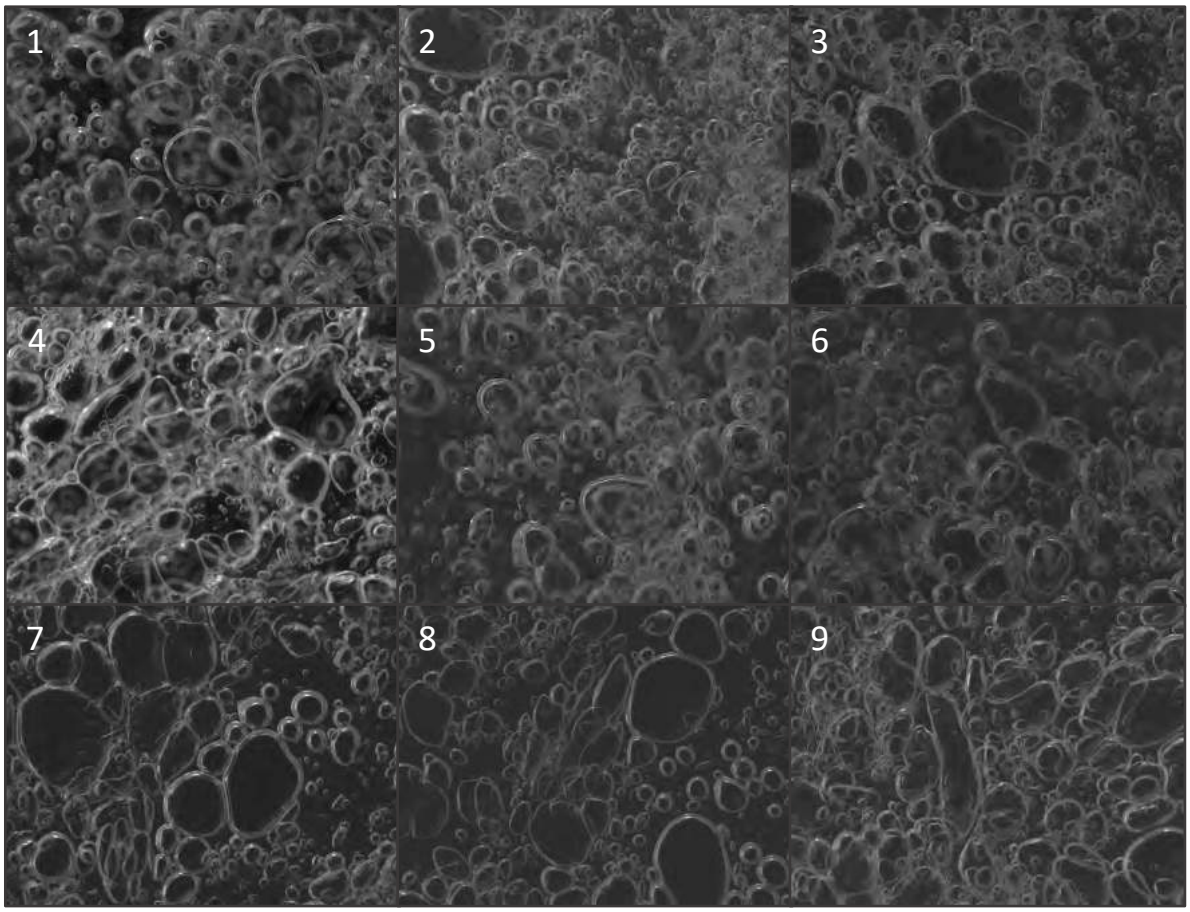

Figure 4.6: Microscope images of foam taken using 4X lens. **1-3:** Unloaded foam. **4-6:** Foam loaded with 1mg/ml Nile Red. **7-9:** Foam loaded with 1mg/ml Calcein. All images were taken using freshly defrosted foam.

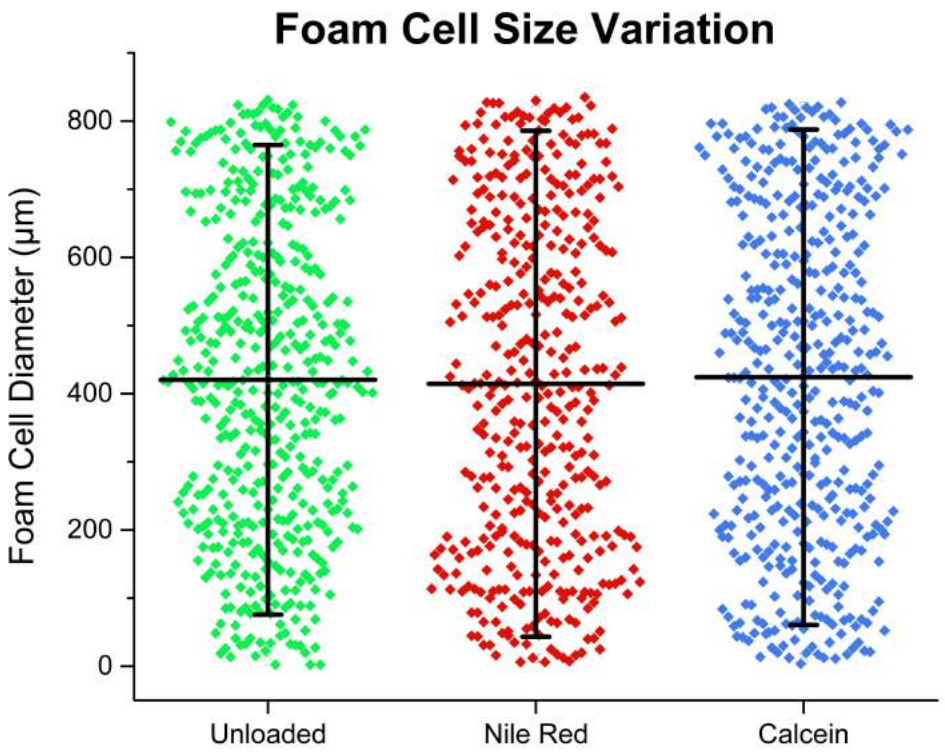

Figure 4.7: Foam cell diameter measurements scatter plot. Ferret diameter of each cell was measured using Fiji software, with a scale set at 1.613pixels/um. Bars on the scatter display 10-90% of data, with centre line representing the mean cell size.

4.4 Rheology:

Rheological properties of foam are usually difficult to measure due to the unstable nature of foams (Arzhavitina *et al.,* 2009). However, *E. pustulosus* foam is highly stable allowing for the collection of rheological data. Rheology is used to investigate elastic and viscous properties of a substance, particularly under shear stress. Previous observations on stability have indicated that the foam displays elasticity and resists shear (Cooper *et al.,* 2005). The elasticity modulus can be used to understand substance structure, while the viscosity modulus shows resistance to flow. Two experiments were carried out, a stress sweep and a time sweep. A foam used for a potential drug delivery system should be able to undergo deformation before breaking.

During the stress sweep the shear stress (τ) was gradually increased. The viscoelasticity moduli and shear strain responses were measured, which allows the linear viscoelastic region (LVR) to be identified. The LVR of a substance determines a range of stress it can withstand before breaking. The LVR was calculated from the stress sweep data (**Fig 4.8**) as 0.0 – 0.5 rads (γ). The *E. pustulosus* foam has a higher LVR than most pharmaceutical foams which usually lies between 0.0 – 0.05 rads (Kealy *et al*., 2008), indicating that it can withstand a higher amount of stress than common topical foams. The yield stress point was calculated as 147Pa. This is the point at which a substance “breaks”. Strong pharmaceutical foams have yield stresses below 60Pa (Kealy *et al*., 2008). The LVR and yield stress indicate the foam is highly stable under stress, withstanding more strain than topical foams and handling more shear stress before breaking.

Time sweep experiments were carried out to measure the foam's response to constant stress over time at 37°C (**Fig 4.9**). Foam elasticity (G') increases over time, indicating it undergoes coarsening and fluid drainage in response to prolonged stress. An increase in elasticity shows that as water is drained the foam structure does not break, reinforcing evidence that it is highly stable.

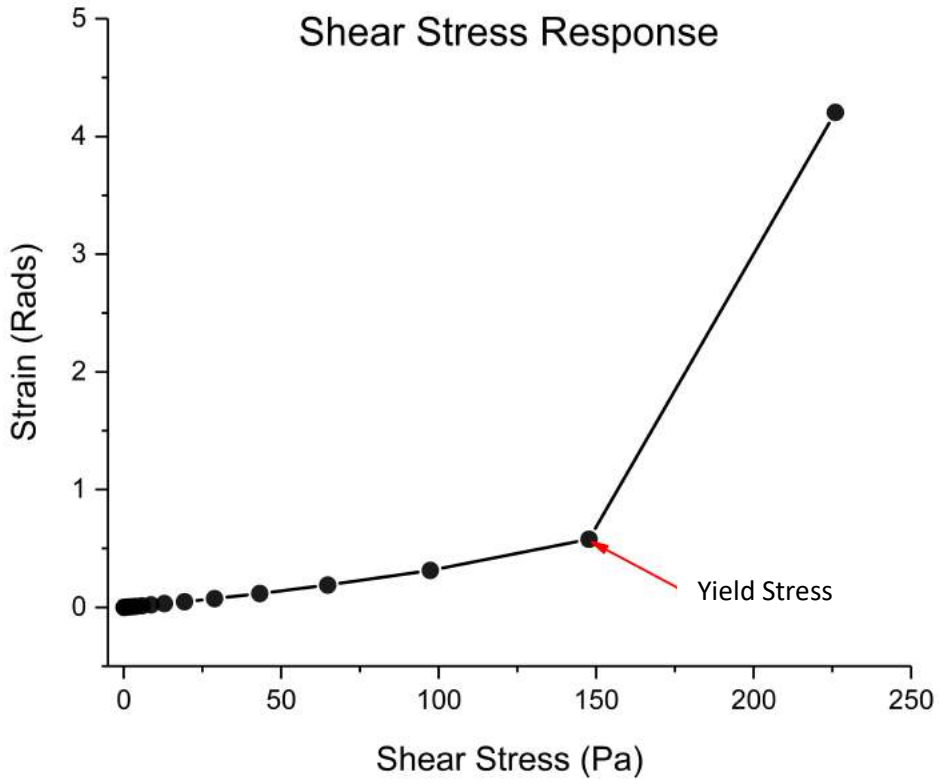

Figure 4.8: Foam stress sweep response. Shear stress was gradually increased from 0.1 – 225Pa. Each measurement taken in triplicate and averaged data is presented. Yield stress point is marked with red arrow. LVR was calculated as the strain range before yield stress point is reached.

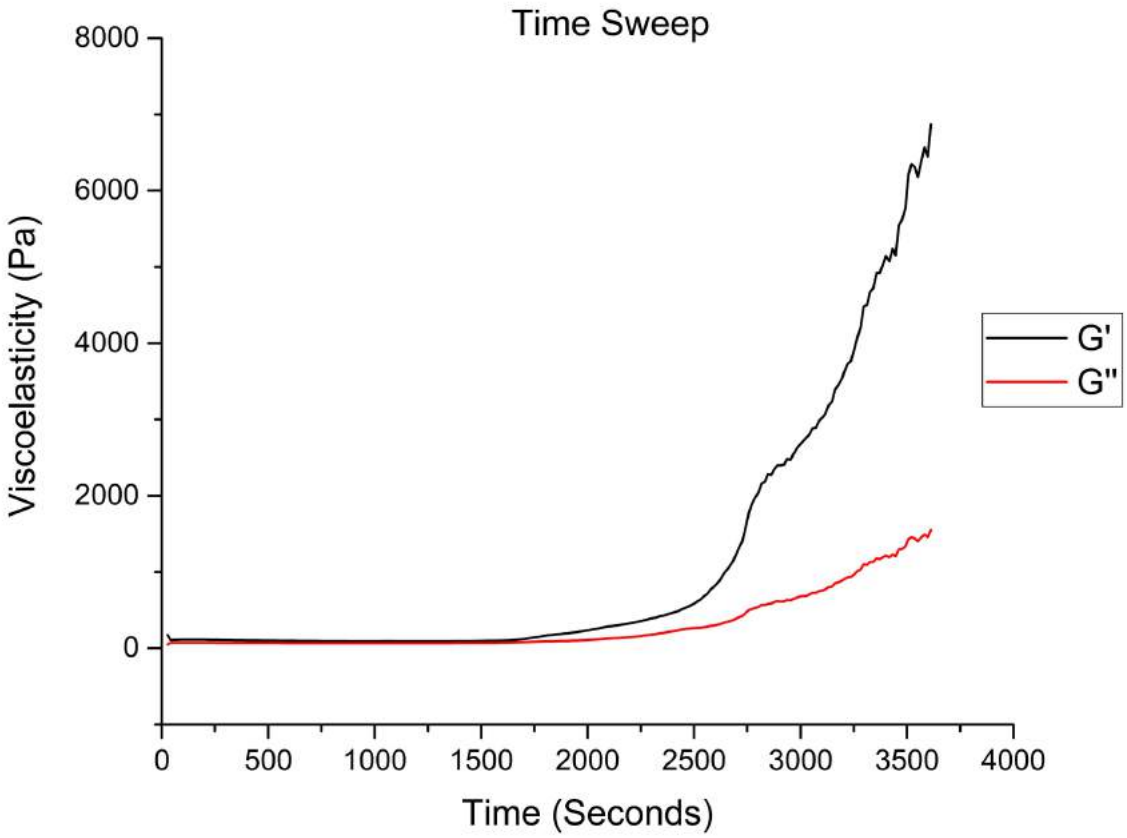

Figure 4.9: Time sweep data for *E. pustulosus* foam. Displaying results for elastic (G') and viscous (G") moduli. G' increased notably at 2500 seconds by stress, but less of an impact can be seen on G'' throughout the experiment. Shear stress was set at 100Pa and measurements were taken every 15 seconds. Each measurement was taken in triplicate, and average data points are displayed.

4.5 Impact on bacterial growth:

A major function of the *E. pustulosus* foam nest is the prevention of microbial predation (Cooper *et al.,* 2004). Previous research has shown the foam nests are contaminated with bacteria and fungus, but that there is no evidence of tadpole degradation indicating that the foam has some antimicrobial properties (Cooper *et al.,* 2010). It was hypothesised that the foam has inhibitory properties that prevent extensive microbial degradation of the nests, however the source of this is unclear. It may be the result of the foams surfactant activity, potentially mediated by the surfactant protein RSN-2 present in the foam (MacKenzie *et al.,* 2009). RSN-3, RSN-4, RSN-5 and RSN-6, have some sequence similarity to lectins, indicating these proteins are potentially carbohydrate binding (Fleming *et al.,* 2009) which may be responsible for the antimicrobial effect. The foams antimicrobial activity could also be a consequence of its macro structure, instead of the function of any individual protein.

To investigate the impact of the foam proteins on bacteria, growth curves were conducted using solubilised foam proteins. This was conducted in a similar way to performing minimum inhibitory concentration assays that are performed for antimicrobial drugs. The protein concentration was determined with a Bradford assay, and a concentration of 1mg/ml was used to test the foam protein mixtures antimicrobial properties. This concentration was chosen as it falls within the normal 1-2mg/ml protein concentration present in an *E. pustulosus* foam nest. To measure the impact on both Gram-positive and Gram-negative bacteria, the growth of *Escherichia. coli* and *Staphylococcus. aureus* was

measured over 12 hours (**Figs 4.10 and 4.11**). Growth curves were calculated by collecting optical density at 600nm (OD) every 10 minutes over 12 hours. Data collected on every hour mark was averaged, and the standard deviation calculated to display any variability in results. The *E. coli* 8739 strain used was a faecal isolated strain used to test antimicrobial agents, and the *S. aureus* 29213 strain was a wound isolated strain used to test antimicrobial agents (ATCC) making them suitable for elucidating any antimicrobial effect of the foam protein mix. The growth of *E. coli* and *S. aureus* were not reduced by the presence of 1mg/ml of foam proteins (**Table 4.1**). The *E. coli* positive control had an average growth rate of $0.153h^{-1}$ and the foam protein treated cells had an average growth rate of $0.148h^{-1}$. A one-way ANOVA was carried out and calculated no significant difference of the treated growth rates to the positive control. The *S. aureus* positive control had an average growth rate of $0.160h^{-1}$, while the foam protein treated *S. aureus* had an average growth rate of $0.189h^{-1}$ and a one-way ANOVA between these samples showed no significant difference in growth rates. However, no tests were performed to calculate if the data was within a normal distribution so very little can be assumed from the statistical results. The growth curve results indicate that the solubilised foam proteins do not have an antimicrobial effect on either Gram-positive or Gram-negative bacteria. FTIR data collected indicates that solubilising the foam doesn't drastically change the protein mixtures secondary structures, however there may some conformational changes occurring during the whipping of the mixture when the foam production. This makes it difficult to determine if there is truly no antimicrobial activity of any RSN protein until they can be individually

tested. Further, it is possible that the foams overall structure may also be responsible for the foam's antimicrobial effect.

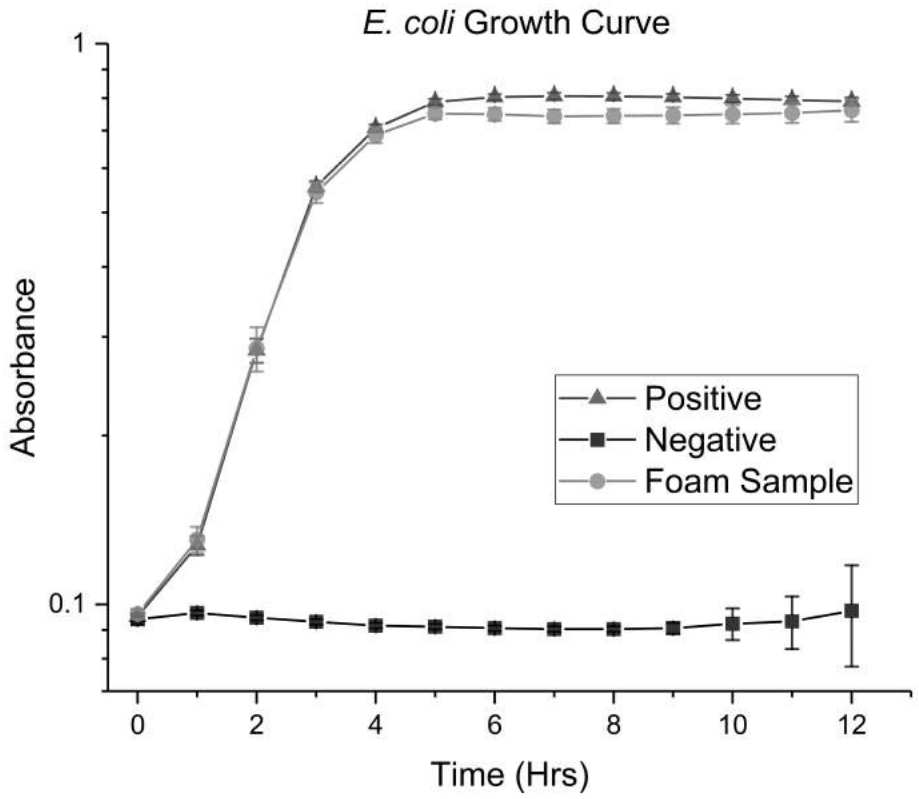

Figure 4.10: Growth curves for *E. coli.* Positive control was *E. coli* grown in LB media. Negative control was *E. coli* in LB with 50 μg ml^{-1} Kanamycin to kill cells. Foam sample had soluble foam protein added to the media to a concentration of 1mg/ml. Optical density was measured at 600nm. Readings for each hour were averaged, and error bars display standard deviation. Both the positive control and the foam sample demonstrate normal growth curves, and the negative control displays no growth.

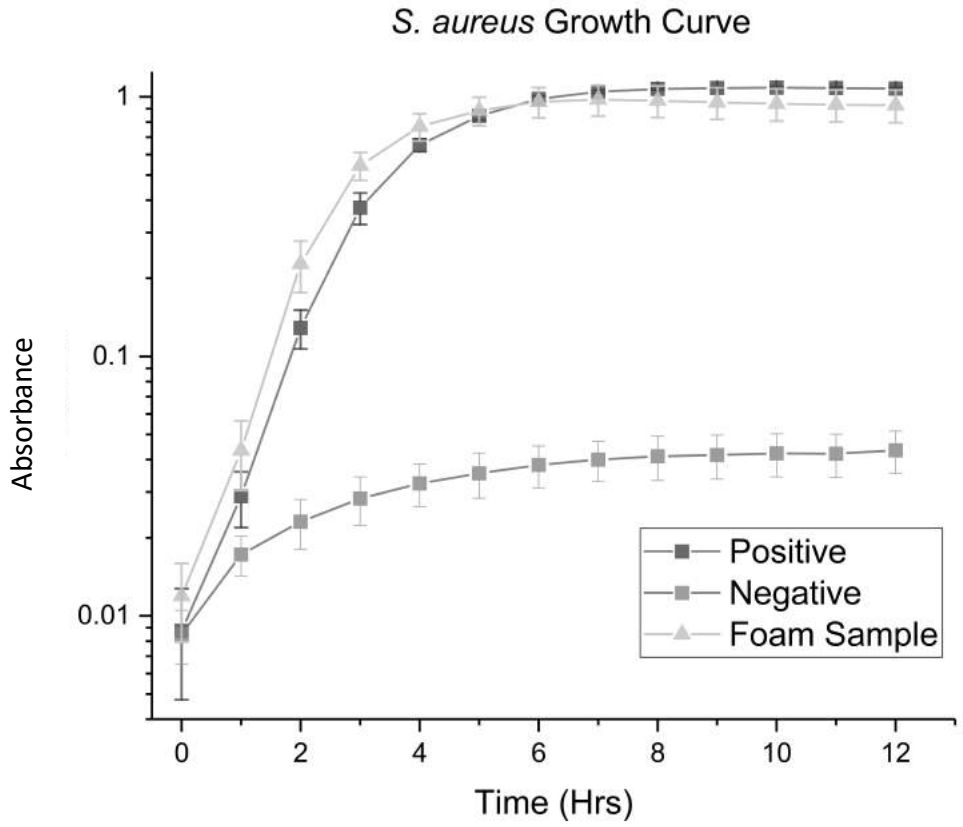

Figure 4.11: Growth curves for *S. aureus.* Positive control was *S. aureus* in LB media. Negative control was *S. aureus* in LB with 50 μg ml^{-1} Kanamycin. Foam sample had soluble foam protein added to the media to a concentration of 1mg/ml. Optical density was measured at 600nm. Readings for each hour were averaged, and error bars display the standard deviation.

Table 4.1: Specific growth rates and one-way ANOVA p-values for *E. coli* and *S. aureus*.

	Positive	**Negative**	**Foam Treatment**
E. coli			
Specific growth rate (h^{-1})	0.153	0.001	0.148
P value		$3.99x10^{-21}$	0.01
S. aureus			
Specific growth rate (h^{-1})	0.160	0.006	0.189
P value		$2.37x10^{-13}$	0.01

4.6 Impact on mammalian cell growth:

E. pustulosus foam does not cause any harm to the eggs, sperm or developing tadpoles placed in the nest, despite the presence of surfactant protein RSN-2. Several RSN proteins have been shown to cause agglutination of human erythrocytes individually (Cooper *et al.,* 2005), but no work has been published on the impact of the whole foam protein mixture on mammalian cells. Biocompatibility is an important property of any pharmaceutical foam and a topical foam drug delivery system should not cause damage to mammalian cells. To investigate the effect that *E. pustulosus* foam has on mammalian cells an MTT cell viability assay using HaCaT cells was conducted using a range of soluble foam protein concentrations (**Fig** 4.**12**). HaCaT cells are an immortal epithelial cell line (Boukamp *et al*., 1988) which have become an established line to use in *in vitro* skin studies (Schoop *et al*., 1999). Four concentrations (1.4mg/ml, 0.3mg/ml, 0.14mg/ml, 0.07mg/ml) of the foam proteins where used to test the impact of the foam mixture on HaCaT cells. Typically, the foam nest has a protein concentration of 1-2mg/ml and treatment 1 (1.4mg/ml) falls within this range. The MTT assay displayed that of the concentrations of *E. pustulosus* foam mixture tested none damaged the viability of HaCaT cells. Treatments 1 and 2 resulted in a higher average cell viability than in positive controls, indicating that the foam proteins may encourage cell growth. One-way ANOVAs were carried out for each treatment set in comparison to the positive control results. However, no tests were performed to calculate if the data was within a normal distribution so it is difficult to assign accuracy to the P values produced. The P value of Treatment 1 was 0.0012 and 0.0016 for Treatment 2, indicating that these two

treatment groups are statistically different from the positive control. Treatments 3 and 4 resulted in P values > 0.05 and were not statistically different from the positive control group, showing these groups are similar in cell viability. The foam nests of *E. pustulosus* evolved to act as protective incubation chambers for developing tadpoles, and it has not been established if growth outside of the foam has any negative impacts on tadpoles. It is possible that the foam improves the growth of the tadpoles, and potentially improves the growth of other cells too. The higher absorbance measurements collected from HaCaT cells treated with 1.4mg/ml and 0.3mg/ml of foam proteins indicate that the foam may have a positive impact on epithelial cells. This property would be useful in a dermal foam delivery system potentially aiding healing. It would be valuable to repeat this experiment with higher concentrations of foam proteins that fall beyond the standard concentrations found within the foam to further test their positive impact on cells. This experiment could be developed further by exposing cells to a longer incubation period to understand what the long-term effect of the foam proteins would look like.

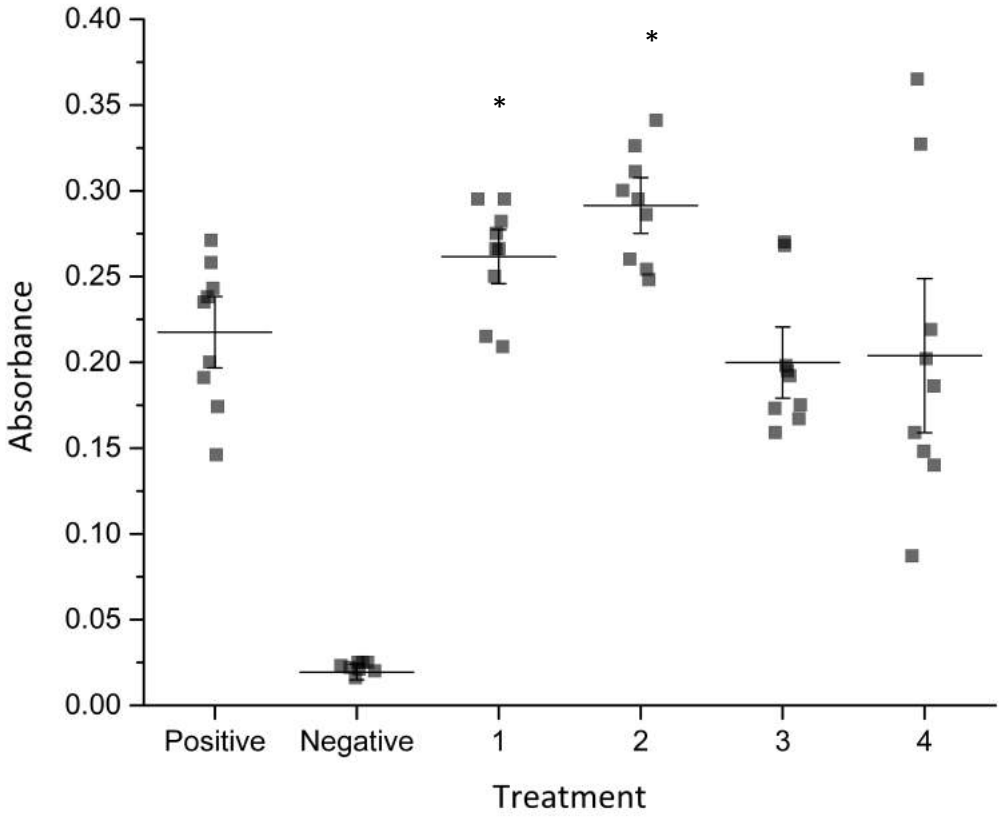

Figure 4.12: MTT assay carried out with HaCaT cells exposed to solubilised foam concentrations over 24 hours at 37^{o}C before absorbance was measured at 570nm. Nine replicates were carried out for each treatment, each replicate was measured in triplicate. Positive control is media alone. The negative controls were treated with DMSO. Treatments 1-4 were a range of foam protein concentrations of 1.4mg/ml, 0.3mg/ml, 0.14mg/ml and 0.07mg/ml respectively. Error bars represent the standard deviation of the data. Asterisk represent data with a p value < 0.05 calculated using a one-way ANOVA in comparison to the positive control.

4.7 Summary:

E. pustulosus foam was characterised in context of a pharmaceutical foam. The foam contains six Ranaspumin proteins ranging from 10-30kDa. FTIR and CD confirmed a high percentage of β secondary structure in foam protein mixture. Whole foam characterisation revealed the foam bubbles are heterogeneous in nature, with cell sizes ranging from 10 – 800µm in diameter. This analysis showed that loading foam with a hydrophobic and a hydrophilic dye does not impact foam structure. Rheology results demonstrate foam is highly stable and resistant to shear. MTT assay data demonstrated that some concentrations of foam proteins may improve mammalian cell viability. A foam that can be loaded with dyes, remains highly stable and has a positive impact on mammalian cells could be a good candidate for a novel topical drug delivery system.

5.0 Drug Release Capacity of *E. pustulosus* Foam:

Pharmaceutical based foams have been proposed as drug delivery systems since the 1950's (Boe., 1950), but typically foams are considered quick release drug delivery systems. Traditionally the drug incorporated is an integral part of the foam formulation, similar to a cream, rather than being loaded to an existing structure. They are then applied to the treatment area and as the foam collapses the drug is released in one step (Zhao *et al*., 2010), making degradation of the foam a key part of the drug delivery system. The value of longer-term drug delivery is now recognised, and many additional systems have been designed for prolonged drug delivery including nanoparticles, hydrogels and liposomes (Zhao *et al*., 2010). There are many drawbacks with these systems - in some, the drug-load is released too rapidly resulting in ineffective long-term treatment (Sabaeifard *et al.,* 2016), In other systems, the drug is rapidly taken up, but they fail to release a sufficient concentration for effective treatment (Zhao *et al.,* 2010). This suggests that there is a need for new drug delivery systems.

The hydrophilic or hydrophobic nature of a drug molecule in delivery systems plays an important role in their release profile. Hydrophilic drugs are difficult to transport across membranes, making loading in to delivery systems difficult. Hydrophobic drugs are challenging to encourage release from delivery systems and have issues with bioavailability (Maherani *et al*., 2013). An ideal drug delivery/release system requires a suitable

concentration of a given drug to be delivered in an appropriate time to enable the delivery of an effective treatment dose in a given location.

To understand the long-term release profile of *E. pustulosus* foam, the same methodology used to test *in vitro* release of drug-mimicking molecules and drug molecules from nanoparticles were applied. Dynamic dialysis method is most commonly used and widely validated technique for *in vitro* analysis of drug delivery (D'Souza *et al*., 2014) and has been frequently used to define delivery as a prerequisite to *in vivo* analysis (Modi *et al.,* 2013). Dynamic dialysis works by adding a loaded drug delivery vehicle, in this case foam, into dialysis tubing and submerging this into a known volume of buffer or a "sink". Samples are removed from the sink at given time points, the quantity of release molecule is analysed, and the concentration of compound released is calculated by comparing to a reference set. This method was applied to the foam using two model dyes, Nile Red and Calcein, which allowed the analysis of drug concentration to be calculated. This was then followed by a clinically used antibiotic molecule – Rifampicin. The use of multiple substances to study the release from *E. pustulosus* foam allowed assessment of the ability to release hydrophobic and hydrophilic compounds and if this approach will work on a clinically relevant drug molecule.

5.1 Nile Red Release:

Nile red is a hydrophobic dye often used as a model to characterize release from nanoparticles (Borgia *et al*., 2005). Nile Red concentration can be determined using absorbance at 520nm against a standard (Dutta *et al*., 1996). Nile red release from *E. pustulosus* foam was measured over a week, with the concentration calculated, considering the sink volume, using a standard calibration curve (**Fig 5.1**). In order to determine release, the volume of Nile Red uptake had to be defined. The uptake of the foam was evaluated by mixing, with a vortex, known volumes of dye solutions to known weights of foam until no more dye would uptake. This determined that 400mg of *E. pustulosus* foam would comfortably and completely uptake 250µl of Nile Red dye solution. The concentration of Nile Red released from *E. pustulosus* foam was analysed over a week of incubation (**Fig 5.2**). Most dermal foams deliver their drug immediately and require multiple applications. One week was chosen to evaluate the foams ability to release a model over a longer time period to understand its potential as a drug release system. In a dialysis system Nile Red was released from the foam in a linear profile, releasing on average approximately 1µg each hour. A total of 170µg of Nile Red was released from a 400µg foam sample over 168 hours (1 week). This is 69% of the total Nile Red loaded in to the foam sample. A week-long release period is a novel finding for a foam drug delivery system. There is a wide range of data for Nile red release from a variety of potential drug delivery systems making direct comparisons difficult. However, many drug delivery systems fail to release more than 10% of their drug load, and others have a drug release time of 24 hours or less (Alvarez-Roman *et al.,* 2004,

Borgia *et al*., 2005, Cheng *et al*., 2013, Vij *et al*., 2010). The *E. pustulosus* foam release profile displays a high percentage release over a long time period, indicating a more stable release profile than previously shown for Nile Red based systems.

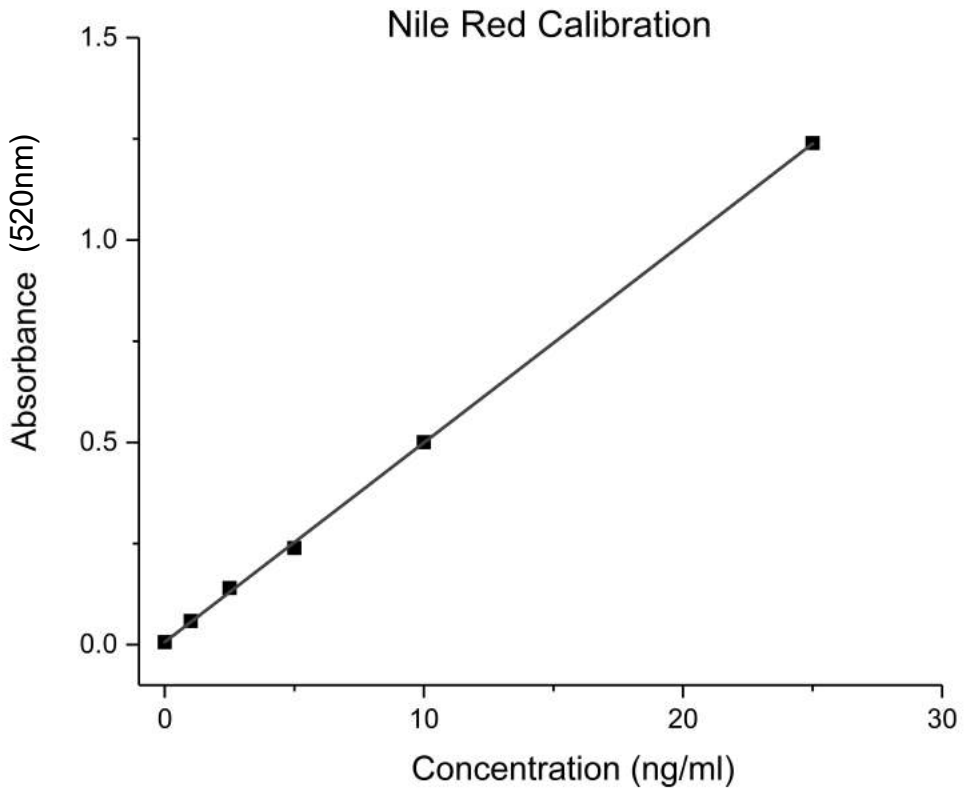

Figure 5.1: Nile Red calibration curve. Absorbance was measured at 520nm and all measurements were read in triplicate. Measurements were averaged, and the standard deviation used for the error bars. The regression line was plotted, and the equation of the line calculated as: $y = 0.0493x + 0.0068$ $R^2 = 0.991$.

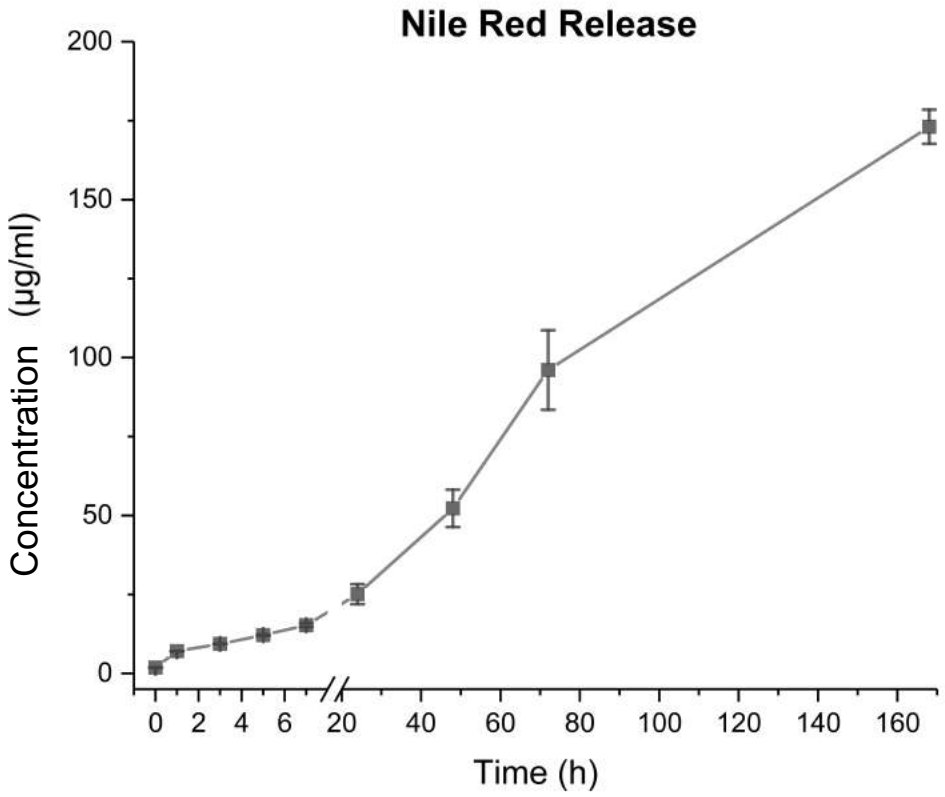

Figure 5.2: Nile Red release from *E pustulosus* foam. All time points were measured in triplicate and each time point was carried out in triplicate to cover both machine and human error. Error bars display standard deviation. Cumulative release was calculated as a percentage of total Nile Red loaded. Foam released 170µg of Nile Red over 168 hours in a linear release profile.

5.2 Calcein Release:

Calcein is a hydrophilic dye which has been used as a model for drug release (Maherani *et al*., 2013), including from liposomes (Allen *et al*., 1980) and for topical release systems (Borgia *et al.,* 2005). Calcein release from *E pustulosus* foam was measured using the dynamic dialysis method under the same conditions as the Nile Red release (see above). Calcein absorbance was measured at 495nm (Litvinchik *et al*., 2009) and the concentration of Calcein released was calculated using calibration curve (**Fig 5.3**). Prior to release measurements, the foams uptake of Calcein solution was determined. It was established that 400mg of foam would fully uptake 350µl of Calcein.

Calcein was released from *E. pustulosus* foam in a burst release profile (**Fig 5.4**). The total release was 294µg of Calcein from a 400mg foam sample over 168 hours. This was 84% of the total load. Approximately 50% of the Calcein was released within the first day, and a further 34% was released over the next week. Similar to Nile Red there is a large volume of release profiles for Calcein from a variety of drug delivery systems so direct comparisons are hard. Some systems release low volumes around 2% (Maherani *et al*., 2013) while others manage higher releases of 50% or 100% but over short time frames of 8-24 hours (Litvinchik *et al*., 2009, Marianecci *et al*., 2011). The foam was able to release a high percentage of its load over a longer time frame. One similarity that can be drawn is that most other delivery systems release Calcein in a burst release profile. Although release of Calcein from the foam is higher overall than for Nile Red release, it is not linear and most of the release happens within 24 hours.

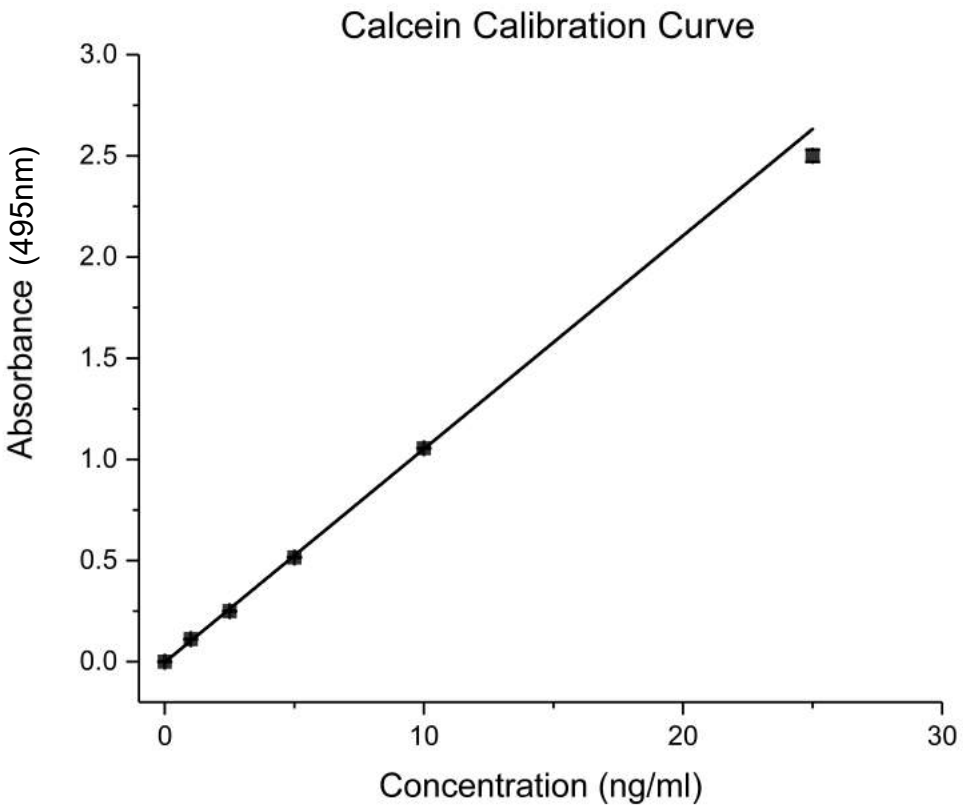

Figure 5.3: Calcein calibration curve. Absorbance was measured at 495nm, and all points were measured in triplicate. Measurements were averaged, and the standard deviation used for the error bars. The regression line was plotted, and the equation of the line calculated as: $y = 0.0985x + 0.0183$ $R^2 = 0.991$

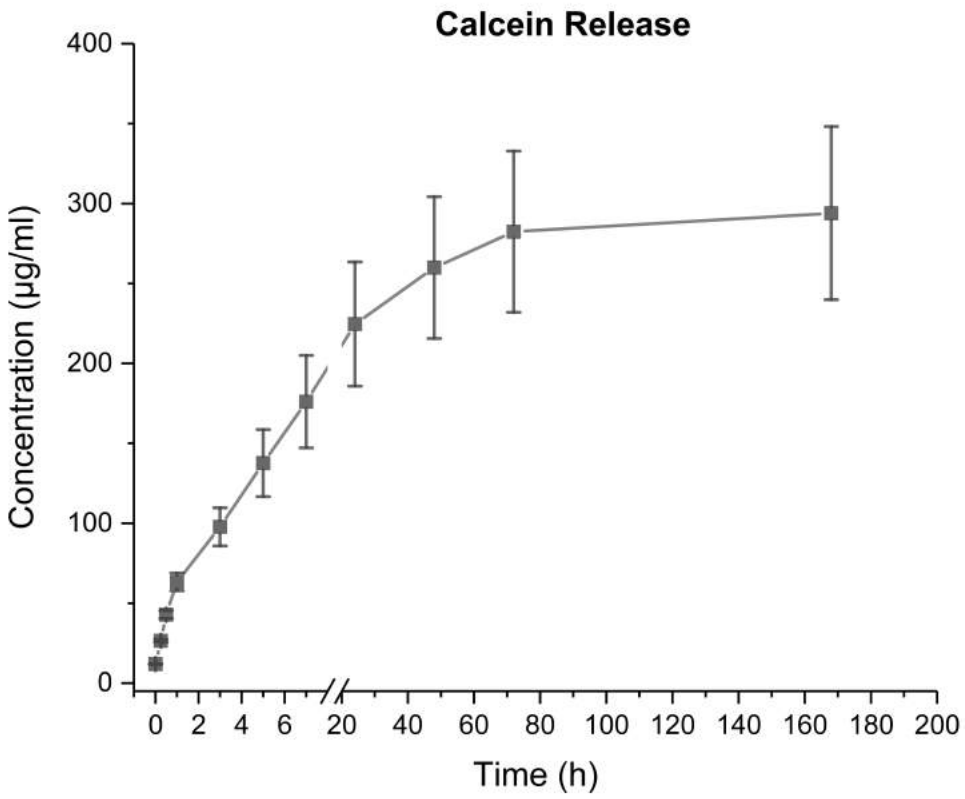

Figure 5.4: Calcein Release from *E. pustulosus* foam. Each time point was measured in triplicate and each time point was carried out in triplicate to cover both machine and human error. Error bars represent standard deviation. Cumulative release was calculated as a percentage of total Calcein loaded. An average of 294µg of Calcein was released from the foam over 168hrs in a burst release profile.

5.3 Rifampicin Release:

Rifampicin is a red pigmented polyketide antibiotic which blocks transcription by inhibiting the β-subunit of RNA polymerase (Wehnli, 1983). Rifampicin is a key treatment for tuberculosis, however it has also been used to treat methicillin resistant *Staphylococcus aureus* infections in prosthesis patients (Aboltins *et al*., 2009).

Rifampicin release from *E. pustulosus* foam was measured using two methods. The dialysis method as carried out above with Nile Red and Calcein, and an additional membrane method using Transwell inserts. Transdermal drug release can be tested using Franz cell diffusion systems, which mimic skin diffusion by separating a donor and receptor chamber with a membrane (Ng *et al.,* 2010). However, this system is an expensive investment for early testing, so a novel method was developed during this research to create a similar system using cheaper and more straightforward equipment by using Transwell inserts to act as a donor chamber and provide a separating "skin like" membrane. This method involved placing loaded foam into Transwell insert with a cellulose membrane in the base and placing this into a 24 well plate with buffer in the lower compartment. This new approach to measure drug release was designed to mimic a Franz cell system at a smaller scale and allow for *in vitro* topical drug release to be measured with multiple replicates, and no similar method has been proposed in the current literature. Rifampicin absorbance was measured at 475nm (Benetton *et al*., 1998), and the concentration of released rifampicin was calculated using a calibration curve (**Fig 5.5**). The Transwell inserts could only hold 100mg of foam, and both experiments used the same weight of foam to ensure the results

were comparable. The foams loading capacity for Rifampicin was determined to be 100µl of Rifampicin in 100mg of foam.

Dynamic dialysis method results show that, similar to Calcein, Rifampicin was released in a burst release profile (**Fig 5.6**). Rifampicin is hydrophobic (Weiss *et al*., 1983), with a similar partition coefficient to Nile Red so a burst release profile was not expected. However, Nile Red has been shown to strongly interact with native proteins (Sackett *et al*., 1987) which may explain its more linear release in comparison to Rifampicin. In all, 85% of Rifampicin was released from a 100µg foam sample over 48 hours, with 80% of release occurring within the first 8 hours. In comparison, dynamic dialysis release data from nanoparticles loaded with rifampicin showed an 80% release in 8hr time frame, with majority of release occurring in first hour (Benetton *et al*., 1998). The foam also released a similar percentage of rifampicin, over a slightly longer time frame, demonstrating that the use of foam could improve the length of delivery of Rifampicin.

The Transwell method also followed a burst release profile (**Fig 5.7**). These measurements showed a 100mg *E. pustulosus* foam released 52% of the loaded rifampicin over 48 hours, with 45% of the release occurring within the first 8 hours of monitoring. This release is lower than the dynamic dialysis method, but the overall profile is similar. However, the Transwell method tested release across a single membrane, instead of a fully submerged system and this likely explains the lower release. Further, a control was carried out were a Transwell insert was loaded with 100µl of Rifampicin and within 24 hours 100% of the Rifampicin had passed through the membrane. The control demonstrates that the foam is responsible for

the release rate, instead of simple diffusion across the membrane. Although this method displays a lower percentage release, the release is slower than release from rifampicin loaded nanoparticles. This method may better indicate the foam release behaviour as a topical release system. It would be interesting to further exploit this method to investigate other drugs such as a painkiller like Ibuprofen, a different antibiotic such as Vancomycin or an antimicrobial like Silver sulfadiazine which all have potential applications in topical drug release. This would allow understanding of the foams diverse potential to treat a variety of skin conditions such as pain conditions, wounds or psoriasis.

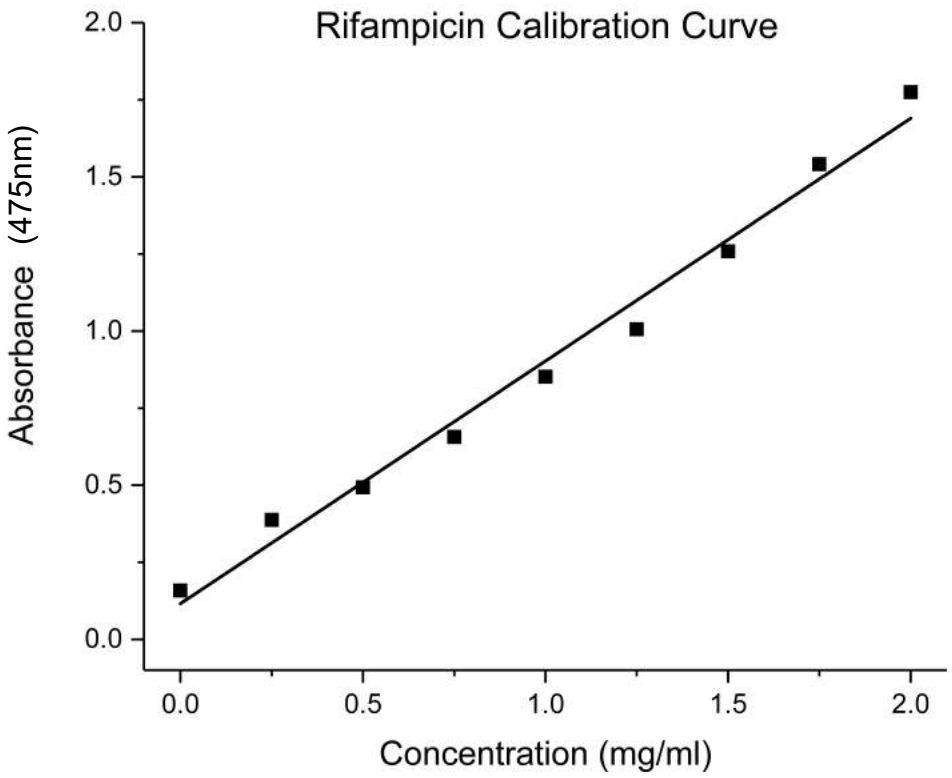

Figure 5.5: Rifampicin calibration curve. Absorbance was measured at 475nm. All measurements were taken in triplicate. Measurements were averaged, and the standard deviation used for the error bars. The regression line was plotted, and the equation of the line calculated as: $y = 0.787x – 0.0808$ $R^2 = 0.986$.

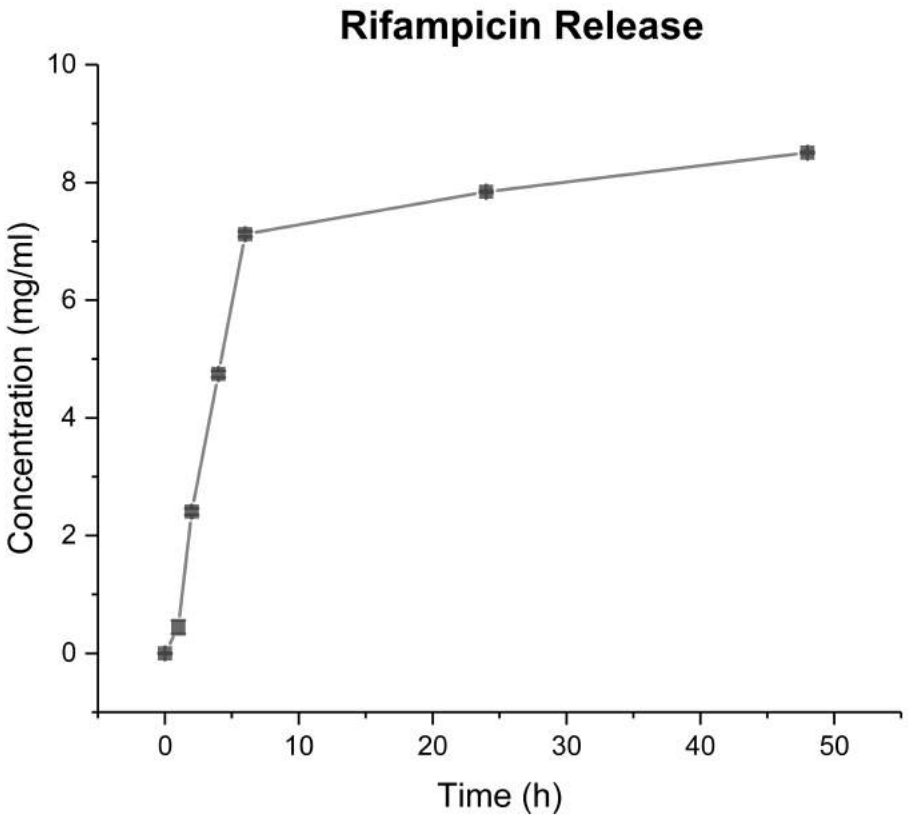

Figure 5.6: Rifampicin release from *E. pustulosus* foam measured using dynamic dialysis method. Each time point was taken in triplicate and each time point was carried out in triplicate to cover both machine and human error. Standard error bars display standard deviation. Percentage release was calculated as a percentage of total rifampicin loaded. The foam released 8.5mg/ml of Rifampicin over 48 hours in a burst release profile.

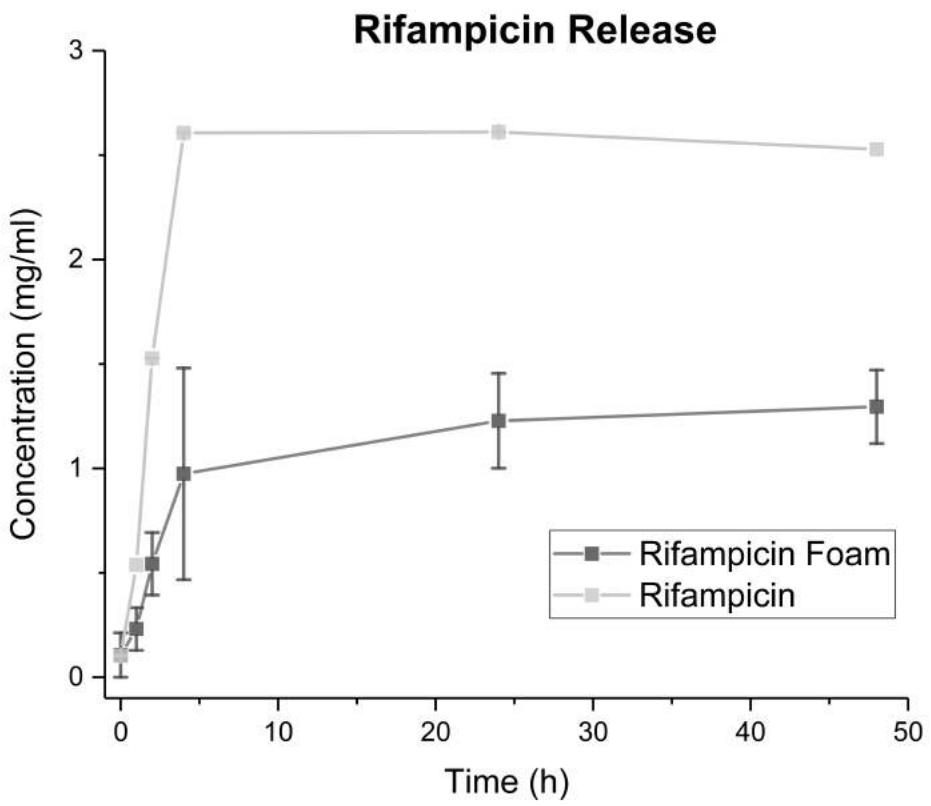

Figure 5.7: Rifampicin release from *E. pustulosus* measured using Transwell release method. All points were taken in triplicate and each time point was carried out in triplicate to cover both machine and human error. Error bars show standard deviation. Percentage release was calculated from the total volume of rifampicin loaded. Free Rifampicin with no drug release system was used a control to highlight drug movement across the membrane. 5.2mg/ml was released from the foam over 48hrs in a burst release profile.

5.4 Summary:

The results presented here demonstrate that *E pustulosus* foam can be loaded with drug mimicking molecules and a clinically relevant antibiotic drug, namely Nile Red, Calcein or Rifampicin and their release profiles defined. This indicates that the foam can take up and release both hydrophobic and hydrophilic substances. Using drug mimics, it was shown that Nile red was released in a linear pattern with 69% of the load released over 168 hours. Calcein was discharged in a burst release profile, and 88% of the total load was released. The methodology was then employed to investigate the release of a clinically relevant antibiotic, Rifampicin. Two methods were used to investigate rifampicin release, dynamic dialysis and a Transwell insert method. These showed release percentages of 85% and 52%, respectively. All these data indicate that foam produced by the Tungara frog could be used as a novel antibiotic drug delivery system.

5.0 Ranaspumin Protein Production

Recombinant proteins are regularly used in biological and medical research, as well as the pharmaceutical industry. Proteins can be produced using a variety of cloning systems and constructs and cell types followed by purification using a range of chromatography-based methods suited to the relevant protein (Bondos *et al.,* 2002, Graslund *et al.,* 2008).

E. pustulosus foam is a mixture of six proteins named Ranaspumin 1-6 (Fleming *et al.,* 2009). In order to utilise this foam as a novel drug delivery system, each Ranaspumin protein must be produced synthetically and fully understood. This may be achieved by overexpressing recombinant RSN proteins in *E. coli* and investigating their properties. However, protein production and purification can be complicated and not all proteins are suitable for expression in all systems (Graslund *et al*., 2008).

Recombinant Ranaspumin's 1, 2, 4 and 6 have previously been produced using T7 Topo TA expression kits and metal affinity chromatography. RSN – 4 and RSN – 6 were purified under denaturing conditions (Fleming *et al.,* 2009). RSN -2, the main surfactant protein present in the foam, has been purified multiple times, its structure solved (MacKenzie *et al.,* 2009) and used to produce a foam for photosynthetic processes (Wendell *et al.,* 2010).

The aim of this work was to attempt to purify each recombinant Ranaspumin starting with a universal method which could be adapted for each specific protein if required. The basic method outline involved sub-cloning each codon optimized *rsn* gene into a pET vector, expressing it in an appropriate *E. coli* strain and used immobilized metal affinity chromatography (IMAC) to purify each recombinant protein.

5.1 Cloning:

Codon bias varies significantly between different hosts, and codon optimization increases the presence of codons which are more frequently translated in a specific organism. Genes for all six Ranaspumin's were codon optimized for *E. coli* expression using IDT's codon optimization tool (https://www.idtdna.com/CodonOpt). Production of recombinant proteins in heterologous hosts can be impacted by codon bias, and optimization has been proven to improve protein expression (Gustafsson *et al.,* 2004). Codon optimized genes where synthesized by Eurofins or IDT into plasmid vectors (pEXA2 or pUCIDT) with synthetic restriction enzyme sites added to facilitate cloning, with added *Nde*I, *BamH*I, *Xho*I and *Nco*I cut sites flanking all genes.

pET vectors are commonly used to express recombinant proteins (Graslund *et al.,* 2008). The pET28a vector was chosen as the ideal expression vector as it contains two hexa-histidine tags allowing the tag to be placed on either the C or the N terminus easily. It is difficult to predict which terminus is best to place a histidine tag on (Graslund *et al.,* 2008) so the restriction enzymes cut sites were specifically added so that the histidine tag could be added to either the N terminus or the C terminus of the protein. By changing the enzymes used to cut both the vector and the gene this could be easily adapted. Further, pET28a has T7 promotor which can be induced by Isopropyl β-D-1-thiogalactopyranoside (IPTG) allowing protein expression to be easily induced. This makes our vector suitable for cloning and over expression in *E. coli* strains containing the gene for T7 RNA polymerase, which is highly specific for the T7 promotor allowing for selective cloning and expression

(Studier *et al.,* 1990). The pET28a vector contains a kanamycin resistance gene, while the pEXA2 and pUCIDT plasmids contain ampicillin resistance, allowing easy resistance screening during sub-cloning.

A full diagram of the cloning method is displayed in **Fig 5.1.** Plasmids containing *rsn* genes and pET28a plasmids were propagated in DH5α and then extracted using a plasmid miniprep kit (Bioline). Both plasmids were then cut with *BamH*I and *Nde*I. The digested plasmids were electrophoresed in 2% agarose gel and the vector or gene fragments were extracted from the gel to be ligated into the expression vector. However, as the *rsn* gene fragments were so small, obtaining a high concentration of quality DNA using gel extraction was difficult. To solve this issue, the vector and genes were digested, and the mixes ligated in one step. The ligation mix was used to transform DH5α, and the resulting colonies were screened by colony PCR (**Fig 5.5**) for successful clones which contained optimized *rsn* genes inserted into pET28a plasmid with his-tag located on the N terminus (**Fig 5.2-5.4**). Unfortunately, the primers used only amplify each *rsn* gene, so could not fully determine if the genes were properly inserted, however all plasmids were then confirmed with sequencing by Eurofins. All six Ranaspumin genes where successfully sub-cloned into pET28a.

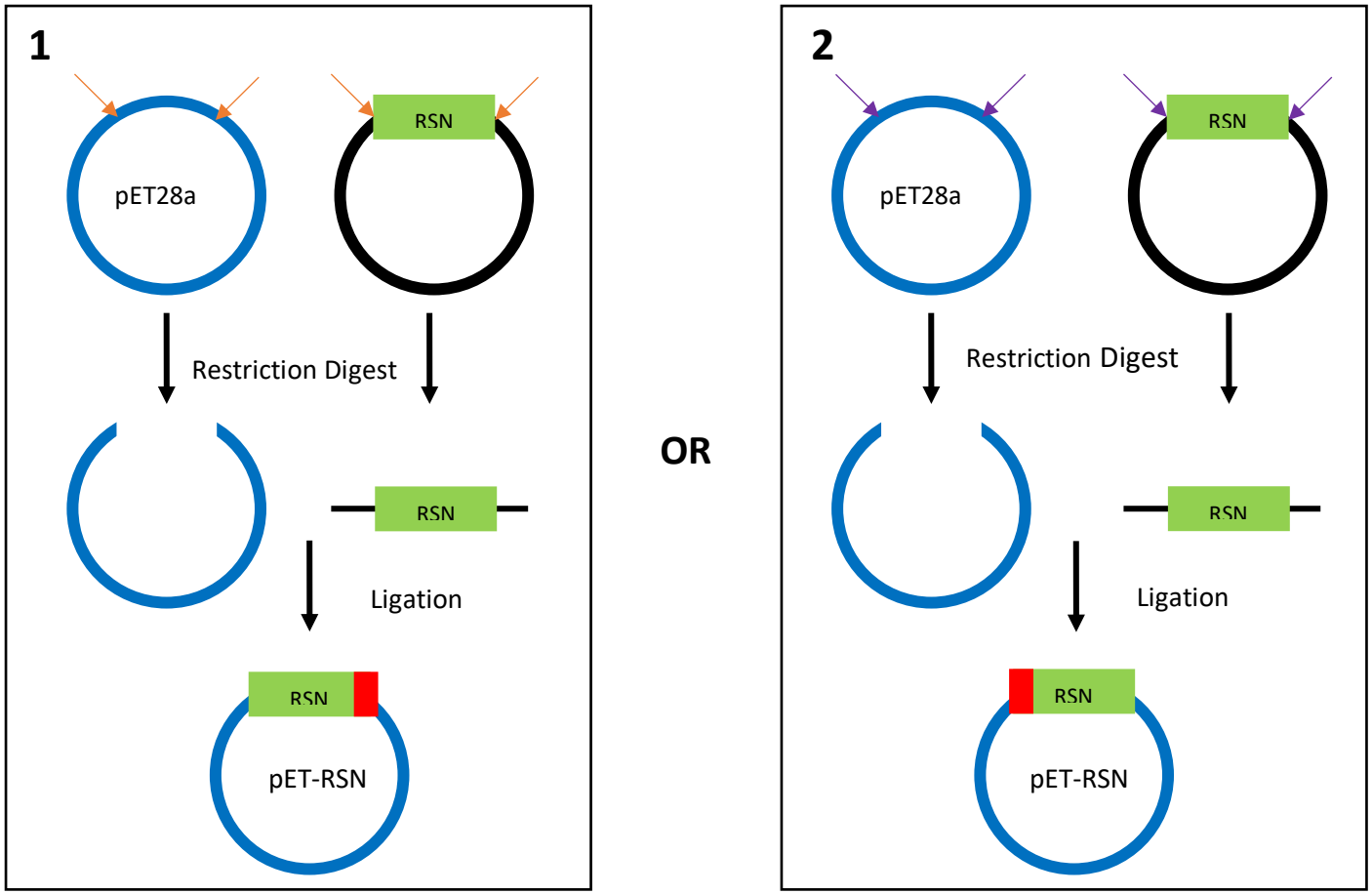

Figure 5.1: Cloning schematic demonstrating how each *rsn* gene could be cut from its synthetic plasmid and ligated into pET28a. Depending on the enzymes used either **1:** *BamHI & NdeI* or **2:** *XhoI & NcoI* would determine whether the histag was located on the N-terminus or C-terminus of the resulting protein.

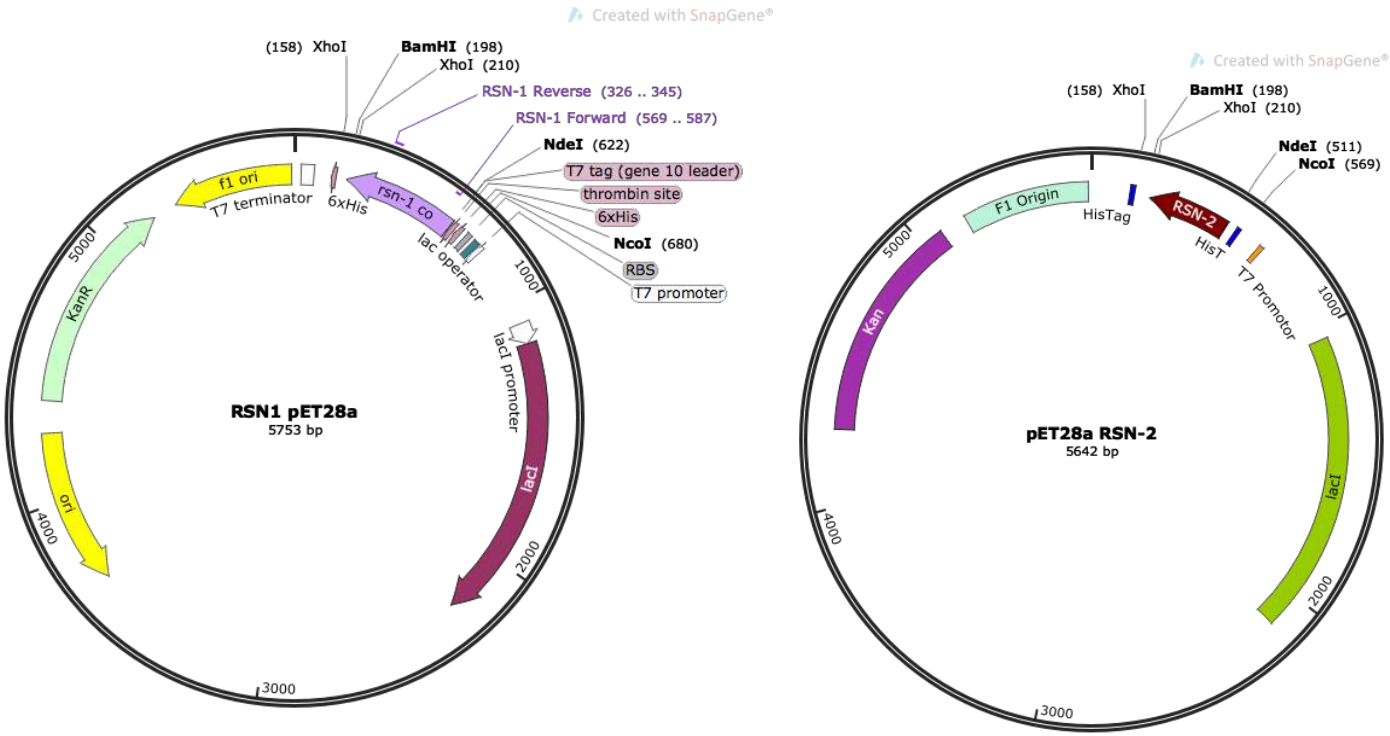

Figure 5.2: Plasmid maps of codon optimized *rsn-1* (408bp) and *rsn-2* (294bp) gene fragments inserted in pET28a plasmid. Maps produced using Snapgene software.

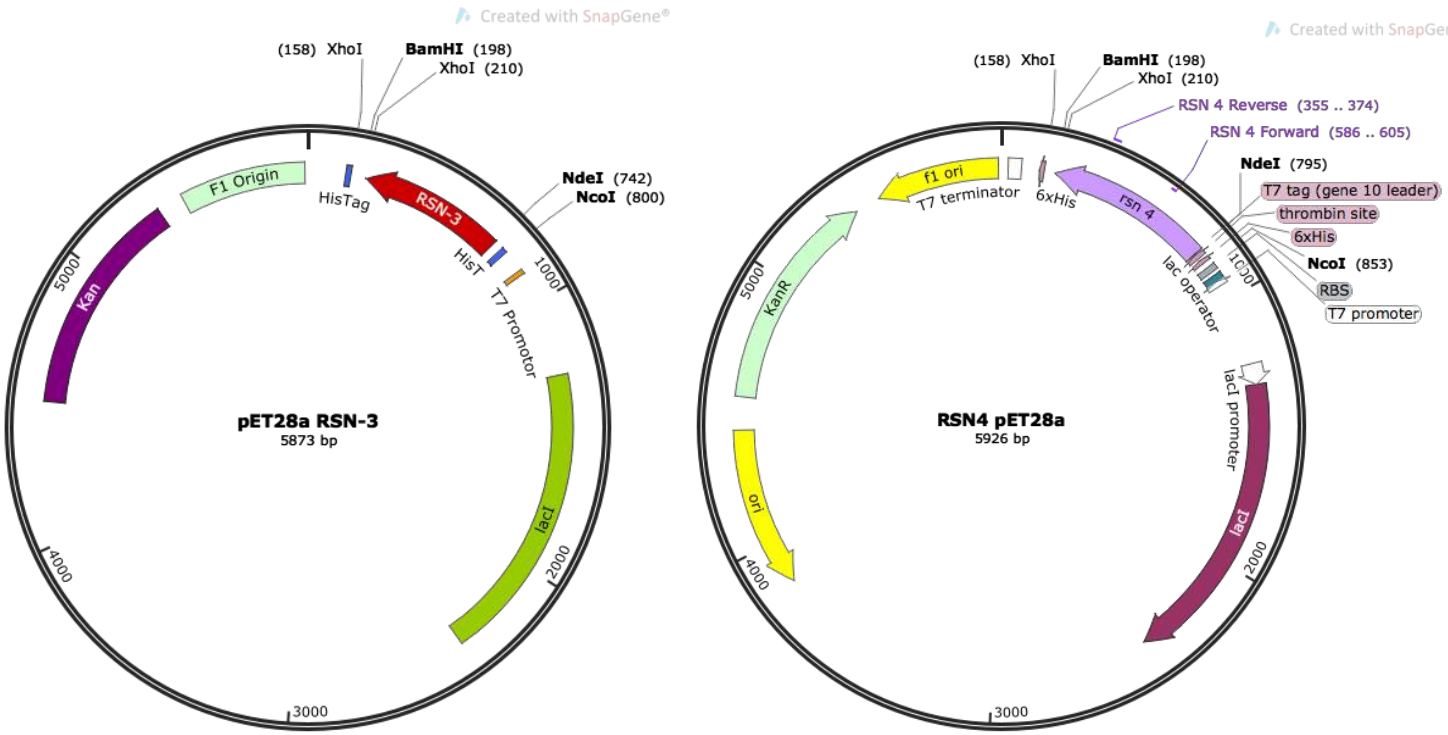

Figure 5.3: Plasmid maps of codon optimized *rsn-3* (525bp) and *rsn-4* (582bp) gene fragments inserted in pET28a plasmid. Maps produced using Snapgene software.

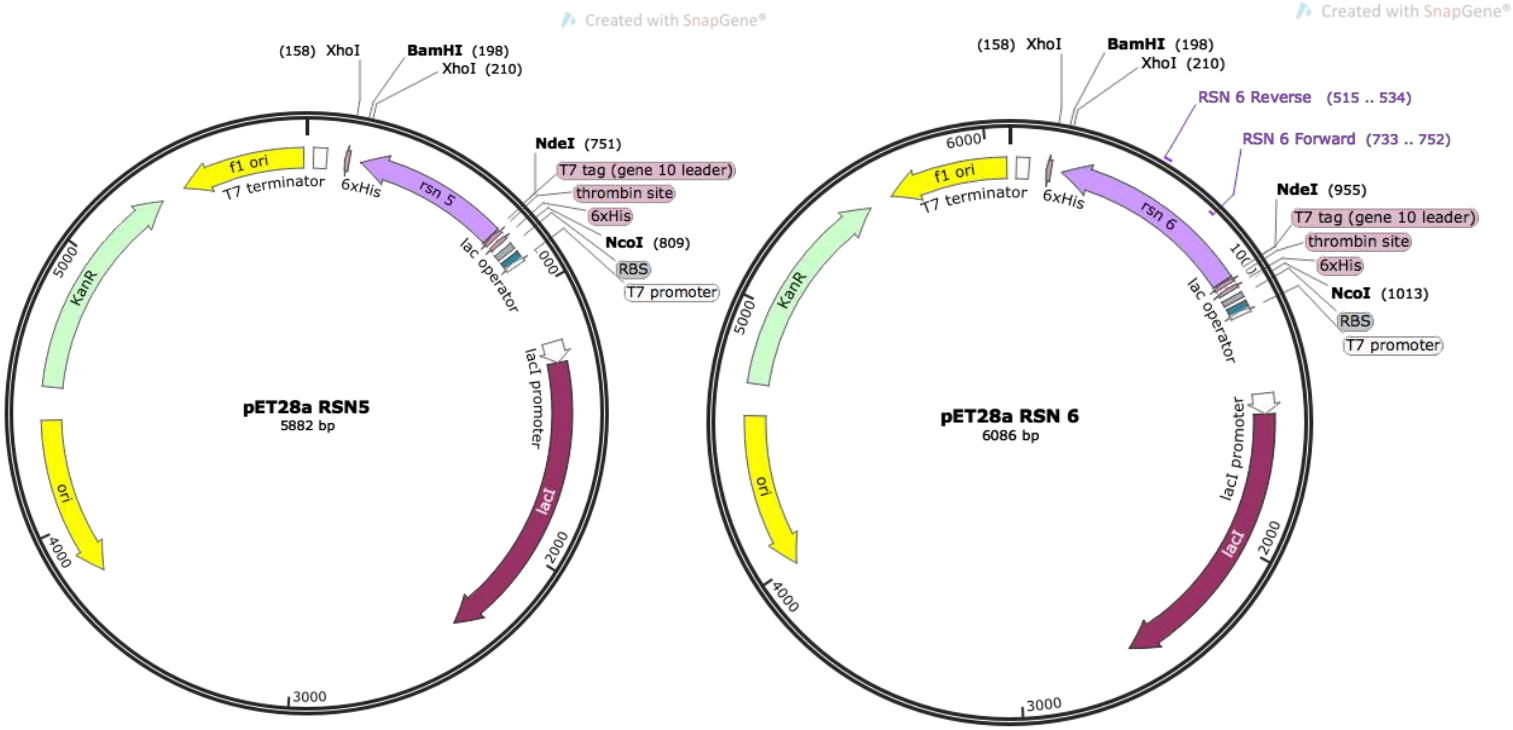

Figure 5.4: Plasmid maps of codon optimized *rsn-5* (537bp) and *rsn-6* (741bp) gene fragments inserted in pET28a plasmid. Maps produced using Snapgene software.

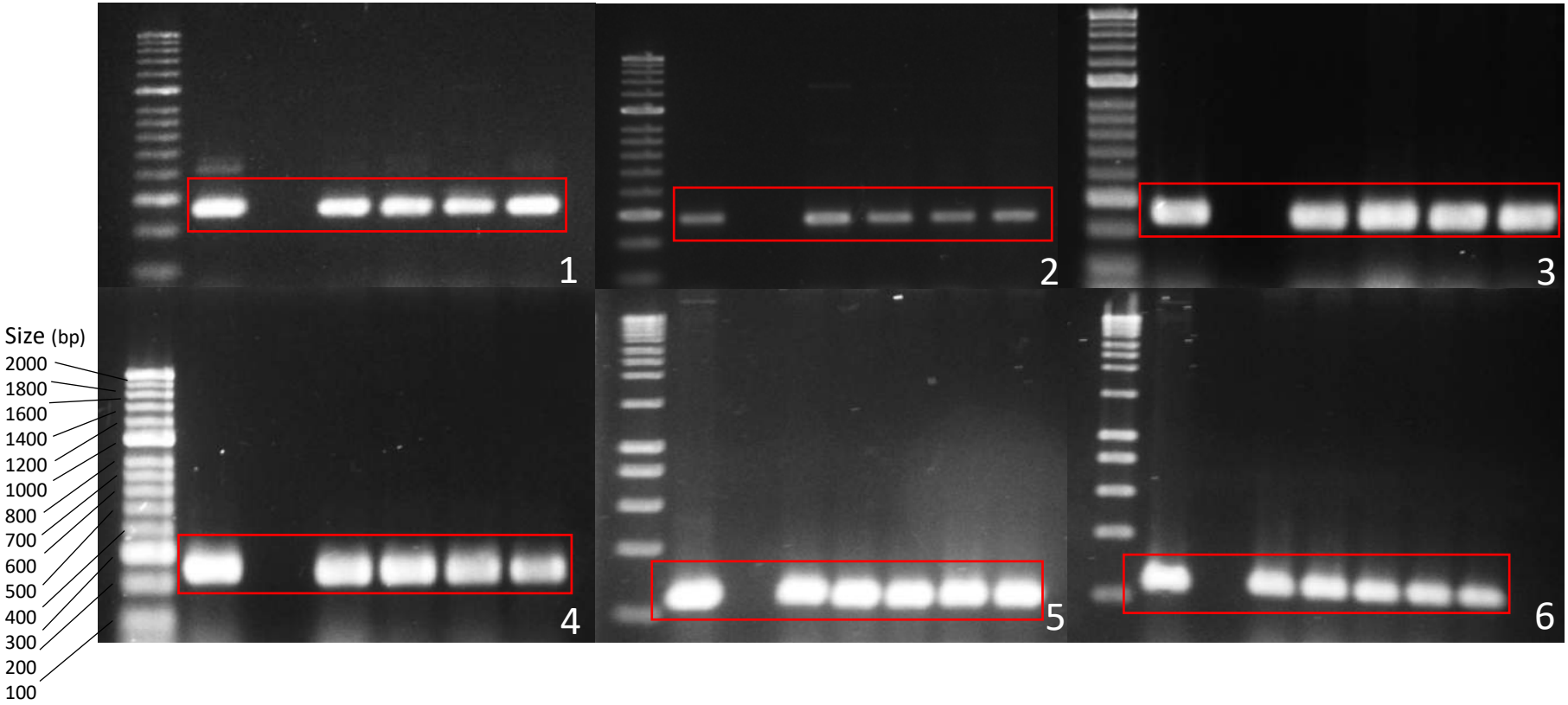

Figure 5.5: Colony PCR verification of pET28aRSN plasmids **1:** pET28A RSN-1 (262bp) **2:** pET28A RSN-2 (275bp) **3:** pET28A RSN-3 (293bp) **4:** pET28A RSN-4 (251bp) **5:** pET28A RSN-5 (247bp) **6:** pET28A RSN-6 (238bp). All gels were run in the same order – Ladder (bioline hyperladder), positive control, negative control and four or five colonies. Original pUC plasmid from IDT with each respective *rsn* gene was used as a positive control. Empty pET28a plasmid was used as a negative control.

5.2 Protein overexpression and optimization:

To produce a synthetic foam using ranaspumin proteins, overexpressing recombinant ranaspumin proteins was required. Multiple cell types, temperatures and IPTG concentrations were screened to identify the optimum expression conditions for each ranaspumin protein. BL21(DE3), BL21*(DE3) and Rosetta (DE3) were the *E. coli* strains chosen for overexpression. All three cell types contain the phage T7 RNA polymerase required to make them compatible with T7 expression vectors but have slightly different qualities. BL21 (DE3) is routinely used for T7 expression systems. BL21* (DE3) is optimized for use with low copy plasmids, such as pET28a. Rosetta(DE3) enhances the expression of rare and unusual codon and is suitable for eukaryotic proteins which may be beneficial in ranaspumin expression. All three cell types were transformed with each pET28a construct containing the genes encoding each ranaspumin protein to be tested under different expression conditions.

All three cell types where tested using 1ml of starter culture in 12 well plates (**Fig 5.6**). Cultures were grown to OD 0.4-0.6 at 37^{o}C before being induced with either 0.2mM, 0.5mM or 1mM of IPTG. Each plate was incubated at a temperature of 15°C, 25°C, 30°C or 37°C. Cultures induced at 15°C and 25°C were allowed to express overnight, and cultures at 30°C or 37°C were incubated for 4 hours. After this time samples were collected from each well and SDS PAGE was carried out for each plate (**Fig 5.7 – 5.12**). This was performed on all six ranaspumin constructs and the best condition for expressing each recombinant protein was identified (**Table 5.1**). RSN-2, RSN-3, RSN-5 and RSN-6 all produced an appropriate

overexpressed protein band in a number of conditions, however in 1ml cultures RSN-1 and RSN-4 failed to provide an overexpressed protein band.

The conditions chosen at small scale were then scaled up from 1ml to 250ml of culture in 1L Erlenmeyer flasks to check they were still appropriate. Samples were taken after cultures were induced under their selected conditions and SDS-PAGE was carried out to confirm the presence of each Ranaspumin (**Fig 5.13**). RSN-1 did not clearly overexpress in either of the condition screens or at scale up size. It is possible that the protein was being expressed at a very low concentration, but it could not be identified on a gel. RSN-4 did not clearly overexpress in condition screens, but it was decided to attempt a scale up at 250ml with Rosetta at 30°C and 1mM IPTG. At a larger scale RSN-4 did overexpress. The remaining four Ranaspumins all expressed well in scale up under the conditions chosen. After confirming that the conditions scaled correctly, purification of each Ranaspumin was attempted.

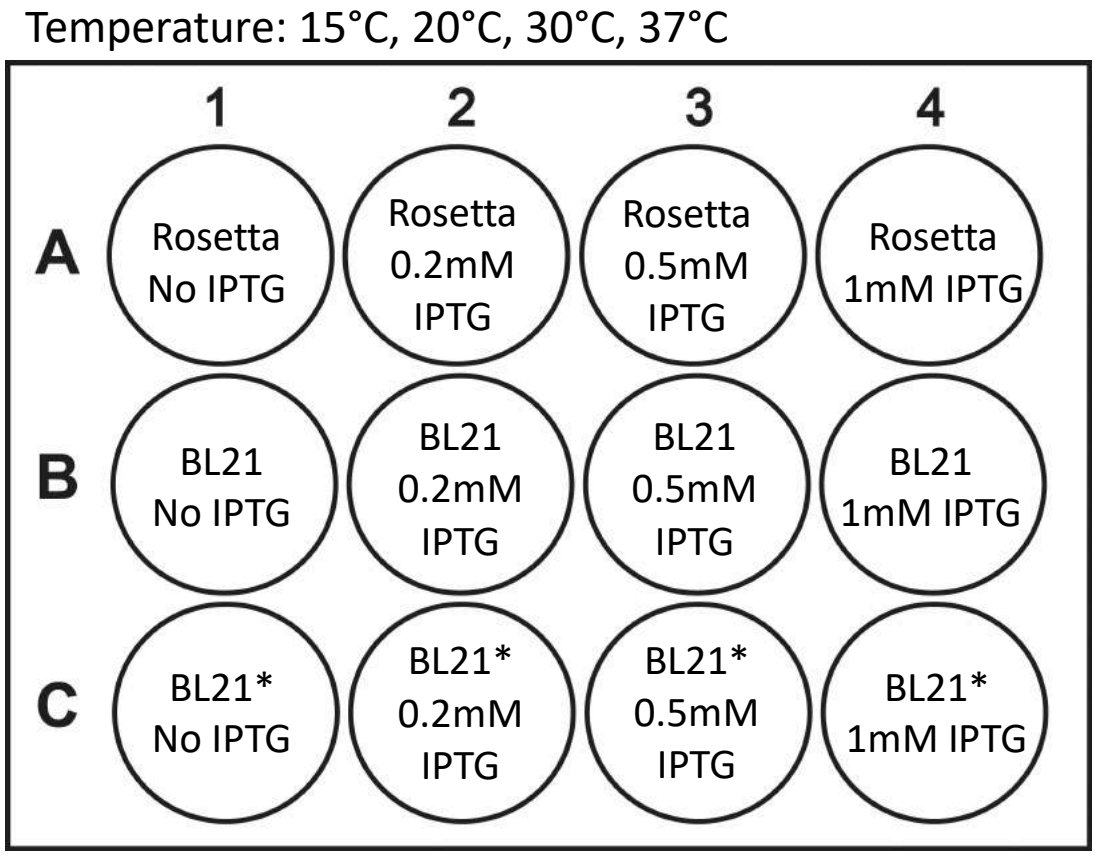

Figure 5.6: 12 well plate layout for condition screening of each recombinant RSN protein.

All wells contained a final working volume of 1ml.

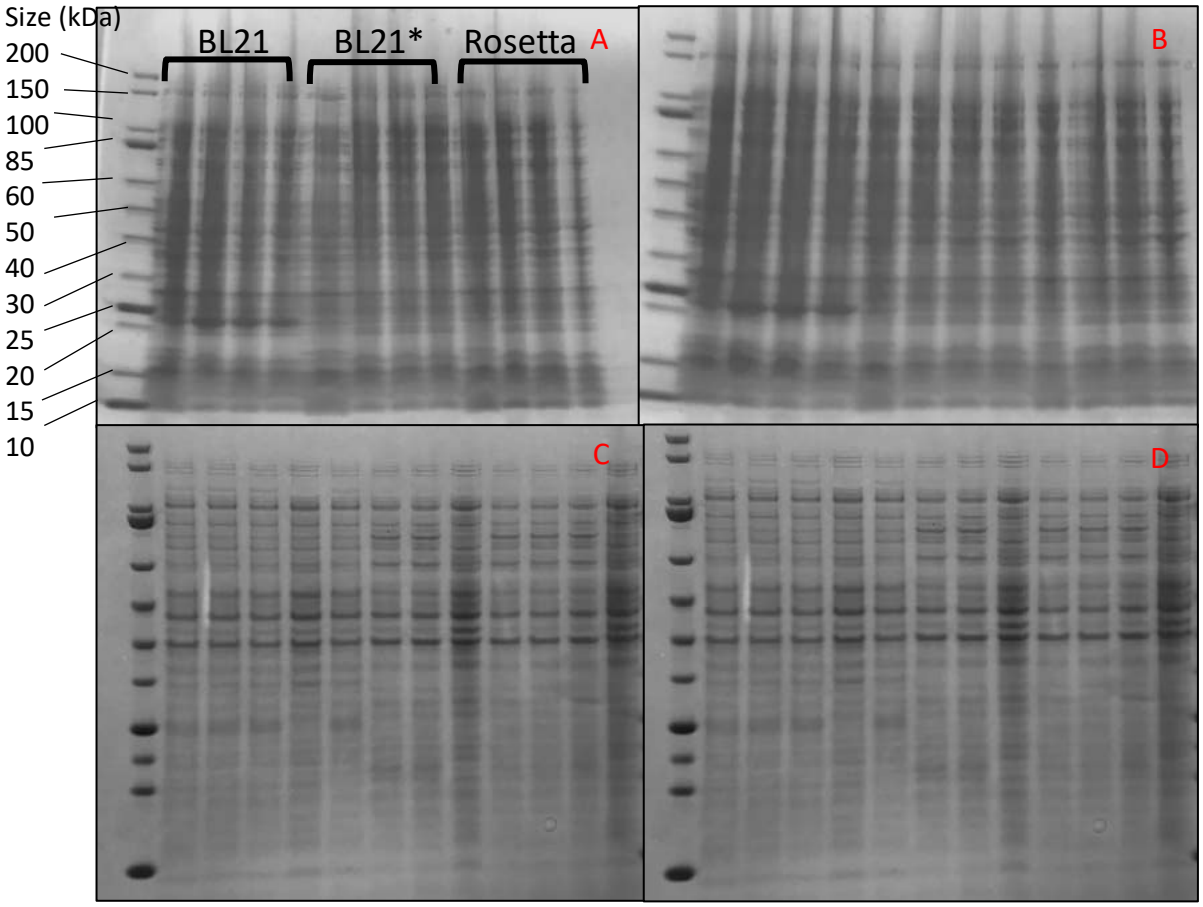

Figure 5.7: Condition screening of pET28a RSN-1 in BL21, BL21* and Rosetta *E. coli* strains. **A** 15°C **B** 25°C **C** 30°C **D** 37°C. **Ladder**: NEB 10-200kDa Broad range marker. **RSN-1** predicted size including HisTag: 15kDa

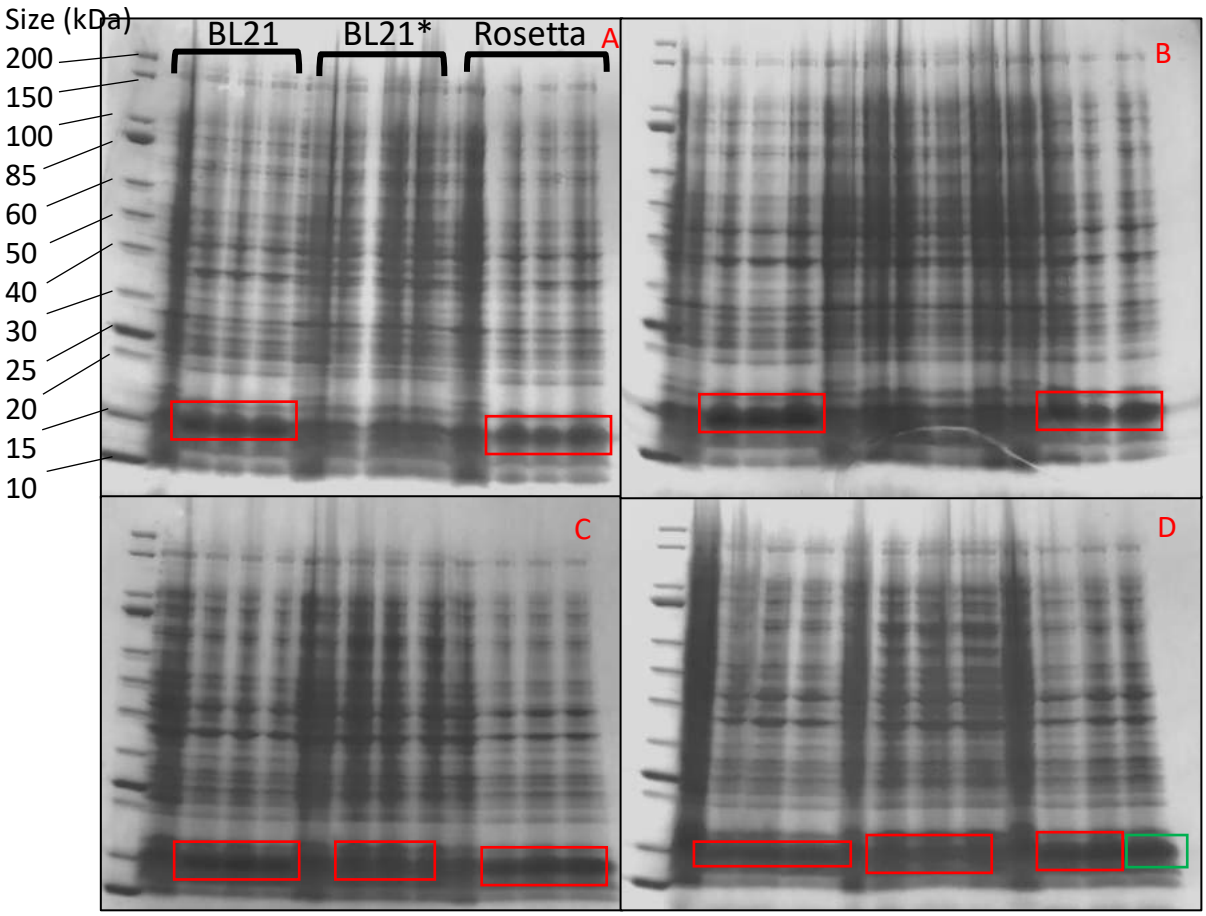

Figure 5.8: Condition screening of pET28a RSN-2 in BL21, BL21* and Rosetta *E. coli* strains. **A** 15°C **B** 25°C **C** 30°C **D** 37°C. **Ladder**: NEB 10-200kDa Broad range marker. **RSN-2** predicted size including HisTag: 12kDa. Expressed protein highlighted with red boxes and condition chosen highlighted with a green box.

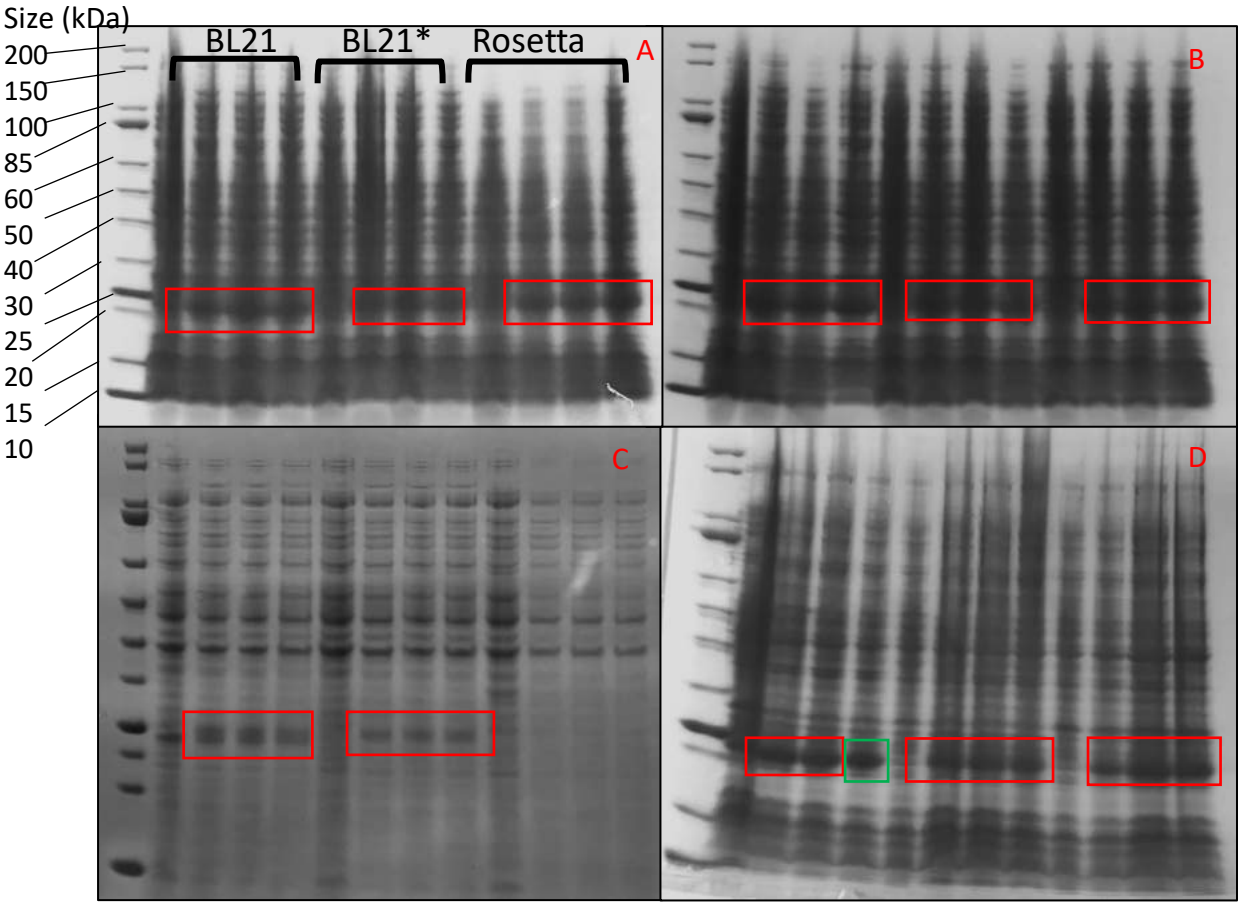

Figure 5.9: Condition screening of pET28a RSN-3 in BL21, BL21* and Rosetta *E. coli* strains. **A** 15°C **B** 25°C **C** 30°C **D** 37°C. **Ladder**: NEB 10-200kDa Broad range marker. **RSN-3** predicted size including HisTag: 19kDa. Expressed protein highlighted with red boxes and condition chosen highlighted with a green box.

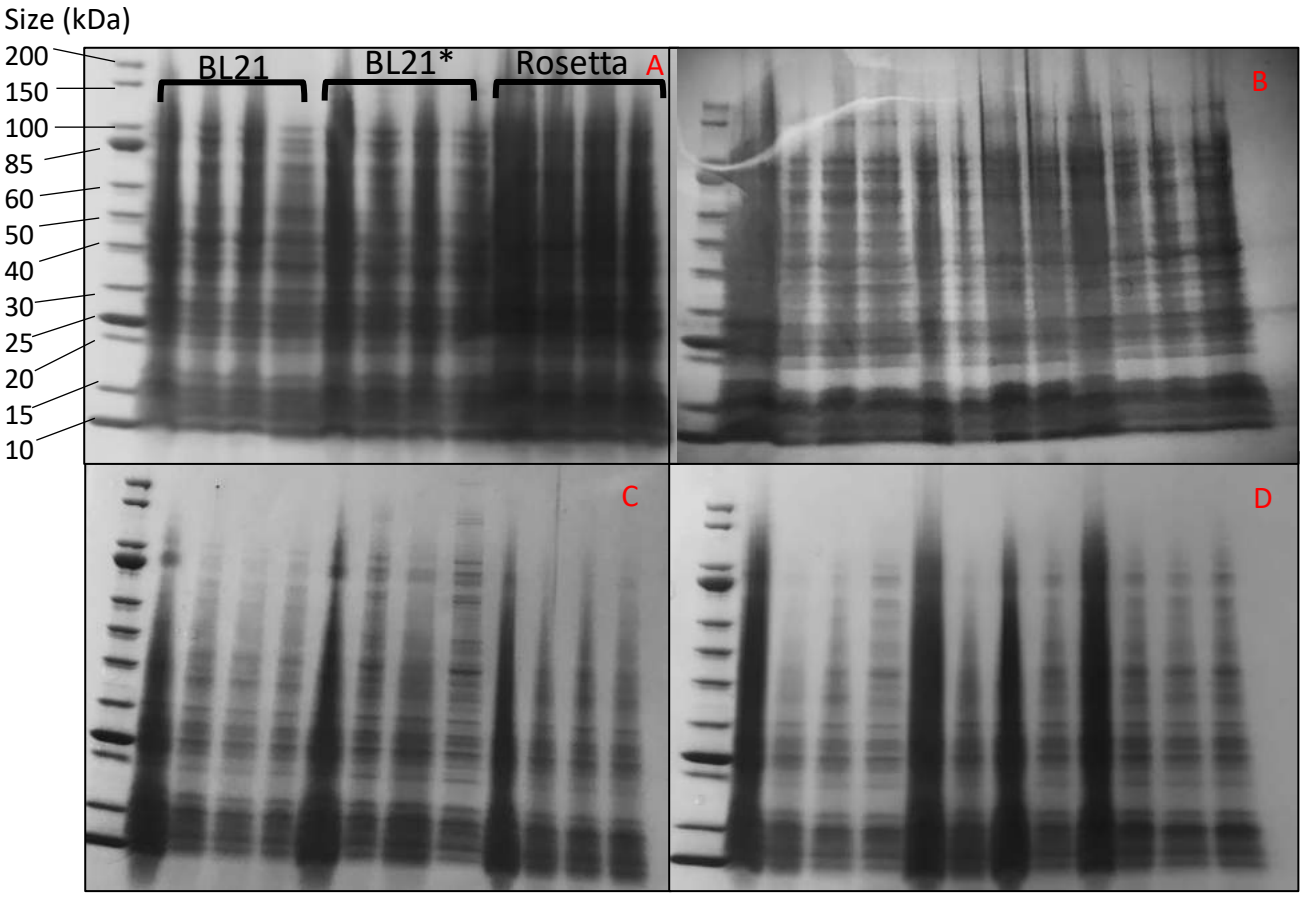

Figure 5.10: Condition screening of pET28a RSN-4 in BL21, BL21* and Rosetta *E. coli* strains. **A** 15°C **B** 25°C **C** 30°C **D** 37°C. **Ladder**: NEB 10-200kDa Broad range marker. **RSN-4** predicted size including HisTag: 22kDa

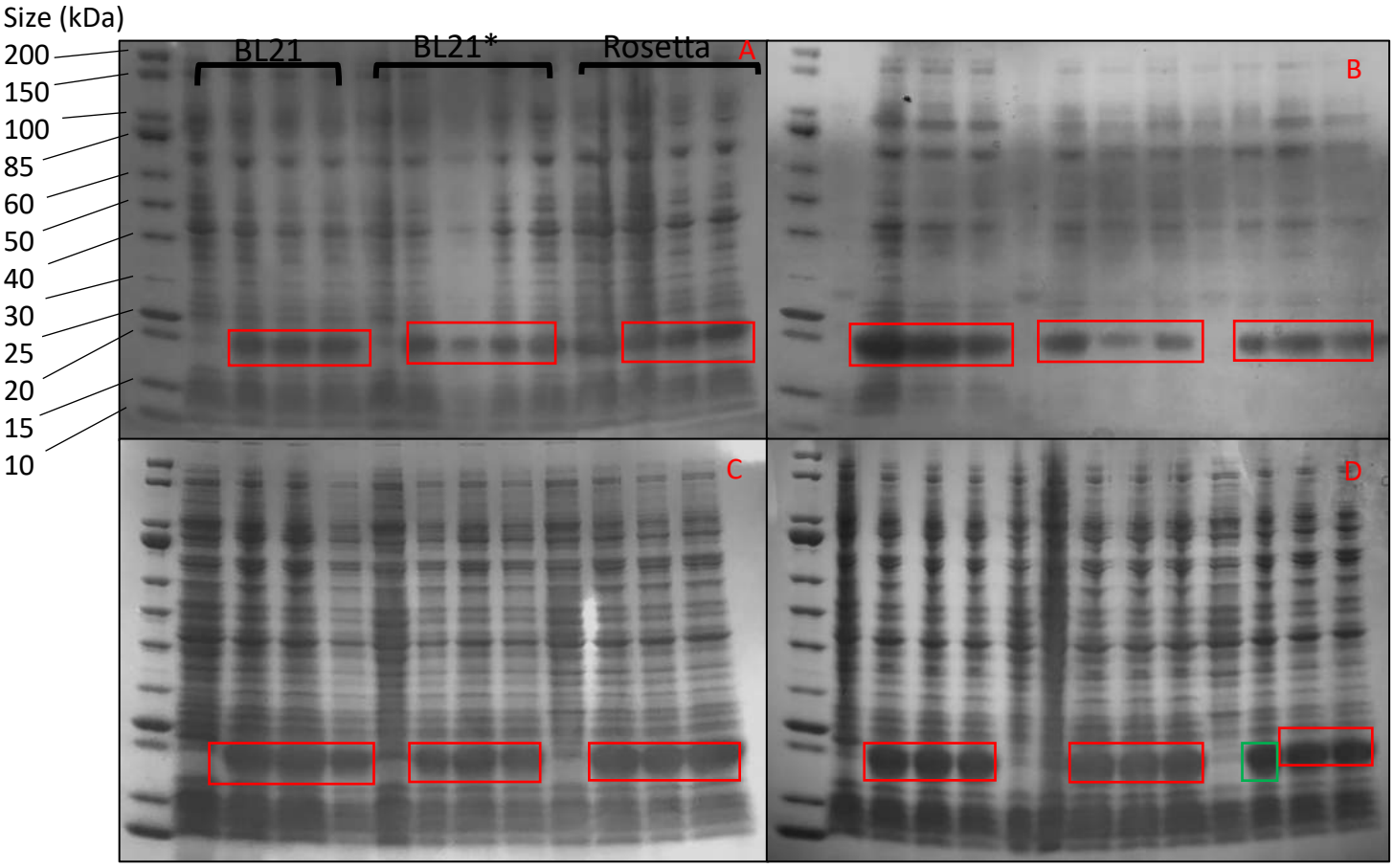

Figure 5.11: Condition screening of pET28a RSN-5 in BL21, BL21* and Rosetta *E. coli* strains. **A** 15°C **B** 25°C **C** 30°C **D** 37°C. **Ladder**: NEB 10-200kDa Broad range marker. **RSN-5** predicted size including HisTag: 20kDa Expressed protein highlighted with red boxes and condition chosen highlighted with a green box.

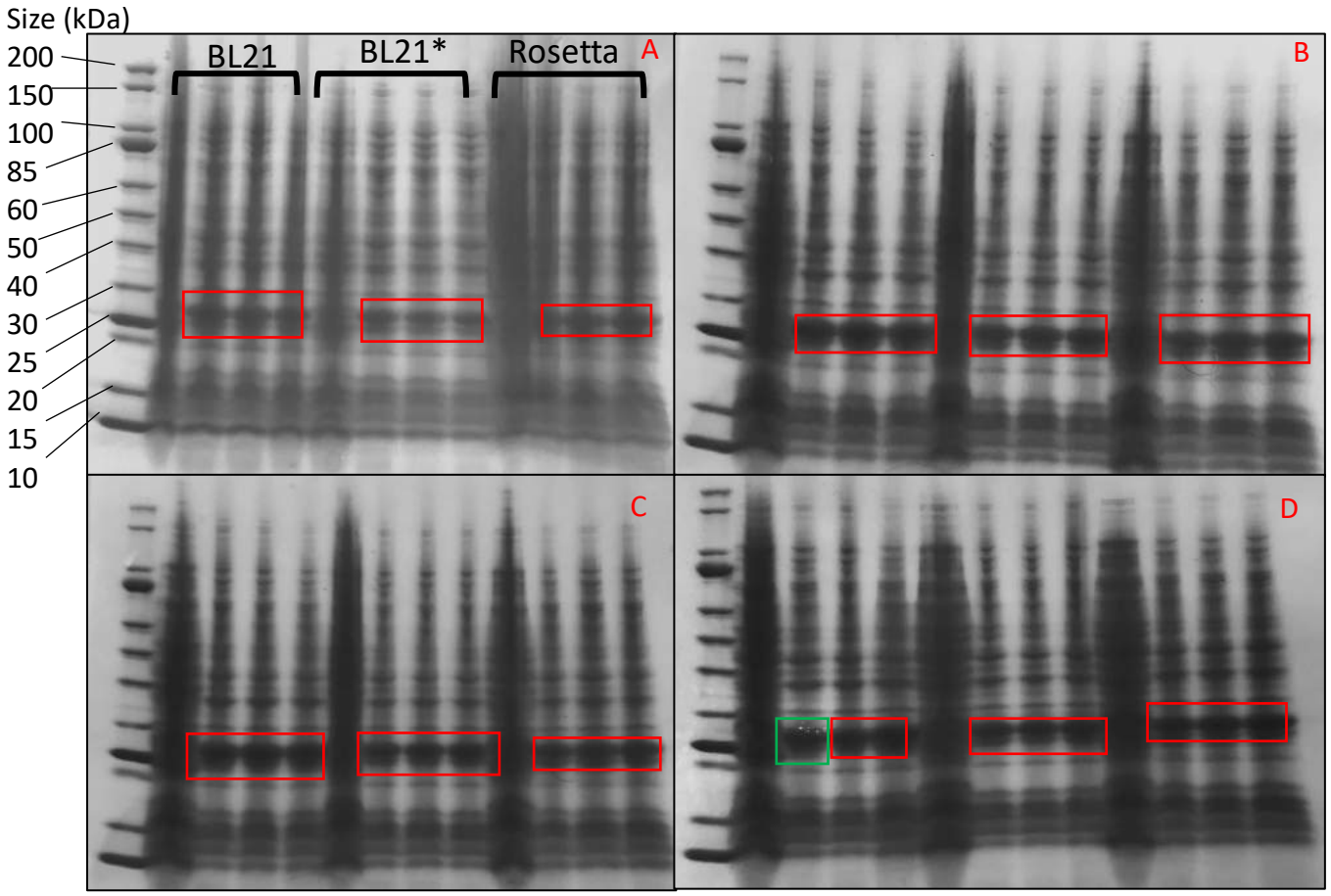

Figure 5.12: Condition screening of pET28a RSN-6 in BL21, BL21* and Rosetta *E. coli* strains. **A** 15°C **B** 25°C **C** 30°C **D** 37°C. **Ladder**: NEB 10-200kDa Broad range marker. **RSN-6** predicted size including HisTag: 28kDa Expressed protein highlighted with red boxes and condition chosen highlighted with a green box.

Table 5.1: Optimum expression conditions for recombinant Ranaspumin proteins

Protein	Cell Type	Temperature (C)	IPTG Concentration (mM)
Ranaspumin 1	-	-	-
Ranaspumin 2	BL21	37	1
Ranaspumin 3	Rosetta	37	1
Ranaspumin 4	Rosetta	30	1
Ranaspumin 5	Rosetta	37	0.2
Ranaspumin 6	BL21	37	0.2

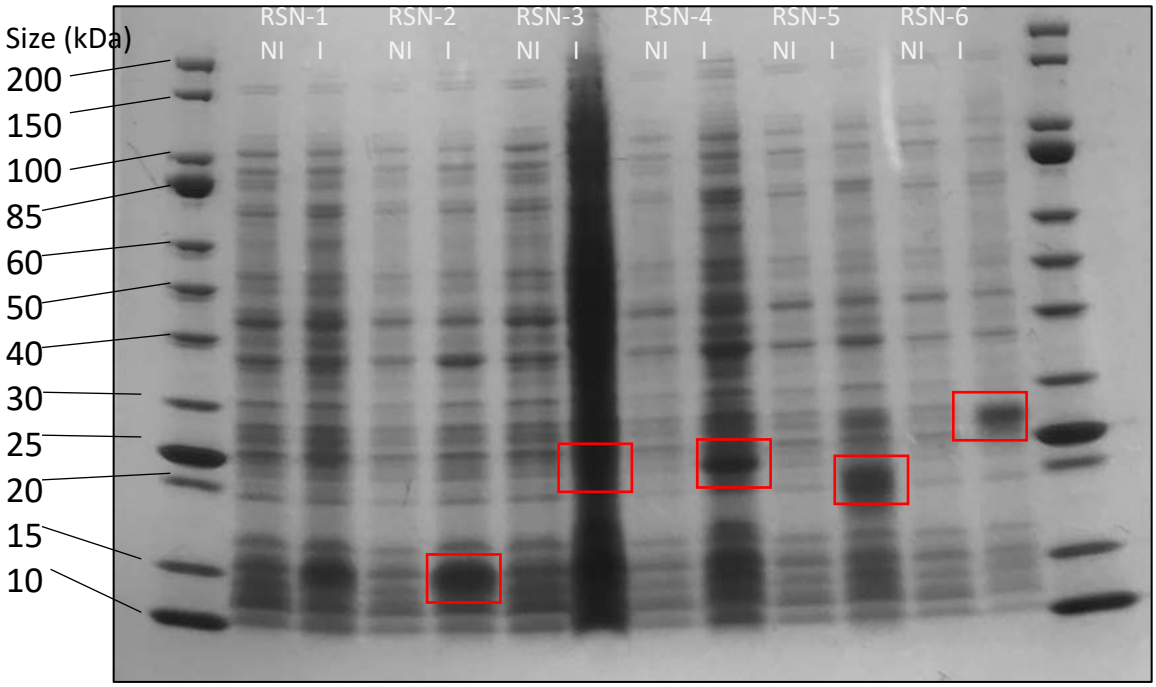

Figure 5.13: Scale up of RSN expression under respective optimal conditions at 250ml. **NI** indicates no IPTG added to culture, **I** indicates induced with appropriate IPTG concentration. **Ladder**: NEB 10-200kDa Broad range marker. **RSN-1:** 15kDa **RSN-2:** 12kDa **RSN-3:** 19kDa **RSN-4:** 22kDa **RSN-5:** 20kDa **RSN-6:** 28kDa. Expressed protein highlighted with a red box.

5.3 Purification:

Metal affinity chromatography was carried out using an AKTA chromatography system (GE Healthcare) to attempt to purify recombinant *E. pustulosus* Ranaspumin proteins. Each protein was tagged with 6 histidine (HisTag) residues on the N terminus. HisTags were chosen as they rarely impact the activity or solubility of a protein (Graslund *et al*., 2008). Histidine contains an imidazole side chain which will bind to metal ions such as Ni^{2+}, and this can be exploited for protein purification through IMAC. A HisTrap column contains immobilized nickel ions which should bind to the HisTag present on the N terminus of each Ranaspumin. Buffer containing free imidazole can then be introduced, and the free imidazole competitively binds the metal ions allowing the protein to be dislodged and collected.

The cells used to overexpress each protein were harvested by centrifugation and then chemically lysed using BugBuster MasterMix (Millipore). Protease inhibitor cocktail (cOpmlete; Roche) was added to the lysate to prevent break down of any protein by proteases. The lysate was run through a HisTrap column. The column was then washed with buffer (Buffer A) to clear any unbound protein. A second buffer (Buffer B) which contains free imidazole is then added in an isocratic gradient to elute the bound protein. The UV absorbance is monitored as the gradient of buffer B increases, and fractions are collected as the absorbance increases.

Buffer conditions contribute to protein solubility and aggregation (Bondos *et al*., 2002). Two different buffer solutions were used: A Sodium Phosphate based buffer and a Tris HCL based buffer. Both buffers are compatible with HisTrap columns, and their pH is similar. Both buffers have a pH well suited with the predicted pI's of all Ranaspumin proteins to allow them to be soluble in the buffer. Tris buffer also contained glycerol, which can improve protein stability (Graslund *et al*., 2008).

Samples were taken at each step of the purification process, starting with the un-induced culture, the induced culture, after centrifugation, after lysing, column flow through, initial buffer A flow through and then fractions of purified protein. SDS-PAGE was carried out with each sample, allowing each step to be monitored for problems or progress.

RSN-1 could not be expressed or purified. Each step was screened using Rosetta grown at 30°C with 1mM of IPTG to confirm (**Fig 5.14**).

Recombinant RSN-2 was purified from lysed BL21(DE3) cells using a HisTrap column (**Fig 5.15**). Purification was carried out with both Sodium Phosphate and Tris HCL based buffers, and Tris HCL buffer resulted in the better purification. Protein concentration was determined using Bradford assay as around 1.7mg/ml. The fractions were pooled and concentrated to 10mg/ml then stored at -80°C until needed for further use.

RSN-3 (**Fig 5.16**) and RSN-6 (**Fig 5.19**) did not appear to be soluble in BugBuster MasterMix, and therefore were not purified. This may be caused by incomplete or improper lysis, and a range of different approaches could be used including enzymatic lysis with lysozyme or sonication in lysis buffer (Peti *et al*., 2007). RSN-6 has been previously been purified under

denaturing conditions (Fleming *et al*., 2009), which may improve protein solubility (Bornhorst *et al*., 2000).

RSN-4 (**Fig 5.17**) and RSN -5 (**Fig 5.18**) both appear to be soluble but did not bind to the HisTrap column. The HisTag could be buried in the protein due to tertiary structure. In order to solve this issue, the HisTag could be moved from the N-terminus to the C-terminus, which pET28a plasmid easily allows. The purification could be carried out in denaturing conditions (Bornhorst *et al.,* 2000), which was previously carried out on RSN-4 (Fleming *et al*., 2009).

Proteins that are part of a complex often require the presence of the other complex proteins to be soluble, and this can be exploited for purification by co-expressing the proteins (Graslund *et* al., 2008, Vera *et* al., 2006). RSN-2 reliably purifies and is a surfactant protein which may increase solubility of other proteins. As a final attempt to purify recombinant ranaspumins, RSN-3, 5 & 6 cultures were mixed with a culture of RSN-2 and lysed. The lysate was then run through a HisTrap column and Tris buffer used to try purification. It was decided to not attempt this with RSN-1 as it had not expressed well during any previous stage. Further, it was chosen to not carry RSN-4 forward as it only expressed at very low levels previously. Neither RSN-3 (**Fig 5.20**) or RSN-6 (**Fig 5.20**) become soluble in the presence of RSN-2. RSN-5 remained soluble but did not bind to the column in the presence of RSN-2.

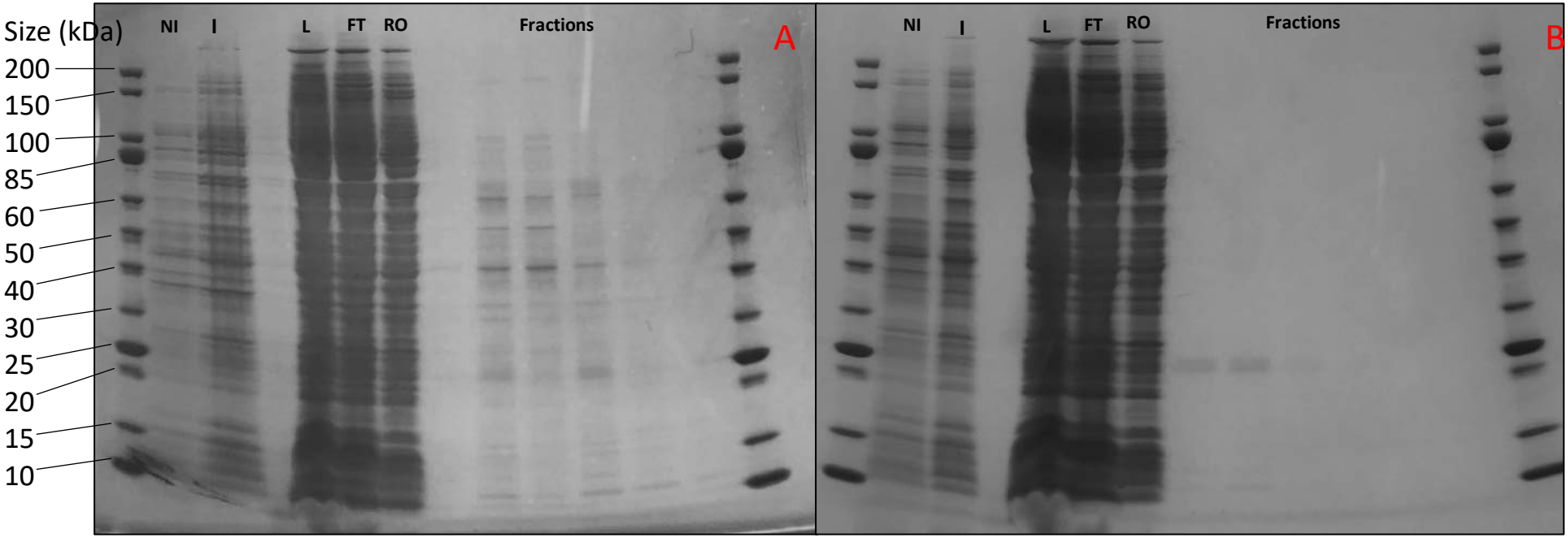

Figure 5.14: HisTrap purification of recombinant RSN-1 harvested from lysed Rosetta culture, grown at 30°C and induced with 1mM of IPTG. **A:** Purification attempted with Sodium Phosphate buffer. **B:** Purification attempted with Tris HCL buffer. **Ladder**: NEB 10-200kDa Broad range marker. . **Running order: NI** not induced culture, **I** induced culture, **L** lysed cells, **FT** Flow through, **RO** run off from buffer A **F** fractions.

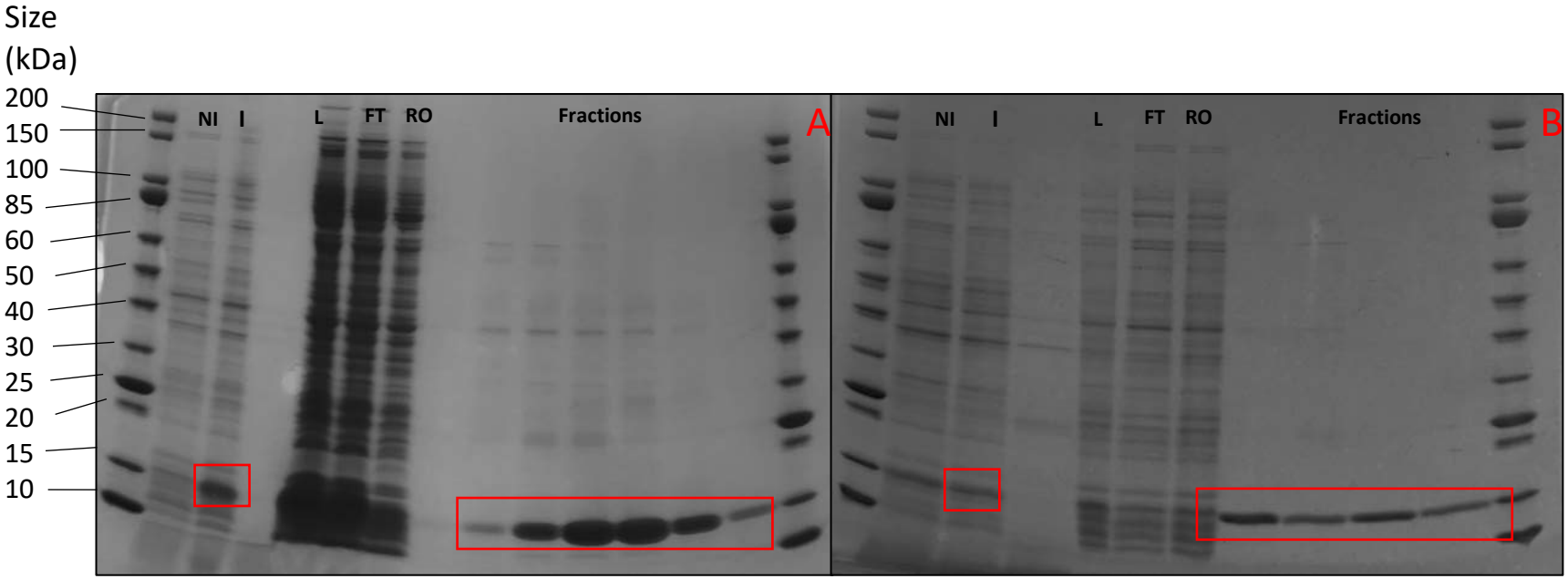

Figure 5.15: HisTrap purification of recombinant RSN-2 harvested from lysed BL21 culture, grown at 37°C and induced with 1mM of IPTG. **A:** Purification attempted with Sodium Phosphate buffer. **B:** Purification attempted with Tris HCL buffer. **Ladder**: NEB 10-200kDa Broad range marker. . **Running order: NI** not induced culture, **I** induced culture, **L** lysed cells, **FT** Flow through, **RO** run off from buffer A **F** fractions. Purified protein is highlighted with a red box.

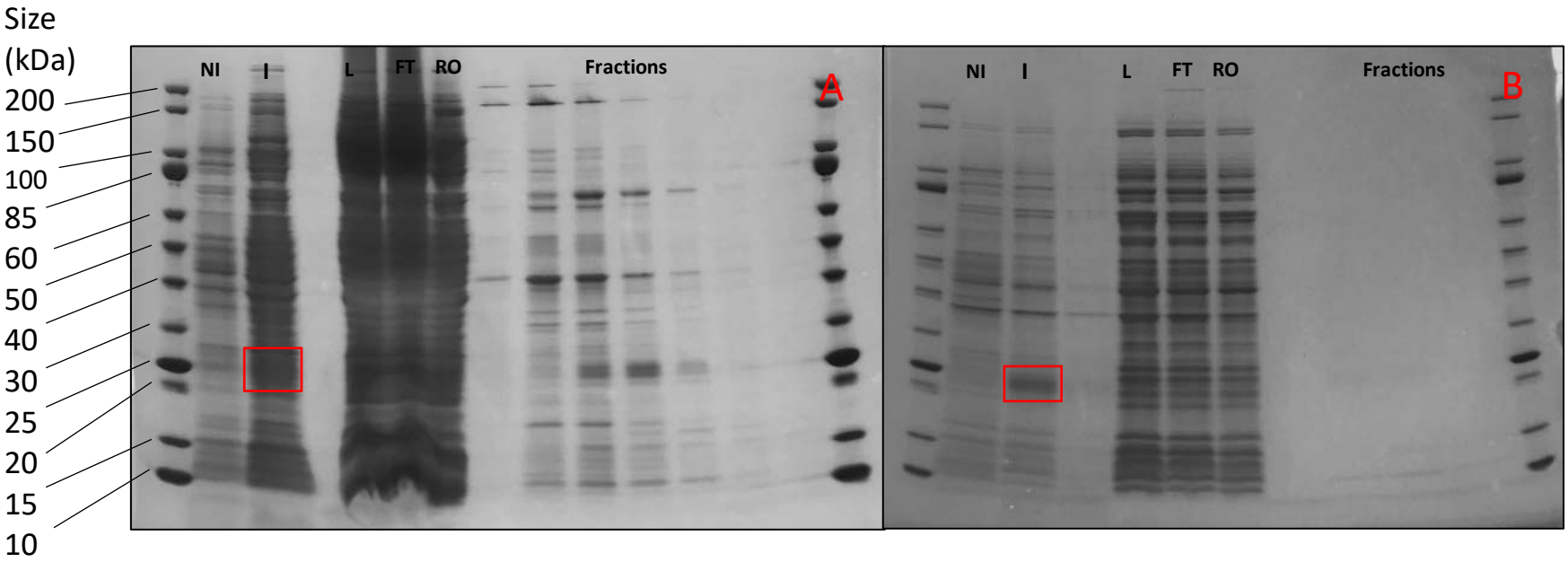

Figure 5.16: HisTrap purification of recombinant RSN-3 harvested from lysed Rosetta culture, grown at 37°C and induced with 1mM of IPTG. **A:** Purification attempted with Sodium Phosphate buffer. **B:** Purification attempted with Tris HCL buffer. **Ladder**: NEB 10-200kDa Broad range marker. . **Running order: NI** not induced culture, **I** induced culture, **L** lysed cells, **FT** Flow through, **RO** run off from buffer A **F** fractions.

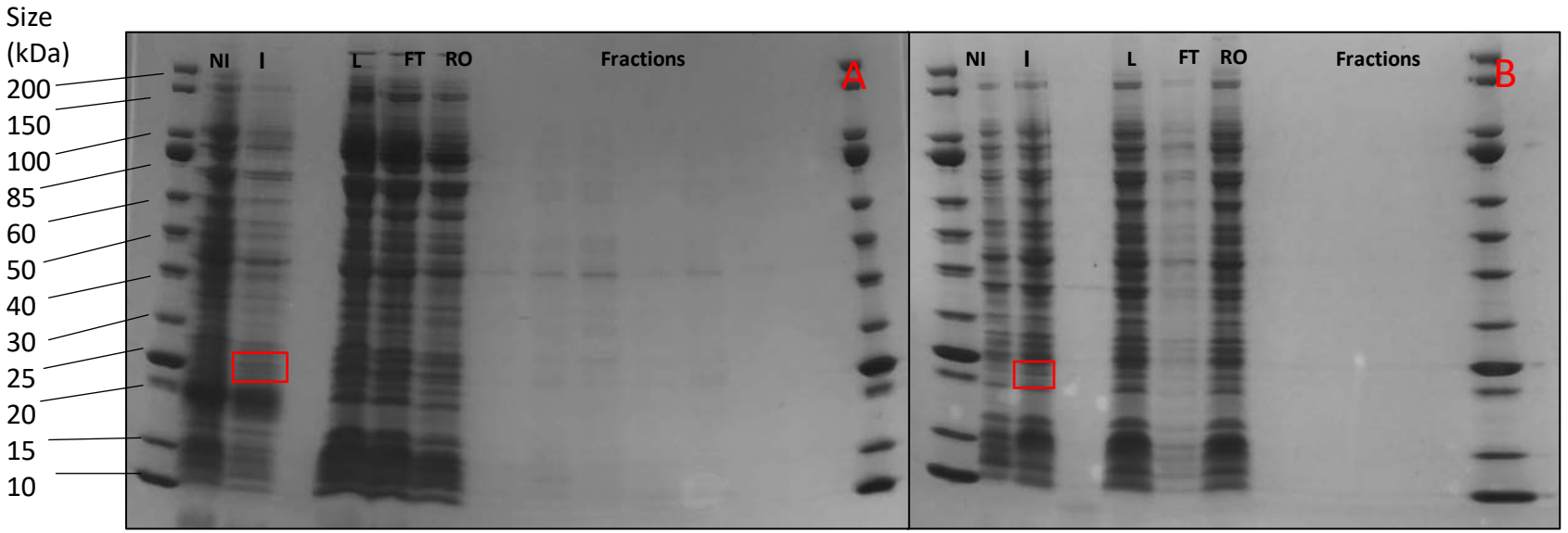

Figure 5.17: HisTrap purification of recombinant RSN-4 harvested from lysed Rosetta culture, grown at 30°C and induced with 1mM of IPTG. **A:** Purification attempted with Sodium Phosphate buffer. **B:** Purification attempted with Tris HCL buffer. **Ladder**: NEB 10-200kDa Broad range marker. . **Running order: NI** not induced culture, **I** induced culture, **L** lysed cells, **FT** Flow through, **RO** run off from buffer A **F** fractions.

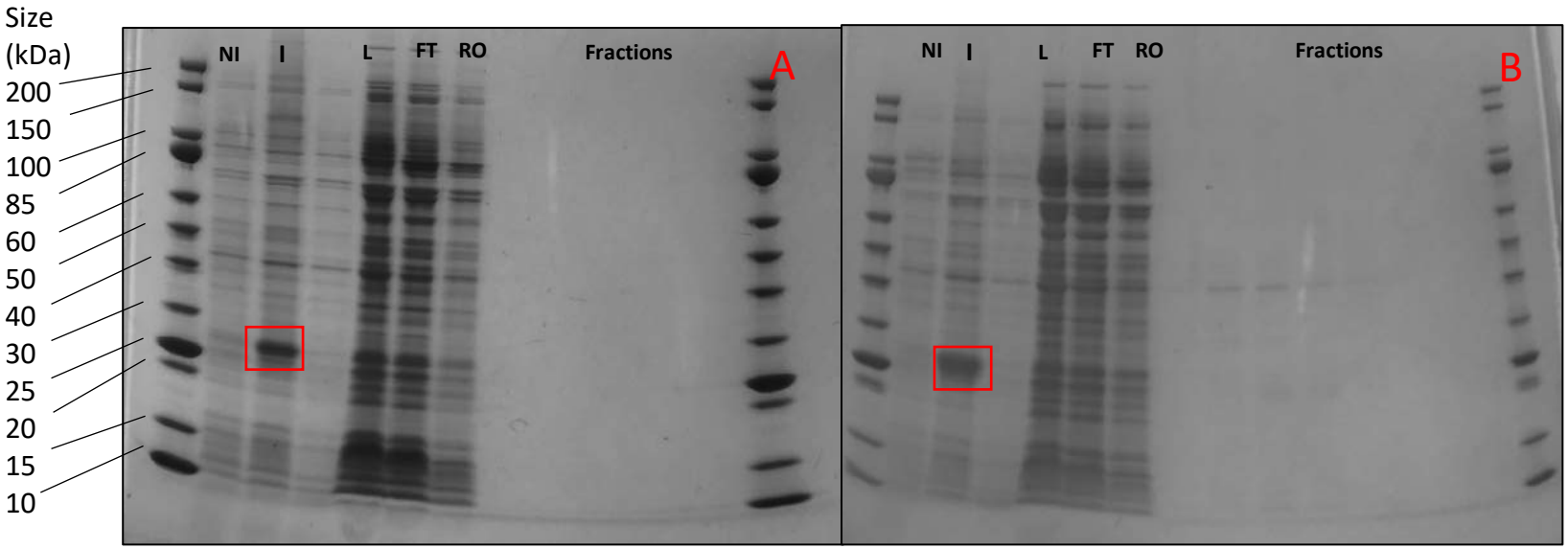

Figure 5.18: HisTrap purification of recombinant RSN-5 harvested from lysed Rosetta culture, grown at 37°C and induced with 0.2mM of IPTG. **A:** Purification attempted with Sodium Phosphate buffer. **B:** Purification attempted with Tris HCL buffer. **Ladder**: NEB 10-200kDa Broad range marker. Running order: Un-induced culture, induced culture, supernatant, lysed cells, column flow through, buffer A run off and fractions.

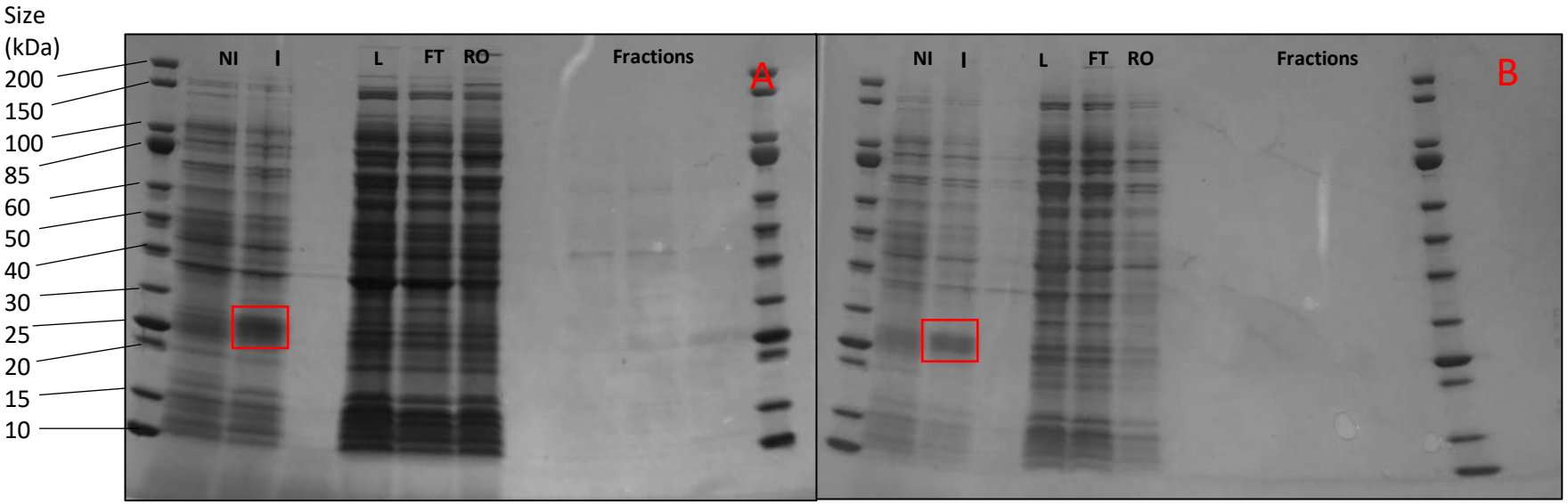

Figure 5.19: HisTrap purification of recombinant RSN-6 harvested from lysed Rosetta culture, grown at 37°C and induced with 0.2 mM of IPTG. **A:** Purification attempted with Sodium Phosphate buffer. **B:** Purification attempted with Tris HCL buffer. Ladder: NEB 10-200kDa Broad range marker. . **Running order: NI** not induced culture, **I** induced culture, **L** lysed cells, **FT** Flow through, **RO** run off from buffer A **F** fractions.

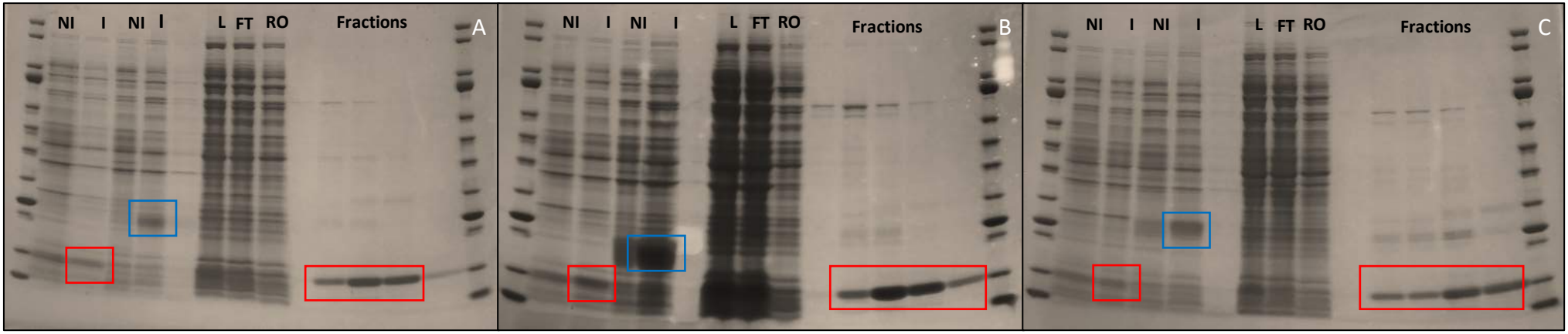

Figure 5.20: SDS-Page analysis of RSN co-purification using HisTrap column. **A** RSN-2 (BL21 37°C) RSN-3 (Rosetta 37°C) co-purification **B** RSN-2 (BL21 37°C) and RSN-5 (Rosetta 37°C) co-purification. **C** RSN-2 (BL21 37°C) and RSN-6 (Rosetta 37°C) co-purification. **Ladder**: NEB 10-200kDa Broad range marker. **Running order: NI** not induced culture, **I** induced culture, **L** lysed cells, **FT** Flow through, **RO** run off from buffer A **F** fractions. Red boxes indicate RSN-2, blue boxes indicate other RSN.

5.4 Summary:

Codon optimized *rsn* genes were sub-cloned into pET28a plasmids, adding an N-terminal HisTag, and used to transform *E. coli* expression strains. Optimum conditions for production of each recombinant Ranaspumin protein were assessed and scaled in preparation for purification. Each Ranaspumin was expressed under their respective conditions, the cells harvested and lysed to be used for purification. IMAC was used to evaluate if purification of recombinant Ranspumins was possible utilizing HisTrap columns and two different buffer sets. RSN-2 was successfully purified. The other Ranaspumins failed to purify which is hypothesized is a result of the inability of the HisTag to strongly bind to the column or issues with solubility.

7.0 Recombinant RSN-2 Analysis

Ranaspumin-2 (RSN-2) is the best characterized protein from the *E. pustulosus* foam nest. RSN-2 is an 11kDa surfactant protein within the foam nest protein mixture. Its structure is described as a single α-helix over a four stranded β-sheet, folded into a globular form. RSN-2 is uniformly polar in solution and its mechanism of action proposed as a conformational change occurring at the air-water interface, where the protein unhinges exposing a hydrophobic region to the air. This conformational change causes the tension at the air-water interface to be reduced and allows for foam formation (MacKenzie *et al*., 2009, Cooper *et al*., 2010). Its role as a surfactant protein has been utilized in other processes including the production of magnetic nanoparticles (Choi *et al* 2012) and studying photosynthetic foam for carbon source production (Wendell *et al.,* 2010). The role it may play in foam drug delivery systems has not been previously explored.

Pharmaceutical foams are widely accepted as useful topical drug delivery systems. These topical foams are usually made up of active agents, solvents and surfactants (Zhao *et al*., 2010). RSN-2 is the surfactant component of *E. pustulosus* foam which has potential as a drug release system so characterization of RSN-2 properties for pharmaceutical use is key to the further development of the foam delivery system. However, it may be relevant to drug delivery as a surfactant in its own standing as current topical release systems also require surfactants to produce reliable and stable foams. Stable foam production, biocompatibility and drug release potential were investigated to identify if RSN-2 alone could be useful in a drug release setting.

7.1 Foam Production:

Recombinant RSN-2 was expressed using a codon optimized *rsn-2* gene in a pET28a plasmid using BL21 *E. coli* cells. It was purified from *E. coli* lysed cells using IMAC via a HisTrap column. The fractions collected during purification of RSN-2 were pooled and concentrated to 10mg/ml, which was confirmed by Bradford assay (Bradford, 1976). SDS-Page was carried out on concentrated samples to ensure purity before being used for further experiments. Purified recombinant RSN-2 was tested to identify if it could be used to produce a foam by adding RSN-2 to water and then agitating the mixture with a pipette. This method is essentially a method analogous to extrusion methods to produce the foam (Dalgetty *et al.,* 2010). This was attempted with 1mg/ml, 0.5mg/ml and 0.1mg/ml of RSN-2 and all three easily formed foams (**Fig 7.1**). The foam looks similar to the foam produced by *E. pustulosus* as it has tightly packed vesicles, but the RSN-2 foam is less dense and less stable. Previous studies have stated that RSN-2 foams for a few minutes and then collapses (Mackenzie *et al*., 2009) and while this was true if the RSN-2 water mixture was vortexed, the foam created from pipetting was stable for much longer. A foam produced using 0.1mg/ml of RSN-2 was monitored for foam stability over time (**Fig 7.2**). Initially the foam produced was around 20mm in height. After 24 hours the foam had started to collapse and was approximately 14mm tall but was still holding a foam like structure. It took four days for RSN-2 foam to collapse to a few small bubbles less than 5mm high, demonstrating that RSN-2 is vital for foam formation in *E. pustulosus* nests but that the remaining five Ranaspumin proteins and complex carbohydrates present are essential for long term persistence of the *E. pustulosus*

foam nests. Producing a foam using recombinant RSN-2 that does not collapse for multiple days is the first step in building a synthetic replicant of the *E. pustulosus* foam. Further, foams are considered to be unstable entities so producing a foam that is stable for multiple days is an important property of RSN-2 which could be exploited for drug delivery as surfactants are required for topical foam release systems (Zhoa *et al.,* 2010). In order to better understand the RSN-2 based foam, further characterisation experiments could be carried out such as those conducted on the whole *E. pustulosus* foam in Chapter 2 such as microscopy, foam density calculations and rheology.

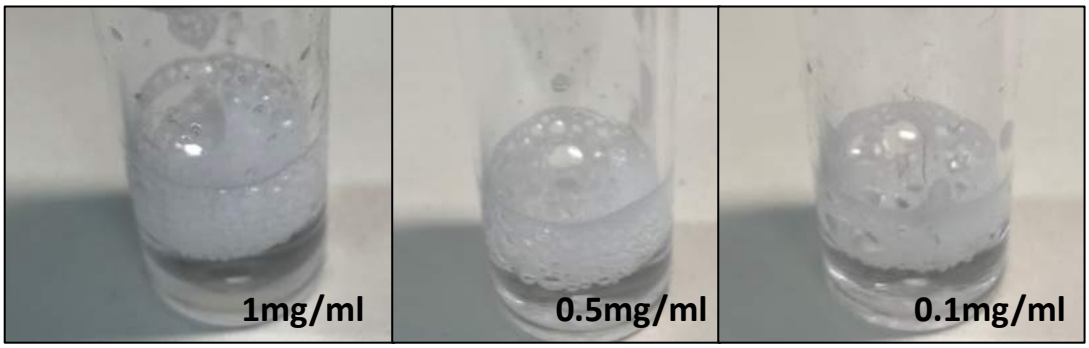

Figure 7.1: Foams produced by multiple concentrations of recombinant RSN-2. Each foam was produced by pushing RSN-2 mixed with distilled water through a 1ml Starlab pipette tip.

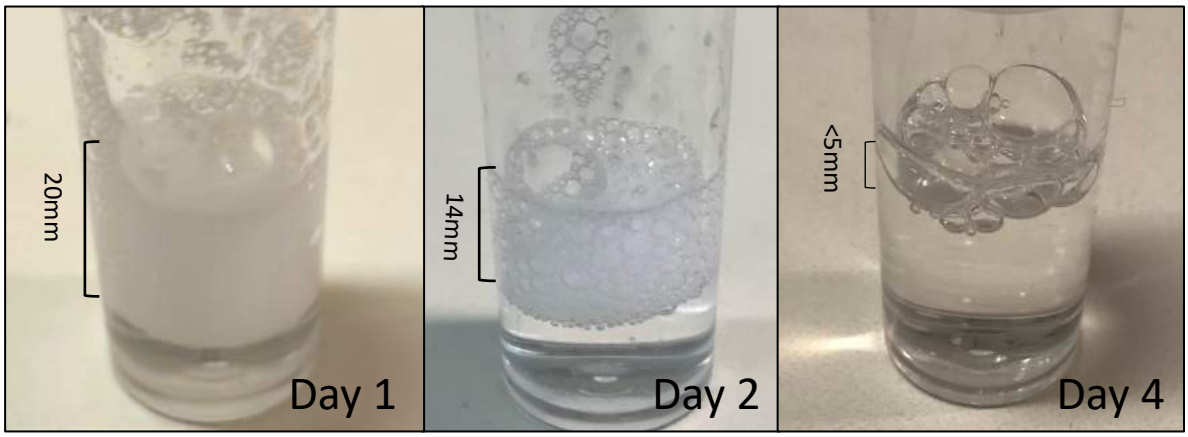

Figure 7.2: Images displaying the collapse of 0.1mg/ml RSN-2 foam over four days. Foam was produced by pushing RSN-2 mixed with distilled water through a 1ml Starlab pipette tip.

7.2 Bacterial Growth Curves:

Previous research has indicated that RSN-2 is non-toxic at low concentrations to eukaryotic cells as it does not damage the sperm or eggs of *E. pustulosus* present in the foam nests, and it is easily over expressed in *E. coli* (MacKenzie *et* al 2009, Fleming *et al.,* 2010). Furthermore, earlier studies carried out during this project showed that solubilized foam does not impact the growth of *E. coli* or *S. aureus* (Chapter 5.0). However, to date no work has been carried out to directly demonstrate the impact of RSN-2 on the growth of bacteria. Bacterial growth curves were carried out in the presence of 1mg/ml, 0.5 mg/ml and 0.1mg/ml of recombinant RSN-2 in LB medium, to investigate any potential antimicrobial activity against Gram-negative (*E. coli*) and Gram-positive (*S. aureus*) organisms. The presence of RSN-2 permitted growth of both Gram-positive and negative species at a range of concentrations. The *E. coli* 8739 strain used was a faecal isolated strain used to test antimicrobial agents, and the *S. aureus* 29213 strain was a wound isolated strain used to test antimicrobial agents (ATCC) making them suitable for this analysis.

Protein concentration was measured using a Bradford assay, and SDS-Page was used to check purified recombinant RSN-2 didn't contain other proteins which could impact results. As RSN-2 was stored in Tris-HCL buffer, a buffer control was added to ensure growth was not reduced by the buffer solution. The positive control contained only media to allow for normal growth, and kanamycin was added negative control to prevent bacterial growth. In both experiments, the buffer control had a slight impact on cell growth. Growth curves were calculated by collecting optical density (OD) every 10 minutes over 12 hours. Data collected

on every hour mark was averaged, and the standard deviation calculated to display any variability in results.

These experiments demonstrated that the growth rate of *E. coli* was significantly reduced by 1mg/ml of RSN-2 protein (**Fig 7.3**). The growth of the positive control was 10 times faster than the positive control. Treatment with 0.5mg/ml and 0.1mg/ml of RSN-2 had no significant effect on the growth rate. The slight reduction in both growth rates can likely be accounted for by the presence of the buffer from purification. The growth of *S. aureus* was also significantly reduced by adding 1mg/ml of RSN-2 (**Fig 7.4**). The growth of the positive control was 6X faster than cell treated with 1mg/ml of RSN-2. The buffer control displayed slightly reduced growth. The growth of cells treated with 0.5mg/ml had a slightly reduced growth rate, and the treatment with 0.1mg/ml had no significant impact on *S. aureus* growth. The growth rates and the p-values calculated for these experiments are displayed in **Table 7.1**. However, no tests were carried out to check the data fell within a normal distribution so the resulting P-values may be inaccurate. These results indicate that at 1mg/ml concentration RSN-2 damages the growth of both *E. coli* and *S. aureus*. However, the concentration necessary for this antimicrobial effect is higher than would naturally occur in a *E. pustulosus* foam nest or be needed for an industrial process, implying that it is unlikely that RSN-2 is cause of antimicrobial protection offered by the foam nests.

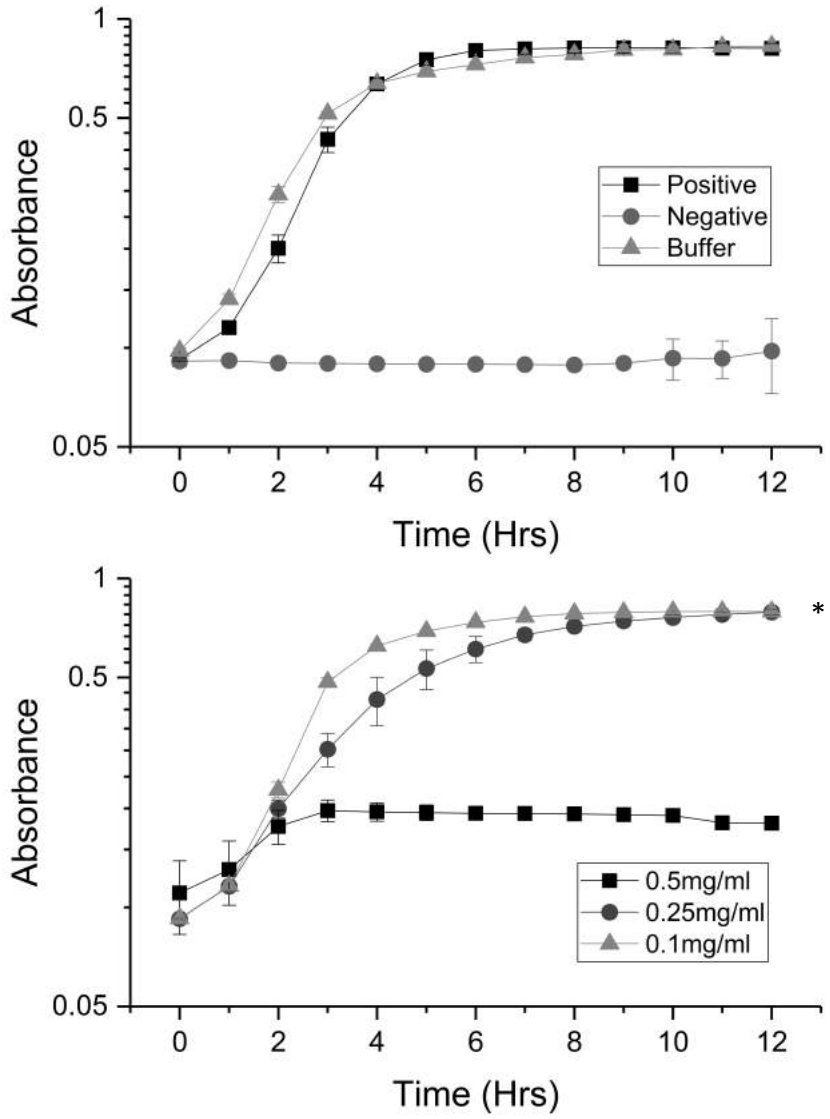

Figure 7.3: Growth curves showing the growth of *E. coli* over 12 hours. Each optical density reading was measured at 600nm in triplicate, and 12 samples were present for each concentration and control. The mean was taken to produce each data point for each hour. Error bars display the standard deviation. P-values are highlighted in **Table 7.1.**

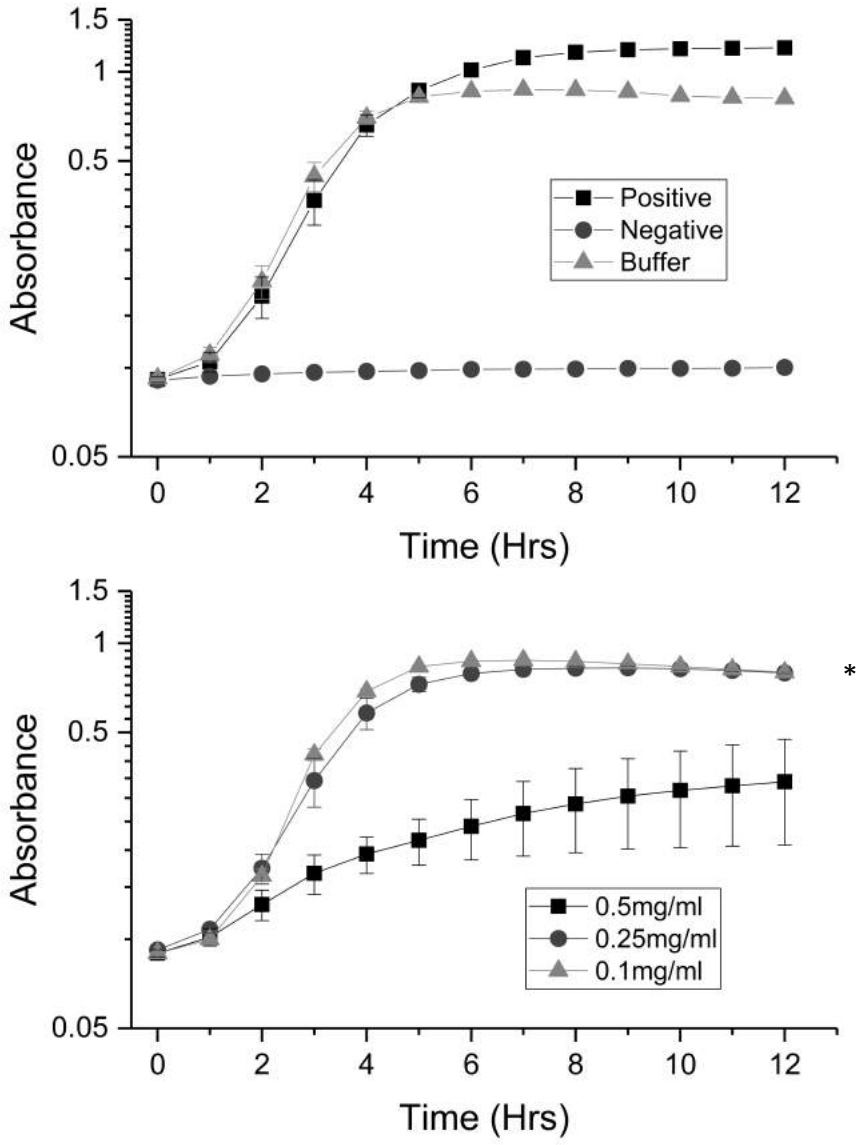

Figure 7.4: Growth curves showing the growth of *S. aureus* over 12 hours. Each optical density reading was measured at 600nm in triplicate, and 12 samples were present for each concentration and control. The mean was taken to produce each data point for each hour. Error bars display the standard deviation. P-values are highlighted in **Table 7.1.**

Table 7.1: Average growth rates of *E. coli and S. aureus*.

P-values calculated using a One-way Anova test, comparing each set of growth rates to the positive control.

	Positive	**Negative**	**Buffer**	**1mg/ml**	**0.5mg/ml**	**0.1mg/ml**
E. coli						
Growth Rate (H^{-1})	0.160	0.001	0.138	0.016	0.104	0.149
P-Value		$5.1x10^{-17}$	0.0920	0.0031	0.0760	0.154
S. aureus						
Growth Rate (H^{-1})	0.190	0.001	0.178	0.029	0.155	0.184
P-Value		$1.39x10^{-15}$	0.0170	0.0009	0.0195	0.7090

7.3 Cell Toxicity:

Biocompatibility is important for any pharmaceutically relevant protein, and for a drug delivery system the toxicity of any given component should be well understood. It is not known if RSN-2 is toxic at any concentration to mammalian cells. Eggs, sperm and tadpoles are not damaged by *E. pustulosus* foam, so at the concentration necessary (0.1mg/ml) for producing a foam nest RSN-2 should not harm mammalian cells. An MTT assay carried out earlier in this research with whole foam enforces this, as solubilized foam did not reduce cell viability of HaCaT cells (Chapter 5). To analyze the impact of recombinant RSN-2 on a mammalian cells an MTT assay was conducted using HaCaT cells. HaCaT cells are an immortal epithelial cell line (Boukamp *et al*., 1988) which have become an established line to use in *in vitro* skin studies (Schoop *et al*., 1999). Similar to the bacterial growth curves, the MTT assays were carried out with a range of concentrations (1mg/ml, 0.5 mg/ml, 0.1mg/ml) and a Tris-HCL buffer control to ensure the buffer RSN-2 was stored in did not have an impact on cell viabilty (**Fig 7.5**). HaCaT cells were incubated with each of the treatments for 24 hours and then the cell metabolic activity was assessed. Cells treated with 1mg/ml of RSN-2 had significantly reduced cell viability when compared to the media only positive control. The remaining treatments had slightly reduced cell viability in comparison to the positive control. However, this reduction was similar to the buffer control indicating that RSN-2 may not be directly responsible for this. ANOVA tests carried out comparing each treatment to the positive control and the buffer control confirm that the 1mg/ml treatment is statistically different from both the positive control and the buffer control. The other

treatments were statically different from the positive control but not the buffer control, indicating that RSN-2 was not responsible for the decreased cell viability in these treatments. However, no tests were carried out to check the data fell within a normal distribution, so the resulting P-values may be inaccurate. Surfactants often damage cells so RSN-2 impacting cell viability at a high concentration is not surprising, but at the lower concentrations which would be required for producing a foam for a drug delivery system *in vitro* data indicates that it should not harm epithelial cells. This shows that RSN-2 is potentially safe for use as part of a foam drug delivery system. It would be useful to carry out similar experiments for a longer treatment time, which would be similar in length to drug release experiments carried out in previous chapters. In order to investigate the safety of the foam even further, *in vivo* animal models would be required as there is no current data available describing immunogenicity to these proteins.

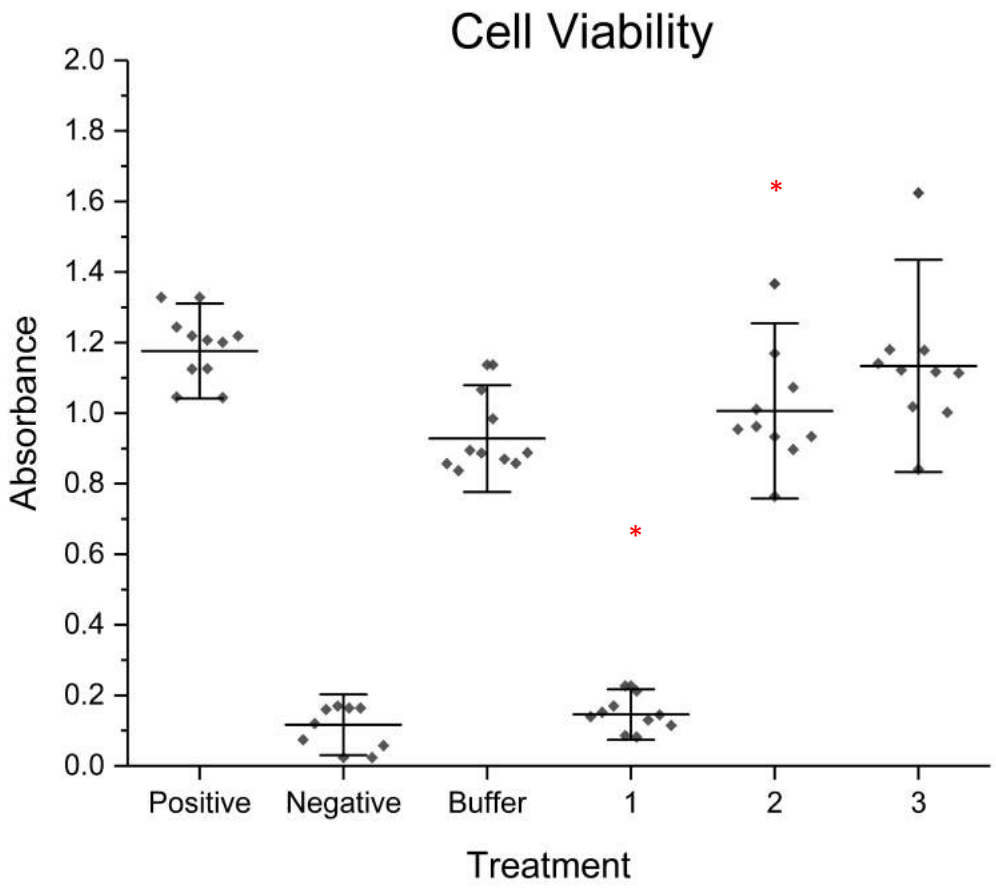

Figure 7.5: Cell viability of HaCaT cells treated for 24 hours with different concentrations of recombinant RSN-2. **Treatment 1**: 1mg/ml RSN-2. **Treatment 2**: 0.5mg/ml. RSN-2 **Treatment 3**: 0.1mg/ml RSN-2. Nine replicates were carried out for each treatment and the controls. Centre line indicates the mean, and upper and lower lines indicate the standard deviation. One way ANOVA tests were carried out and * indicate samples which have a $p < 0.05$ in comparison to the positive control. P values for each treatment are: 2.48×10^{-17}, 0.012 and 0.05 respectively.

7.4 Drug Release:

Topical foams are an established method for dermal drug delivery and many of these foams are made of a surfactant drug combination which collapses quickly upon application to deliver its load onto the skin (Zhoa *et al* 2010). The overall aim of this research was to develop a topical drug release system using *E. pustulosus* foam. This could not be fully investigated as the majority of the RSN proteins were unable to be purified to try and produce a synthetic *E. pustulosus* foam. However, RSN-2 is a surfactant protein and a foam could be produced to investigate if RSN-2 itself could be used as part of a foam drug delivery system.

Nile Red is a model dye frequently used to study *in vitro* release (Borgia *et al* 2005). Previous research carried out highlighted that Nile red had the most stable release from *E. pustulosus* foam (Chapter 5.0), so it was decided to use this to investigate RSN-2 foams drug release potential. A foam was produced by mixing RSN-2 with Nile Red and agitated using a pipette. The foam created was then used to measure Nile Red release from an RSN-2 based foam using the Transwell method developed earlier in this work (Chapter). 400ul of Nile Red RSN-2 foam was added to a Transwell insert, which was then placed in a 12 well plate well containing 1ml of PBS buffer. A blank, unloaded foam for baseline measurements and a Nile Red control were set up in the same manner. The Nile Red control contained only Nile Red solution with no release vehicle at the same concentration and volume as the foam. This allowed for direct comparison of Nile Red passing through the Transwell insert with and without the addition of foam. The plate set up is displayed in (**Fig 7.6).** Measurements were

collected over 8 hours, in triplicate and the concentration released calculated (**Fig 7.7**). Over 8 hours 400µl of foam released 3.4µg of Nile red in a linear release pattern at an approximate release rate of 0.2µg/H. In comparison, the Nile Red control allowed 9.5µg to pass through the Transwell insert in a burst profile at a rate of around 1.1µg/H. The different between the results indicates that the RSN-2 foam slow and controls the release of Nile Red out with normal equilibrium and linearises the burst release. Due to a limited volume of Nile Red RSN-2 foam, further samples could not be produced, but over the 8 hours the foam did not collapse indicating potential for increased release over a longer time period. These results are promising when compared to other Nile Red release data available which highlight that some nanoparticle-based delivery tends to release in around 30 minutes to 6 hours for dermal delivery (Alvarez-Roman *et al.,* 2004). Others release for longer, around 24 hours, but struggle to release more than 3% of the loaded Nile Red (Borgias *et al.,* 2010). There are other systems with better release than presented for the RSN-2 based foam, but foams are popular with patients for dermal delivery making their development important (Marianecci *et al.,* 2011, Zhao *et al.,* 2010). Further, the RSN-2 foam release could potentially be improved with the addition of other RSN proteins. The ability of an RSN-2 based foam to release Nile Red indicates that RSN-2 could be a useful surfactant in producing short term foam delivery systems, as well as being important in long term foam delivery when mixed together with other RSN proteins. The stability of the RSN-2 foam is lower than the natural foam produced by *E. pustulosus* and does not release as effectively, highlighting the importance of the other RSN proteins as a part of the overall foam mixture.

Overall these results demonstrate that RSN-2 could be used to create a novel foam delivery system with an active agent which would remain stable for a minimum of 8 hours based on these data.

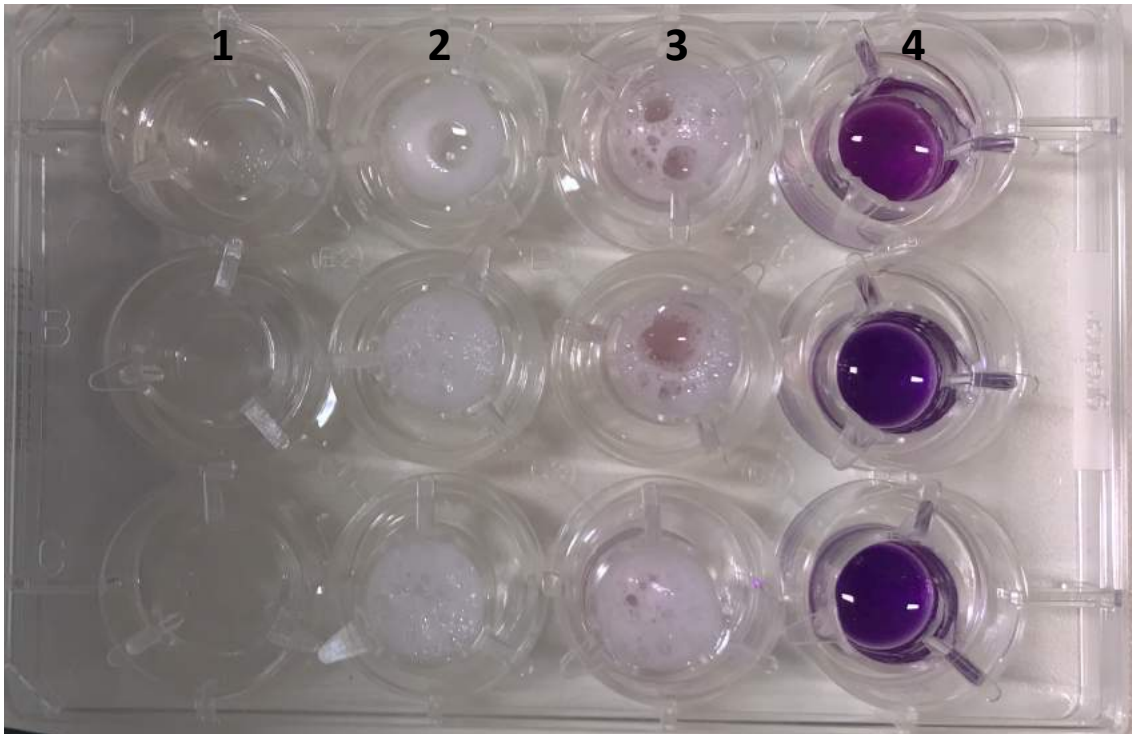

Figure 7.6: Plate layout for RSN-2 foam Transwell release experiment. **1:** Blank wells containing only PBS **2:** Unloaded RSN-2 foam wells for baseline **3:** RSN-2 Nile Red foam wells **4:** Nile Red only control wells. A single plate was used for each time point.

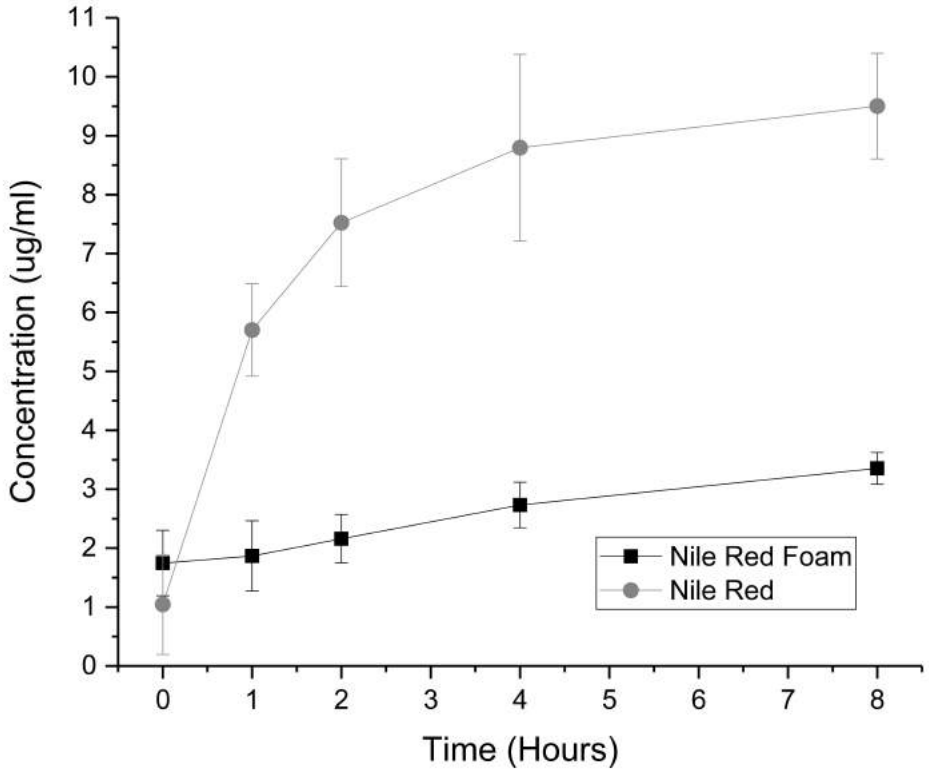

Figure 7.7: Nile Red release from RSN-2 foam and a non-foam control was monitored over 8 hours. Samples were measured at 590nm in triplicate. The concentration of Nile Red released was calculated using a calibration curve against a standard, and the mean concentration for each time point calculated. Error bars indicate the standard deviation. Free Nile Red was used as a control to demonstrate the dyes exchange across the membrane. 3.4µg of Nile Red was released from the RSN-2 based foam over 8 hours in a linear profile.

7.5 Summary:

Recombinant RSN-2 purified during this research can be used to construct a foam at a range of RSN-2 concentrations. Further, the RSN-2 foam produced was stable and took four days to collapse. As RSN-2 is a major component of *E. pustulosus* foam it was important to assess its impact on cells in the context of a pharmaceutical product. Bacterial growth curves were carried out and 1mg/ml concentrations of RSN-2 prevent the growth of *E. coli* and *S. aureus*. MTT assays were conducted and demonstrated that 1mg/ml concentrations of RSN-2 reduce cell viability, but lower concentrations which would be required for a drug delivery foam did not damage cell viability. A Nile Red loaded RSN-2 foam was created and utilized in dye release experiments using a Transwell insert method. The data collected indicated that an RSN-2 foam can successfully release Nile Red in a linear release pattern over 8 hours. RSN-2 protein appears to be non-toxic to epithelial cells at the concentrations required to form a reliable foam, and this concentration of foam can release model dyes indicating that RSN-2 has potential as a topical drug release system. Further, if other RSN proteins can be purified and utilized with the main surfactant protein a more stable foam release system could potentially be produced.

7.0 General Discussion

The foam nests built by *Engystomops pustulosus* have incredible properties. They protect developing tadpoles from environmental stress, insect predation and microbial degradation. These natural incubation chambers are highly stable under tropical conditions and do not cause damage to sperm, eggs or tadpole despite the presence of a surfactant protein (Cooper *et al.,* 2009). The aims of this project were to investigate the basic biophysical properties of the foams and explores the medical and pharmaceutical potential of the foam nests built by *Engystomops pustulosus*. Then using this knowledge, the aim was to attempt to build a synthetic version of the foam. There is a major gap in the drug delivery field, with no existing research considering how natural foams could be utilised for topical treatments. This project explored the antimicrobial properties of the foam and its potential as a novel drug delivery system.

7.1 Foam Characterisation and Drug Release

During this research, bioinformatics analysis was carried out on the Ranaspumin (RSN) sequences and identified that multiple RSNs shared sequence similarities with lectin like proteins and proteins of unknown function from a range of amphibian species. The number of amphibian genomes available has increased since the initial research into the RSN proteins was carried out (Buisine *et al.,* 2015, Session *et al.,* 2016, Hammond *et al.,* 2017, Nowoshilow *et al.,* 2018), allowing for new insights to be made. These frog genomes belong to a variety of species across multiple continents providing a more diverse base for comparison. The sequence similarities between RSNs and other putative

amphibian proteins indicates that the RSN proteins may belong to a broader group of proteins present in anurans that have diverse functionality. Further, many of the homologues contained domains that encoded putative carbohydrate binding lectins (Cooper *et al* 2017). These data are significance for two reasons. Firstly, the foams stability is not fully understood, and the presence of lectins implies that carbohydrate crosslinking may be required to maintain the foams structure. The potential lectin functionality of these proteins is key information when attempting to build a synthetic foam structure. Secondly, lectins often interact with bacteria and these proteins may have important antimicrobial functions (Pistole., 1981) and may explain why the foams are not over grown by microorganisms in the environment. The updated bioinformatics analysis from this research also highlights that RSN-2, the surfactant protein in the foam mixture, remains a unique protein yielding no blast hits from the NCBI database. Unfortunately, it was not possible to produce reasonable structural models for the RSN proteins using the I-TASSER suite. Programs for protein structure modelling rely on identifying solved protein structures with similar sequence motifs to the input sequence and using them as a template for building a model (Roy *et al.,* 2010). The pitfall with this approach is that it relies on similar structures being available in the reference database. The RSNs are not easily comparable to other proteins, and this restricts the usefulness of any structural models generated.

The next logical step in this research was to characterise the foam, especially in the context of a pharmaceutical foam. Many of the methods used had to be improvised or

adapted from characterisations of foams which collapse quickly, or other drug delivery systems. SDS-PAGE, CD and FTIR confirmed that the foam collected contained the six Ranaspumin proteins as prior studies have highlighted, and that the foam proteins are not changed by the centrifugation step used to make them soluble. This meant that the soluble proteins could be used for a range of measurements where the whole foam was impractical. Measurements showed that the foam is low-density, and this is an important quality for a pharmaceutical foam. Low-density foams are considered to be more comfortable when applied topically, particularly in comparison to topical creams, that are less comfortable and feel heavy upon application (Arzhavitina *et al.,* 2010). Rheology data is rarely collected for foams (Arzhavitina *et al.,* 2010), due to their instability, so these data are novel and provided insight into how highly stable foams respond to stress. These experiments proved technically demanding, however they highlight the stability of the foam under shear-stress conditions and demonstrated that the foams elasticity increases as it undergoes coarsening, instead of causing complete structural collapse as is often observed (Kealy *et al.,* 2007). This is important for a topical drug release system as it has to be able to withstand the exterior pressures if it is going to be utilised as a long-term treatment/delivery system. These types of release systems have to be able to withstand itching, rubbing and potentially being wrapped with a bandage so high stability is crucial. The biocompatibility of pharmaceutical foams is a key consideration in the clinic. Using cell viability assays with the epithelial cell line, HaCaT, demonstrated that the foam mixture does not damage the cells and at some concentrations may

stabilise the cells and even improve cell viability. *E. pustulosus* has evolved the use of a foam nest as a strategy to provide its developing eggs with a safe, stable environment to develop. There is anecdotal evidence that the foam nests may aid the growth of the tadpoles although this hasn't been clearly determined, yet with this in mind, the foam components may improve the growth of the cells. Regardless of whether the foam has a genuinely positive impact on epithelial cells, the components did not have a detrimental effect, and this is a good initial indicator for biocompatibility of the foam and the potential for safe use of the foam as a topical release system. However, with this information in mind it's clear that a full toxicology study using mice should be carried out to clearly define the impact on the foam on a whole organism. To study any potential antimicrobial properties of the *Engystomops pustulosus* foam, an assessment of bacterial viability when in contact with the foam proteins was performed. These showed that the soluble foam components did not prevent the growth of Gram-positive or Gram-negative bacteria. Previous work has shown that the foam does have some antimicrobial activity (Cooper *et al.,* 2010), however this research indicates that the concentration of foam proteins present is not the cause of this effect. It is possible that the foam structure as a whole prevents the movement of bacteria and that it the cause of the antimicrobial activity, or that the lectin/carbohydrate binding ability of the foams could potentially interfere with peptidoglycan biosynthesis (Pistole., 1981). Overall the whole foam analysis indicated that the foam was a good candidate for a drug delivery system as it is low density, stable and compatible with mammalian cells.

The main feature of a drug release system is to actually release an active agent to its target site. A key aim of this research was to assess the foams ability to uptake and release an antibiotic. Initial drug release testing was carried out using Calcein and Nile Red as model dyes to understand the foams release of both a hydrophobic and a hydrophilic substance. These release tests acted as a proof of concept experiments and demonstrated that the foam could release both dyes which have been used extensively in the literature as model drug molecules (Borgia *et al*., 2005., Maherani *et al*., 2013). The model molecules were released at different rates with different release profiles for up to one week without the foam completely breaking down. Comparing these data with other pharmaceutical foams, which release their payload faster or the foams degrade quickly (Zha*o et al*., 2010) suggests that *Engystomops pustulosus* derived foam has great potential. Dye release experiments were carried out using a dynamic dialysis method to make it comparable to other drug release profiling data available in the literature. However, one issue with this testing method was that it did not represent the exchange that would occur in a topical release system. To address this, a novel method was required to mimic the system in a patient. To analyse how an antibiotic would be released by the foam, a novel method using Transwell membrane inserts was designed in order to have a model closer to that of a topical system. This method allowed for the exchange of an antibiotic to be monitored across a single membrane instead of a fully submerged dialysis set up. The dynamic dialysis method was still conducted to allow comparison to the Nile Red and Calcein results. The downside of using the Transwell

membrane system was that each replicate required one Transwell insert per time point making the set up more time consuming and involving more equipment and foam than the dynamic dialysis set up. However, the Transwell method eliminated the need for calculating the dilution involved in a dialysis experiment from constantly taking samples and replacing buffer due to sink conditions reducing the overall error. Rifampicin was chosen as it is a red-pigmented antibiotic, which made it easy to measure the drug release by absorbance (475nm). If other antibiotics were to be tested for this research a HPLC method could be employed to improve accuracy, but this would be more expensive and time consuming than absorbance-based measurements. The aim of these experiments was to clearly demonstrate that *E. pustulosus* foam could release an antibiotic for a time-period longer than a typical foam release system. The antibiotic release proved that the foam could release an active agent over 48 hours in both methods tested. The release experiments also highlighted that the foam did not fully collapse over this time indicating it could be used to release for longer than the test period. This data combined with the whole foam analysis makes *E. pustulosus* foam a convincing candidate for a novel drug release system.

Not only does *E. pustulosus* show promise for drug delivery, but this research opens the question of whether other foam nests could be exploited in a similar manner. There are a number of foams produced by a variety of species which have different textures, compositions and unusual properties (Cooper *et al.,* 2010, Hissa *et al.,* 2016, Cooper *et al.,* 2017, Hill *et al.,* 2017). The foams from *Polypedates leucomystax* are blue in colour

and contain a rare blue pigmented protein called Ranasmurfin (McMahon *et al*., 2006), while foams from *Leptodacylus vastus* contain a surfactant protein, Lv-RSN-1, which is different from RSN-2 (Cavalcante-Hissa *et al.,* 2016). There is huge variety in the nests produced, none have been investigated for drug release or pharmaceutical potential, and this should be explored.

7.2 Protein Expression and Foam Production

The collection and egg removal of *E. pustulosus* foam poses a huge limiting factor in its use as a drug release system. It would be impractical to utilise the foam unless a synthetic version could be produced. Further, the RSN proteins themselves may yield useful medical properties and production of pure versions would allow easier research in to their properties. Frog proteins and peptides have widely demonstrated antimicrobial and antifungal properties (Xu *et al*., 2013). To develop a synthetic foam and investigate the medical properties of the RSN proteins, each *rsn* gene had to be cloned into a vector for overexpression, the overexpression conditions evaluated and each RSN purified. This was by far the most challenging part of this research project. In order to make this process as simple as possible a universal cloning strategy was designed for all six RSN proteins. Each *rsn* gene was codon optimised to increase the chance of the proteins overexpressing well in *E. coli* and the synthesised *rsn* gene was inserted into a pET28a vector. This step posed some difficultly as both *rsn-1* and *rsn-4* were hard to clone into pET28a. Multiple attempts were required to gain enough quality DNA for ligation, and in the end the digested synthetic plasmid and digested pET28a were ligated without any

isolation of the *rsn* gene fragments and the colonies screened with colony PCR to identify correct plasmids. pET28a was used as it has two hexa-histidine tags which can be added to either the C-terminus or N-terminus depending on how the plasmid is cut with restriction enzymes. This meant that if a His-Tag placed on one terminus was buried our problematic during overexpression the His-Tag orientation could easily be moved. Unfortunately, the usefulness of this was not tested due to time constraints but provides a bank of clones that can be further manipulated in future work. A variety of bacterial expression strains, temperatures and induction conditions were tested to create the best overexpression conditions possible for each RSN protein. Out of the six RSNs, only RSN-1 was not overexpressed by *E. coli* at any stage of this research. Optimal expression conditions were picked and scaled up for RSN 2-6, and purification was tested for each RSN. Unfortunately, only RSN-2 could be purified using metal affinity chromatography and time did not allow for other protocols to be tested for the other RSNs. Some of the RSN proteins expressed really well but were not soluble. Chemical lysis was chosen as it is fast and simple, however this research would benefit from experimenting with mechanical lysis such a French press or sonication in a more suitable buffer (Graslund *et al*., 2008). Other RSNs expressed well, were soluble after lysis but did the His-Tag did not bind to nickel charged column during purification suggesting that protein folding may bury the tag in the structure, precluding access to the column. Multiple elution buffers were tested to ensure that this could not change the outcome. Moving the HisTag from the N-terminus to the C-terminus could potentially solve this issue. Another approach

would be to attempt purification under denaturing conditions and try to refold the proteins (Graslund *et al*., 2008). This was a limiting step in the research as the properties of the other proteins could not be assessed as a recombinant protein was not obtained. Further, this limited the manner in which a synthetic foam could be produced. An interesting set of experiments would have been to play with the ratio of RSNs concentration and the impact that would have on foam formation, stability and even drug release profile. However, RSN-2 is the surfactant protein in the foam and it purified well so it was decided to carry out some characterisation experiments and investigate the foaming potential of RSN-2.

Despite being utilised in industrial processes and nanoparticle production (Choi *et al.,* 2012, Wendell *et al.,* 2010), there was little information available on the impact of RSN-2 on mammalian or bacterial cells. It was found that high concentrations of RSN-2 damage HaCaT cells, as well as Gram-positive and Gram-negative cells. High concentrations of RSN-2 causing damage is unsurprising as surfactants have negative impacts on cell walls (Denyer and Stewart., 1998, Cooper *et al.,* 2005). However, at the concentrations necessary for foam formation neither mammalian or bacterial cells were affected. Not only is this feature important for the production of a safe synthetic foam, but surfactants are also used in the production of other drug delivery systems such as nanoparticles and liposomes (Choi *et al,* 2012). The use of chemical surfactants in their production is believed to be the cause of some nanoparticles irritant effect (Zhao *et al.,* 2010). It would be interesting to explore if RSN-2 could be utilised in these processes,

given its biocompatibility and if using a less destructive surfactant could impact the efficacy of topical nanoparticulate systems.

Further experiments with RSN-2 demonstrated that the protein could be used to create a foam which was stable for around 48 hours, completely collapsing after 96 hours and a foam could also be created which incorporated Nile Red. This Nile Red loaded foam was used to carry out a Transwell release set up and the release of Nile Red was monitored over 8 hours. These experiments showed that RSN-2 could be used to produce a foam loaded with a model dye and act as a release system. Most pharmaceutical foams available collapse within seconds, and the foam produced in this work functioned as a stable foam release system for two days. The production of an RSN-2 foam was a key step in the production of a novel foam release system and was the first step in achieving the aim of creating a novel drug release system.

7.3 The Overall Impact of a Foam Release System

The interest and research into drug release systems has been growing rapidly (Zhao *et al*., 2010). These systems allow for well-defined active agents to be targeted to particular sites, for drug uptake to be improved or for their overall toxicity to be reduced. In topical applications this can be applied to a range of skin treatments including psoriasis, acne, burns and post-surgical wounds (Purdon *et al.,* 2003). These types of skin treatments require antiseptics, antimicrobials and antibiotics to be delivered directly to the damaged area with an effective concentration whilst keeping patient comfort in mind. Producing a foam release system based on research on *E. pustulosus* foam has multiple

advantages for this kind of delivery. Foams are preferred by patients when compared to the current conventional systems, such as creams and gels (Zhao *et al*., 2010). Foams have fewer issues relating to toxicity and concentration release in comparison to new release systems like nanoparticles and hydrogels. However, long-term foam release has not been previously explored in the literature. The foam investigated here offers a novel concept of providing the advantages of current foam release systems combined with a longer-term delivery model. This work has highlighted the foams ability to release a 'real world drug' (the antibiotic, rifampicin) as well as demonstrating its stability and potential for low toxicity. All of these factors warrant further investigation into naturally occurring stable foams as the basis for a novel type of drug delivery system.

7.4 Future Work

There are multiple avenues for the future work of this research. A protocol should be developed for the purification of each recombinant RSN protein, which would then allow for the characteristics of each protein to be assessed. Production of each RSN protein would not only mean that the antimicrobial properties of each protein could be understood, but each RSNs role within the foam could be more clearly defined. Understanding how the function of each Ranaspumin would lead to the ability to produce a synthetic *E. pustulosus* foam that could be utilised for further drug release research. An interesting part of this would be to fully understand the stoichiometry of the natural foam mixture and is altering the ratio of the RSN proteins to determine this

would alter the stability of the whole foam and if any alterations in the protein combination could improve the foams drug release potential.

On the drug release front, it would be necessary to investigate the foams ability to release other active agents other than an antibiotic. This would broaden the understanding of how this foam could be applicable in a pharmaceutical context. The MTT assays carried out in this work alluded to the potential non-toxicity of the foam but further work is required to assess if the foam could cause any immunogenic response. A general toxicology should be carried out using unloaded foam to investigate the *in vivo* response to the foam or the foam protein components. Alongside this, the foams release potential has only been tested *in vitro*, and an *in vivo* mouse model should be developed to assess the foams ability to release an active agent across a genuine skin barrier. This use of a mouse model would allow for pharmacokinetic/pharmacodynamic modelling to be carried out. Multiple mouse models have been developed to study psoriasis, acne, skin infections and skin burns (Calum *et al.,* 2014, Jang *et al*., 2015, Kugelberg *et al.,* 2005). The models could be utilised to investigate the efficacy of the foam as novel long-term drug release system, which can be loaded with a variety of active agents, as a treatment for skin damage.

There a vast number of amphibians who produce foam nests, and these have huge variety in protein components. The diversity of these foams and their proteins may have value as antimicrobial proteins, novel protein surfactants or as new foam delivery systems. The potential of frog foams should be investigated further.

9.0 References:

Abdel-Mottaleb M, Lamprecht A (2010) Standardized in vitro drug release test for colloidal drug carriers using modified USP dissolution apparatus I. Drug Development and Industrial Pharmacy 37:178–184. doi: 10.3109/03639045.2010.502534

Aboltins C, Page M,(2007) Treatment of staphylococcal prosthetic joint infections with debridement, prosthesis retention and oral rifampicin and fusidic acid. Clinical microbiology infections. 586-91 doi: 10.1111/j.1469-0691.2007.01691.x

Akre KL, Farris HE, Lea AM, et al (2011) Signal perception in frogs and bats and the evolution of mating signals. Science (New York, NY) 333:751–2. doi: 10.1126/science.1205623

Allen TM, Cullis PR (2004) Drug Delivery Systems: Entering the Mainstream. Science 303:1818–1822. doi: 10.1126/science.1095833

Altschul SF, Gish W, Miller W, et al (1990) Basic local alignment search tool. Journal of Molecular Biology 215:403–410. doi: 10.1016/S0022-2836(05)80360-2

Alvarez G, Hélary C, Mebert A, et al (2014) Antibiotic-loaded silica nanoparticle–collagen composite hydrogels with prolonged antimicrobial activity for wound infection prevention. Journal of Materials Chemistry B 2:4660–4670. doi: 10.1039/C4TB00327F

Arzhavitina A, Steckel H (2010) Foams for pharmaceutical and cosmetic application. International Journal of Pharmaceutics 394:1–17. doi: 10.1016/j.ijpharm.2010.04.028

Atiyeh BS, Gunn WS, Hayek SN (2005) State of the Art in Burn Treatment. World Journal of Surgery 29:131–148. doi: 10.1007/s00268-004-1082-2

Azzopardi EA, Azzopardi E, Camilleri L, et al (2014) Gram Negative Wound Infection in Hospitalised Adult Burn Patients-Systematic Review and Metanalysis-. PLoS ONE 9:e95042. doi: 10.1371/journal.pone.0095042

Bertani, G (1951) Studies on Lysogenesis I.: The Mode of Phage Liberation by Lysogenic *Escherichia coli*. Journal of Bacteriology. 293-300

Barillo DJ (2014) Silver in wound care: A review of the state-of-the-art. Burns 40: S1–S2. doi: 10.1016/j.burns.2014.11.007

Barker WC, Garavelli JS, Huang H, et al (2000) The Protein Information Resource (PIR). Nucleic Acids Research 28:41–44. doi: 10.1093/nar/28.1.41

Benetton S, Kedor-Hackmann E, Talanta SM (1998) Visible spectrophotometric and first-derivative UV spectrophotometric determination of rifampicin and isoniazid in pharmaceutical preparations. 639-43

Berman HM, Westbrook J, Feng Z, et al (2000) The Protein Data Bank. Nucleic Acids Research 28:235–242. doi: 10.1093/nar/28.1.235

Bertrand N, Wu J, Xu X, et al (2013) Cancer nanotechnology: The impact of passive and active targeting in the era of modern cancer biology. Advanced Drug Delivery Reviews 2–25

Banyx. F, (1999) Recombinant protein expression in *Escherichia coli*. Current opinion in Biotechnology. 5: 172 https://doi.org/10.1016/S0958-1669(99)00003-8

Blumenthal R (2014) Magnetically Triggered Drug Release from Liposome Embedded Gel. Journal of Nanomedicine & Biotherapeutic Discovery 04: doi: 10.4172/2155-983X.1000130

Boateng, J, S, Matthews, K, H, Stevens, H, N.E, Eccleston, G, N (2008) Wound Healing Dressings and Drug Delivery Systems: A Review. Journal of Pharmaceutical Sciences, VOL. 97, NO. 8.

Bondos SE, Bicknell A (2003) Detection and prevention of protein aggregation before, during, and after purification. Analytical Biochemistry 316:223–231. doi: 10.1016/S0003-2697(03)00059-9

Borgia LS, Regehly M, Sivaramakrishnan R, et al (2005) Lipid nanoparticles for skin penetration enhancement—correlation to drug localization within the particle matrix as determined by fluorescence and parelectric spectroscopy. Journal of Controlled Release 110:151–163. doi: 10.1016/j.jconrel.2005.09.045

Branski LK, Herndon DN, Barrow RE (2012) Total Burn Care (Fourth Edition). 1-7. doi: 10.1016/B978-1-4377-2786-9.00001-1

Buisine N, Ruan X, Bilesimo P, et al (2015) Xenopus tropicalis genome re-scaffolding and re-annotation reach the resolution required for in vivo ChIA-PET analysis. PLOS ONE. doi: 10.1371/journal.pone.0137526

Bureiko A, Trybala A, Kovalchuk N, Starov V (2015) Current applications of foams formed from mixed surfactant–polymer solutions. Advances in Colloid and Interface Science 222:670–677. doi: 10.1016/j.cis.2014.10.001

Calum H, Høiby N (2014) Burn mouse models. *Pseudomonas* Methods and Protocols 793-802 doi: 10.1007/978-1-4939-0473-0_60

Campbell EA, Korzheva N, Mustaev A, et al (2001) Structural Mechanism for Rifampicin Inhibition of Bacterial RNA Polymerase. Cell 104:901–912. doi: 10.1016/S0092-8674(01)00286-0

Carafa M, Marianecci C, Marzio L, et al (2011) A new vesicle-loaded hydrogel system suitable for topical applications: preparation and characterization. Journal of pharmacy & pharmaceutical sciences: a publication of the Canadian Society for Pharmaceutical Sciences, 14:336–46

Chen R (2012) Bacterial expression systems for recombinant protein production*: E. coli* and beyond. Biotechnology Advances 30:1102–1107. doi: 10.1016/j.biotechadv.2011.09.013

Cheng R, Meng F, Deng C, et al (2013) Dual and multi-stimuli responsive polymeric nanoparticles for programmed site-specific drug delivery. Biomaterials 34:3647–3657. doi: 10.1016/j.biomaterials.2013.01.084

Cheng Y, Morshed RA, Auffinger B, et al (2014) Multifunctional nanoparticles for brain tumor imaging and therapy. Advanced Drug Delivery Reviews 66:42–57. doi: 10.1016/j.addr.2013.09.006

Cheong (2001) Wound Dressing Comprising Polyurethane Foam. United States Patent.

Choi H-J, Ebersbacher CF, Myung NV, Montemagno CD (2012) Synthesis of nanoparticles with frog foam nest proteins. Journal of Nanoparticle Research: 14-19. doi: 10.1007/s11051-012-1092-1

Choi H-J, Ebersbacher CF, Quan F-S, Montemagno CD (2013a) pH stability and comparative evaluation of ranaspumin-2 foam for application in biochemical reactors. Nanotechnology 24:55-63. doi: 10.1088/0957-4484/24/5/055603

Choi H-J, Stazak TJ, Montemagno CD, et al (2013) Surface-dependent cytotoxicity on bacteria as a model for environmental stress of halloysite nanotubes. 15:2008 Journal of Nanoparticle Research. doi: 10.1007/s11051-013-2008-4

Church D, Elsayed S, Reid O, et al (2006) Burn Wound Infections. Clinical Microbiology Review 19:403–434

Coe, MJ (1967) Co-operation of three males in nest construction by *Chiromantis rufescens* Gunther (Amphibia: Rhacophoridae). Nature. 112–113 doi: 10.1038/214112b0

Consortium S, Gräslund S, Nordlund P, et al (2008) Protein production and purification. Nature Methods 5:135. doi: 10.1038/nmeth.f.202

Cooper A, Kennedy MW (2010) Biofoams and natural protein surfactants. Biophysical Chemistry 151:96–104. doi: 10.1016/j.bpc.2010.06.006

Cooper A, Kennedy MW, Fleming RI, et al (2005) Adsorption of Frog Foam Nest Proteins at the Air-Water Interface. Biophysical Journal 88:2114–2125. doi: 10.1529/biophysj.104.046268

Cooper A, Vance S, Smith B, Kennedy - MWA and (2017) Frog foams and natural protein surfactants. doi: 10.1016/j.colsurfa.2017.01.049

Downie, JR. (1984) How Leptodactylus fuscus tadpoles make foam, and why. Copeia. doi: 10.2307/1445168.

Correa D, Ramos, C. (2009) The use of circular dichroism spectroscopy to study protein folding, form and function. African Journal of Biochemistry Research Vol.3.

Dalgetty L, Kennedy MW (2010) Building a home from foam—túngara frog foam nest architecture and three-phase construction process. Biology Letters 6:293–296. doi: 10.1098/rsbl.2009.0934

Davidson PT, Le H (1992) Drug Treatment of Tuberculosis - 1992. Drugs 43:651–673. doi: 10.2165/00003495-199243050-00003

Delcour AH (2009) Outer membrane permeability and antibiotic resistance. Biochimica et Biophysica Acta (BBA) - Proteins and Proteomics 1794:808–816. doi: 10.1016/j.bbapap.2008.11.005

D'Souza S (2014) A Review of In Vitro Drug Release Test Methods for Nano-Sized Dosage Forms. Advances in Pharmaceutics 2014:1–12. doi: 10.1155/2014/304757

Duellman W, Trueb L (1986) Biology of amphibians.

Dutta A, Kamada K, Ohta K (1996) Spectroscopic studies of nile red in organic solvents and polymers. Journal of Photochemistry and Photobiology A: Chemistry 93:57–64. doi: 10.1016/1010-6030(95)04140-0

Epstein-Barash H, Gutman D, Markovsky E, et al (2010) Physicochemical parameters affecting liposomal bisphosphonates bioactivity for restenosis therapy: Internalization, cell inhibition, activation of cytokines and complement, and mechanism of cell death. Journal of Controlled Release 146:182–195. doi: 10.1016/j.jconrel.2010.03.011

Erama N, Woody RW (2000) Estimation of Protein Secondary Structure from Circular Dichroism Spectra: Comparison of CONTIN, SELCON, and CDSSTR Methods with an Expanded Reference Set. Analytical Biochemistry 287:252–260. doi: 10.1006/abio.2000.4880

Eue I (2001) Growth inhibition of human mammary carcinoma by liposomal hexadecylphosphocholine: Participation of activated macrophages in the antitumor mechanism. International Journal of Cancer 92:426–433. doi: 10.1002/ijc.1201

Faraji AH, Wipf P (2009) Nanoparticles in cellular drug delivery. Bioorganic & Medicinal Chemistry 17:2950–2962. doi: 10.1016/j.bmc.2009.02.043

Fleming RI, Mackenzie CD, Cooper A, Kennedy MW (2009) Foam nest components of the túngara frog: a cocktail of proteins conferring physical and biological resilience. Proceedings of the Royal Society B: Biological Sciences 276:1787–1795. doi: 10.1098/rspb.2008.1939

Fomina N, McFearin C, Sermsakdi M, et al (2010) UV and Near-IR Triggered Release from Polymeric Nanoparticles. Journal of the American Chemical Society 132:9540–9542. doi: 10.1021/ja102595j

Frey SL, Todd J, Wurtzler E, et al (2015) A non-foaming proteosurfactant engineered from Ranaspumin-2. Colloids and Surfaces B: Biointerfaces 133:239–245. doi: 10.1016/j.colsurfb.2015.05.043

Gallagher JJ, Branski LK, Williams-Bouyer N, et al (2012) Total Burn Care (Fourth Edition). 137-156.e2. doi: 10.1016/B978-1-4377-2786-9.00012-6

Golding A, Guay JA, Herrera-Rincon C, et al (2016) A Tunable Silk Hydrogel Device for Studying Limb Regeneration in Adult Xenopus Laevis. PLOS ONE doi: 10.1371/journal.pone.0155618

Goyal R, Macri LK, Kaplan HM, Kohn J (2016) Nanoparticles and nanofibers for topical drug delivery. Journal of Controlled Release 240:77–92. doi: 10.1016/j.jconrel.2015.10.049

Gradishar WJ, Tjulandin S, Davidson N, et al (2005) Phase III Trial of Nanoparticle Albumin-Bound Paclitaxel Compared With Polyethylated Castor Oil–Based Paclitaxel in Women With Breast Cancer. Journal of Clinical Oncology 23:7794–7803. doi: 10.1200/JCO.2005.04.937

Greenfield NJ (2007) Using circular dichroism spectra to estimate protein secondary structure. Nature Protocols. 2876–2890. doi: 10.1038/nprot.2006.202

Griffiths PR, Haseth JA (2007) Fourier transform infrared spectrometry. John Wiley & Sons

Griffiths, H.R, Thornton, K.L, Clements, C.M, Burge, T.S, Kay, A.R, Young, A.E.R (2006) The cost of a hot drink scald. Burns, Volume 32, Issue 3, Pages 372-374

Gurtner GC, Werner S, Barrandon Y, Longaker MT (2008) Wound repair and regeneration. Nature 453:314–321. doi: 10.1038/nature07039

Haddad CFB, Hodl W (1997) New Reproductive Mode in Anurans: Bubble Nest in Chiasmocleis leucosticta. Copeia 585–558

Haley B, Frenkel E (2008) Nanoparticles for drug delivery in cancer treatment. Urologic Oncology: Seminars and Original Investigations 26:57–64. doi: 10.1016/j.urolonc.2007.03.015

Hammond S, Warren R, (2017) The North American bullfrog draft genome provides insight into hormonal regulation of long noncoding RNA. Nature. 1433. doi: 10.1038/s41467-017-01316-7

Haney EF, Hunter HN, Matsuzaki K, Vogel HJ (2009) Solution NMR studies of amphibian antimicrobial peptides: Linking structure to function? Biochimica et Biophysica Acta (BBA) - Biomembranes 1788:1639–1655. doi: 10.1016/j.bbamem.2009.01.002

Hawkins MJ, Soon-Shiong P, Desai N (2008) Protein nanoparticles as drug carriers in clinical medicine. Advanced Drug Delivery Reviews 60:876–885. doi: 10.1016/j.addr.2007.08.044

Heunis T, Dicks L (2010) Nanofibers Offer Alternative Ways to the Treatment of Skin Infections. Journal of Biomedicine and Biotechnology 2010:510682. doi: 10.1155/2010/510682

Heyer RW, Rand SA (1977) Foam Nest Construction in the Leptodactylid Frogs Leptodactylus pentadactylus and Physalaemus pustulosus (Amphibia, Anura, Leptodactylidae). Journal of Herpetology 11:225. doi: 10.2307/1563148

Hill C, Eastoe J (2017) Foams: From nature to industry. Advances in Colloid and Interface Science 247:496–513. doi: 10.1016/j.cis.2017.05.013

Hissa D, Bezerra W, Freitas C, et al (2016) Frog Foam Nest Protein Diversity and Synthesis. Journal of Experimental Zoology Part A: Ecological Genetics and Physiology 325:425–433. doi: 10.1002/jez.2027

Hissa D, Vasconcelos I, Carvalho A, et al (2008) Novel surfactant proteins are involved in the structure and stability of foam nests from the frog Leptodactylus vastus. Journal of Experimental Biology 211:2707–2711. doi: 10.1242/jeb.019315

Hoop V, Mirancea N, Fusenig N (1999) Epidermal organization and differentiation of HaCaT keratinocytes in organotypic coculture with human dermal fibroblasts. The Journal of investigative dermatology 112:343–53. doi: 10.1046/j.1523-1747.1999.00524.x

Housman T, Mellen BG, Rapp SR, et al (2002) Patients with psoriasis prefer solution and foam vehicles: a quantitative assessment of vehicle preference. Cutis 70:327–332

Hu L, Olsen C, Maddux N, et al (2011) Investigation of Protein Conformational Stability Employing a Multimodal Spectrometer. Analytical Chemistry 83:9399–9405. doi: 10.1021/ac201995c

Huang T, Dibildox M (2012) The use of skin grafts, skin flaps and tissue expansion in burn deformity reconstruction. In: Total Burn Care

Iakoucheva LM, Brown CJ, Lawson J, et al (2002) Intrinsic disorder in cell-signaling and cancer-associated proteins. Journal of molecular biology 323:573–84

III HA, Rugo HS, Vukelja SJ, et al (2010) Phase II Study of the Antibody Drug Conjugate Trastuzumab-DM1 for the Treatment of Human Epidermal Growth Factor Receptor 2 (HER2) –Positive Breast Cancer After Prior HER2-Directed Therapy. Journal of Clinical Oncology 29:398–405. doi: 10.1200/JCO.2010.29.5865

Jang Y, Lee K, Lee S-J, et al (2014) HR-1 Mice: A New Inflammatory Acne Mouse Model. Annals of Dermatology 27:257–264. doi: 10.5021/ad.2015.27.3.257

Jeník J (2002) Tropical Forest Ecology: a View from Barro Colorado Island. Springer.

Johal H, Garg T, Rath G, Goyal A (2014) Advanced topical drug delivery system for the management of vaginal candidiasis. Drug Delivery 23:550–563. doi: 10.3109/10717544.2014.928760

Jones SM, Morgan M, Humphrey TJ, Lappin-Scott H (2001) Effect of vancomycin and rifampicin on meticillin-resistant *Staphylococcus aureus* biofilms. The Lancet 357:40–41

Jong DW, Borm, PJA (2008) Drug delivery and nanoparticles: applications and hazards. International Journal of Nanomedicine. 133–149

Kealy T, Abram A, Hunt B, Buchta R (2008) The rheological properties of pharmaceutical foam: Implications for use. International Journal of Pharmaceutics 355:67–80. doi: 10.1016/j.ijpharm.2007.11.057

Kelly SM, Jess TJ, Price NC (2005) How to study proteins by circular dichroism. Biochimica et Biophysica Acta (BBA) - Proteins and Proteomics 1751:119–139. doi: 10.1016/j.bbapap.2005.06.005

Killion JJ, Fidler IJ (1998) Therapy of Cancer Metastasis by Tumoricidal Activation of Tissue Macrophages Using Liposome-Encapsulated Immunomodulators. Pharmacology & Therapeutics 78:141–154. doi: 10.1016/S0163-7258(98)00004-7

King JD, Leprince J, Vaudry H, et al (2008) Purification and characterization of antimicrobial peptides from the Caribbean frog, *Leptodactylus validus* (Anura: Leptodactylidae). Peptides 29:1287–1292. doi: 10.1016/j.peptides.2008.04.005

Kluger R, Alagic A (2004) Chemical cross-linking and protein–protein interactions—a review with illustrative protocols. Bioorganic Chemistry 32:451–472. doi: 10.1016/j.bioorg.2004.08.002

Kraft JC, Freeling JP, Wang Z, Ho RJ (2014) Emerging Research and Clinical Development Trends of Liposome and Lipid Nanoparticle Drug Delivery Systems. Journal of Pharmaceutical Sciences 103:29–52. doi: 10.1002/jps.23773

Krychowiak M, Grinholc M, Banasiuk R, et al (2014) Combination of Silver Nanoparticles and Drosera binata Extract as a Possible Alternative for Antibiotic Treatment of Burn

Wound Infections Caused by Resistant *Staphylococcus aureus*. PLoS ONE. doi: 10.1371/journal.pone.0115727

Kugelberg E , Norström, T(2005) Establishment of a superficial skin infection model in mice by using *Staphylococcus aureus* and *Streptococcus pyogenes*. Antimicrobial agents chemotherapy 3435-41. doi: 10.1128/AAC.49.8.3435-3441.2005

Leigh E (1999) Tropical forest ecology: a view from Barro Colorado Island
Lewis G, M, Heimbach D, M, Gibran N, (2002) Evaluation of the burn wound management decisions. Total Burn Care.

Litvinchuk S, Lu Z, Rigler P, et al (2009) Calcein Release from Polymeric Vesicles in Blood Plasma and PVA Hydrogel. Pharmaceutical Research 26:1711–1717. doi: 10.1007/s11095-009-9881-7

Lu X-Y, Wu D-C, Li Z-J, Chen G-Q (2011) Progress in Molecular Biology and Translational Science. 104:299–323. doi: 10.1016/B978-0-12-416020-0.00007-3

Ma T, Wang L, TingyuanYang, et al (2014) PLGA–lipid liposphere as a promising platform for oral delivery of proteins. Colloids and Surfaces B: Biointerfaces 117:512–519. doi: 10.1016/j.colsurfb.2014.02.039

Mackenzie CD, Smith BO, Meister A, et al (2009) Ranaspumin-2: structure and function of a surfactant protein from the foam nests of a tropical frog. Biophysical journal 96:4984–4992 doi: 10.1016/j.bpj.2009.03.044

Mackenzie CD, Smith BO, Meister A, et al (2009) Ranaspumin-2: Structure and Function of a Surfactant Protein from the Foam Nests of a Tropical Frog. Biophysical Journal 96:4984–4992. doi: 10.1016/j.bpj.2009.03.044

MacMillan B (1981) The control of burn wound sepsis. Intensive Care Medicine 7:63–69. doi: 10.1007/BF01687262

Maherani B, Arab-Tehrany E, Kheirolomoom A, et al (2013) Calcein release behavior from liposomal bilayer; influence of physicochemical/mechanical/structural properties of lipids. Biochimie 95:2018–2033. doi: 10.1016/j.biochi.2013.07.006

Marze S, Guillermic R, Saint-Jalmes A (2009) Oscillatory rheology of aqueous foams: surfactant, liquid fraction, experimental protocol and aging effects. Soft Matter 5:1937–1946. doi: 10.1039/B817543H

Marze SPL, Saint-Jalmes A, Langevin D (2005) Protein and surfactant foams: linear rheology and dilatancy effect. Colloids and Surfaces A: Physicochemical and Engineering Aspects 263:121–128. doi: 10.1016/j.colsurfa.2005.01.014

Mazzeo, FA (2008) Importance of Oscillatory Time sweep in rheology. TA Instruments manual.

McMahon SA, Walsh MA, Ching RTY, et al (2006) Crystallization of Ranasmurfin, a blue-coloured protein from *Polypedates leucomystax*. Acta Crystallographica Section F: Structural Biology and Crystallization Communications 62:1124–1126. doi: 10.1107/S1744309106040036

Mi F, Wu Y, Shyu S, et al (2002) Control of wound infections using a bilayer chitosan wound dressing with sustainable antibiotic delivery. Journal of Biomedical Materials Research 59:438–449. doi: 10.1002/jbm.1260

Modi S, Anderson BD (2013) Determination of Drug Release Kinetics from Nanoparticles: Overcoming Pitfalls of the Dynamic Dialysis Method. Molecular Pharmaceutics 10:3076–3089. doi: 10.1021/mp400154a

Mody VV, Cox A, Shah S, et al (2014) Magnetic nanoparticle drug delivery systems for targeting tumor. Applied Nanoscience 4:385–392. doi: 10.1007/s13204-013-0216-y

Mogoşanu G, Grumezescu A (2014) Natural and synthetic polymers for wounds and burns dressing. International Journal of Pharmaceutics 463:127–136. doi: 10.1016/j.ijpharm.2013.12.015

Morey M, Pandit A (2018) Responsive triggering systems for delivery in chronic wound healing. Advanced drug delivery reviews. 169-193 doi: 10.1016/j.addr.2018.02.008

Morris RJ, Brandani GB, Desai V, et al (2016) The Conformation of Interfacially Adsorbed Ranaspumin-2 is an Arrested State on the Unfolding Pathway. Biophysical Journal. 732-742. doi: 10.1016/j.bpj.2016.06.006

Murzin AG, Murzin AG (1992) Structural principles for the propeller assembly of sheets: the preference for sevenfold symmetry. Proteins: Structure, Function, and Bioinformatics 14:191–201. doi: 10.1002/prot.340140206

Naik A, Kalia Y, Guy R, research FH (2004) Enhancement of topical delivery from biodegradable nanoparticles. doi: 10.1023/B:PHAM.0000045235.86197.ef

Ng S-F, Rouse JJ, Sanderson FD, et al (2010) Validation of a Static Franz Diffusion Cell System for In Vitro Permeation Studies. AAPS PharmSciTech 11:1432–1441. doi: 10.1208/s12249-010-9522-9

Nielsen SL, Frimodt-Møller N, Kragelund BB, Hansen PR (2007) Structure–activity study of the antibacterial peptide fallaxin. Protein Science 16:1969–1976. doi: 10.1110/ps.072966007

Nowoshilow S, Schloissnig S, Fei J-F, et al (2018) The axolotl genome and the evolution of key tissue formation regulators. Nature 554:50. doi: 10.1038/nature25458

Orive G, Hernández R, Gascón A, et al (2003) Drug delivery in biotechnology: present and future. Current Opinion in Biotechnology 14:659–664. doi: 10.1016/j.copbio.2003.10.007

P&G (2015) Shaving compositions. US Patent.

Pardeike J, Hommoss A, Müller RH (2009) Lipid nanoparticles (SLN, NLC) in cosmetic and pharmaceutical dermal products. International Journal of Pharmaceutics 366:170–184. doi: 10.1016/j.ijpharm.2008.10.003

Peti W, Page R (2007) Strategies to maximize heterologous protein expression in *Escherichia coli* with minimal cost. Protein expression and purification 51:1–10

Peti W, Page R (2007) Strategies to maximize heterologous protein expression in *Escherichia coli* with minimal cost. Protein expression and purification 51:1–10. doi: 10.1016/j.pep.2006.06.024

Piazza L, Gigli J, Bulbarello A (2008) Interfacial rheology study of espresso coffee foam structure and properties. Journal of Food Engineering 84:420–429. doi: 10.1016/j.jfoodeng.2007.06.001

Pistole, TG (1981) Interaction of bacteria and fungi with lectins and lectin-like substances. Annual Reviews Microbiology doi: 10.1146/annurev.mi.35.100181.000505

Prausnitz MR, Langer R (2008) Transdermal drug delivery. Nature Biotechnology doi: 10.1038/nbt.1504

Purdon CH, Haigh JM, Surber C, Smith EW (2003) Foam Drug Delivery in Dermatology. American Journal of Drug Delivery 1:71–75. doi: 10.2165/00137696-200301010-00006

Pyron AR, Wiens JJ (2011) A large-scale phylogeny of Amphibia including over 2800 species, and a revised classification of extant frogs, salamanders, and caecilians. Molecular Phylogenetics and Evolution 61:543–583. doi: 10.1016/j.ympev.2011.06.012

Qin J, Li R, Raes J, et al (2010) A human gut microbial gene catalogue established by metagenomic sequencing. Nature. 59–65 doi: 10.1038/nature08821

Rinaldi AC (2002) Antimicrobial peptides from amphibian skin: an expanding scenario: Commentary. Current Opinion in Chemical Biology 6:799–804. doi: 10.1016/S1367-5931(02)00401-5

Riss TL, Moravec RA, Minor L (2016) Cell Viability Assays. Assay Guidence Manual

Roberts, Mohammed Y, Pastore M, et al (2017) Topical and cutaneous delivery using nanosystems. Journal of Controlled Release 247:86–105. doi: 10.1016/j.jconrel.2016.12.022

Rodgers, M, Epstein, D, Bojke, L, Yang, H, Craig, D, Fonseca, T, Myers, L, Bruce,I Chalmers, S Bujkiewicz, Woolacott, N (2011) Etanercept, infliximab and adalimumab for the treatment of psoriatic arthritis:a systematic review and economic evaluation. Health Technology Assessment 2011; Vol. 15: No. 10

Rollins-Smith LA, King JD, Nielsen PF, et al (2005) An antimicrobial peptide from the skin secretions of the mountain chicken frog *Leptodactylus fallax* (Anura: Leptodactylidae). Regulatory Peptides 124:173–178. doi: 10.1016/j.regpep.2004.07.013

Ron SR, Santos JC, Cannatella DC (2006) Phylogeny of the túngara frog genus *Engystomops* (= Physalaemus pustulosus species group; Anura: Leptodactylidae). Molecular phylogenetics and evolution 39:392–403. doi: 10.1016/j.ympev.2005.11.022

Rosenholm JM, Sahlgren C, Lindén M (2010) Towards multifunctional, targeted drug delivery systems using mesoporous silica nanoparticles – opportunities & challenges. Nanoscale 2:1870–1883. doi: 10.1039/C0NR00156B

Roy A, Kucukural A, Zhang Y (2010) I-TASSER: a unified platform for automated protein structure and function prediction. Nature Protocols. doi: 10.1038/nprot.2010.5

Ryan MJ (1983) SEXUAL SELECTION AND COMMUNICATION IN A NEOTROPICAL FROG, *PHYSALAEMUS PUSTULOSUS*. Evolution; international journal of organic evolution 37:261–272. doi: 10.1111/j.1558-5646.1983.tb05536.x

Ryan MJ, Rand SA (1990) THE SENSORY BASIS OF SEXUAL SELECTION FOR COMPLEX CALLS IN THE TÚNGARA FROG, *PHYSALAEMUS PUSTULOSUS* (SEXUAL SELECTION FOR SENSORY EXPLOITATION). Evolution 44:305–314. doi: 10.1111/j.1558-5646.1990.tb05200.x

Sabaeifard P, Abdi-Ali A, Soudi M, et al (2016) Amikacin loaded PLGA nanoparticles against Pseudomonas aeruginosa. European Journal of Pharmaceutical Sciences 93:392–398. doi: 10.1016/j.ejps.2016.08.049

Sackett D, Wolff J (1987) Nile red as a polarity-sensitive fluorescent probe of hydrophobic protein surfaces. Analytical biochemistry 167:228–34

Saint-Jalmes A (2006) Physical chemistry in foam drainage and coarsening. Soft Matter 2:836–849. doi: 10.1039/B606780H

Salamone JC, Salamone A, Swindle-Reilly K, et al (2016) Grand challenge in Biomaterials-wound healing. Regenerative Biomaterials 3:127–128. doi: 10.1093/rb/rbw015

Savjani KT, Gajjar AK, Savjani JK (2012) Drug Solubility: Importance and Enhancement Techniques. ISRN Pharmaceutics 2012:195727. doi: 10.5402/2012/195727

Schäfer-Korting M, Mehnert W, Korting H-C (2007) Lipid nanoparticles for improved topical application of drugs for skin diseases. Advanced Drug Delivery Reviews 59:427–443. doi: 10.1016/j.addr.2007.04.006

Schor M, Reid JL, MacPhee CE, Stanley-Wall NR (2016) The Diverse Structures and Functions of Surfactant Proteins. Trends in biochemical sciences 41:610–620. doi: 10.1016/j.tibs.2016.04.009

Shahrudin S, Ismail M, Kwan S, Najimudin N (2017) Ecology and Protein Composition of Polypedates leucomystax (Gravenhorst, 1829) (Anura: Rhacophoridae) Foam Nests from Peninsular Malaysia. Annual Research & Review in Biology 14:1–10. doi: 10.9734/ARRB/2017/34211

Sheridan R, Care R (2007) Alternative wound coverings. Total Burn Care.

Sørensen H, Mortensen K (2005) Advanced genetic strategies for recombinant protein expression in *Escherichia coli.* Journal of Biotechnology 115:113–128. doi: 10.1016/j.jbiotec.2004.08.004

Session A, Uno Y, Kwon T, et al (2016) Genome evolution in the allotetraploid frog *Xenopus laevis*. Nature 538:336. doi: 10.1038/nature19840

Straight P, Willey J (2006) Interactions between *Streptomyces coelicolor* and *Bacillus subtilis*: role of surfactants in raising aerial structures. Journal of Bacteriology. 4918-25. doi: 10.1128/JB.00162-06

Studier F, Rosenberg A, Dunn J, Dubendorff J (1990) Use of T7 RNA polymerase to direct expression of cloned genes. Methods in enzymology 185:60–89

Sun G, Zhang X, Shen Y-I, *et al* (2011) Dextran hydrogel scaffolds enhance angiogenic responses and promote complete skin regeneration during burn wound healing. Proceedings of the National Academy of Sciences 108:20976–20981. doi: 10.1073/pnas.1115973108

Sung JC, Padilla DJ, Garcia-Contreras L, *et al* (2009) Formulation and Pharmacokinetics of Self-Assembled Rifampicin Nanoparticle Systems for Pulmonary Delivery. Pharmaceutical Research 26:1847–1855. doi: 10.1007/s11095-009-9894-2

Susi H, Byler DM (1986) Methods in Enzymology. 130:290–311. doi: 10.1016/0076-6879(86)30015-6

Tagalakis AD, Kenny GD, Bienemann AS, et al (2014) PEGylation improves the receptor-mediated transfection efficiency of peptide-targeted, self-assembling, anionic nanocomplexes. Journal of Controlled Release 174:177–187. doi: 10.1016/j.jconrel.2013.11.014

Tamarkin DA (2016) Foam: A Unique Delivery Vehicle for Topically Applied Formulations. Handbook of Formulating Dermal Applications: A Definitive Practical Guide

Toppo F, Pawar, RS (2015) Novel drug delivery strategies and approaches for wound healing managements. Journal of Critical Reviews. 2394-5125

Torchilin VP (2014) Multifunctional, stimuli-sensitive nanoparticulate systems for drug delivery. Nature Reviews Drug Discovery 13:813–827. doi: 10.1038/nrd4333

Toussaint J, Chung W, Osman N, et al (2015) Topical Antibiotic Ointment Versus Silver-containing Foam Dressing for Second-degree Burns in Swine. Academic Emergency Medicine 22:927–933. doi: 10.1111/acem.12723

UniProt Consortium T (2017) UniProt: the universal protein knowledgebase. Nucleic Acids Research 45: D158–D169. doi: 10.1093/nar/gkw1099

Valle M de, López F, Navarro A (2008) Development and validation of an HPLC method for vancomycin and its application to a pharmacokinetic study. Journal of Pharmaceutical and Biomedical Analysis 48:835–839. doi: 10.1016/j.jpba.2008.05.040

VanCompernolle S, Smith PB, Bowie JH, et al (2015) Inhibition of HIV infection by caerin 1 antimicrobial peptides. Peptides 71:296–303. doi: 10.1016/j.peptides.2015.05.004

Vera A, González-Montalbán N, Arís A, Villaverde A (2007) The conformational quality of insoluble recombinant proteins is enhanced at low growth temperatures. Biotechnol Bioeng 96:1101–1106. doi: 10.1002/bit.21218

Vijayakumar A, Sharon E, Teena J, et al (2014) A clinical study on drug-related problems associated with intravenous drug administration. Journal of Basic and Clinical Pharmacy 5:49–53. doi: 10.4103/0976-0105.134984

Villa J, armid R, Gallardo J (1982) Arthropod predators of leptodactylid frog foam nests. Brenesia

Wang C, Li H-B, Li S, et al (2012) Antitumor effects and cell selectivity of temporin-1CEa, an antimicrobial peptide from the skin secretions of the Chinese brown frog (*Rana chensinensis*). Biochimie 94:434–441. doi: 10.1016/j.biochi.2011.08.011

Waterhouse AM, Procter JB, Martin DM, et al (2009) Jalview Version 2—a multiple sequence alignment editor and analysis workbench. Bioinformatics 25:1189–1191. doi: 10.1093/bioinformatics/btp033

Weaire D (2002) Foam Physics. Advanced Engineering Materials 10:723–725

Weaire D (2013) Applied physics. A fresh start for foam physics. Science (New York, NY) 340:693–4. doi: 10.1126/science.1238247

Wehrli, W. (1983) Rifampin: mechanisms of action and resistance. Reviews of Infectious Diseases. Vol 5. doi: 10.1093

Weiss J, Victor M, Elsbach P (1983) Role of Charge and Hydrophobic Interactions in the Action of Bactericidal/Permeability-increasing Protein of Neutrophils on Gram-negative Bacteria. Journal of Clinical Investigation 71:540–549. doi: 10.1172/JCI110798

Wendell D, Todd J, Montemagno C (2010) Artificial Photosynthesis in Ranaspumin-2 Based Foam. Nano Letters 10:3231–3236. doi: 10.1021/nl100550k

Wicki A, Witzigmann D, Balasubramanian V, Huwyler J (2015) Nanomedicine in cancer therapy: Challenges, opportunities, and clinical applications. Journal of Controlled Release 200:138–157. doi: 10.1016/j.jconrel.2014.12.030

Wilde P. (2000) Interfaces: their role in foam and emulsion behaviour. Current Opinion in Colloid & Interface Science 5:176–181. doi: 10.1016/S1359-0294(00)00056-X

Willey J, Santamaria R, Guijarro J, et al (1991) Extracellular complementation of a developmental mutation implicates a small sporulation protein in aerial mycelium formation by S. coelicolor. Cell 65:641–650. doi: 10.1016/0092-8674(91)90096-H

Williams K, Piddock L (1998) Accumulation of rifampicin by *Escherichia coli* and *Staphylococcus aureus*. Journal of Antimicrobial Chemotherapy 42:597–603. doi: 10.1093/jac/42.5.597

Wilson AJ (2013) Foams: physics, chemistry and structure. Springer Science & Business Media

Wu J, Hou S, Ren D, Mather PT (2009) Antimicrobial Properties of Nanostructured Hydrogel Webs Containing Silver. Biomacromolecules 10:2686–2693. doi: 10.1021/bm900620w

Wu J, Liu H, Yang H, et al (2011) Proteomic Analysis of Skin Defensive Factors of Tree Frog *Hyla simplex*. Journal of Proteome Research 10:4230–4240. doi: 10.1021/pr200393t

Xu X, reviews LR (2015) The chemistry and biological activities of peptides from amphibian skin secretions. 1760–1846 doi: 10.1021/cr4006704

Yah C, Simate G, (2012) Nanoparticles toxicity and their routes of exposures. IS journal. 477-91.

Yamanaka K, Reynolds KA, Kersten RD, et al (2014) Direct cloning and refactoring of a silent lipopeptide biosynthetic gene cluster yields the antibiotic taromycin A. Proceedings of the National Academy of Sciences 111:1957–1962. doi: 10.1073/pnas.1319584111

Yeaman MR, Yount NY (2003) Mechanisms of Antimicrobial Peptide Action and Resistance. Pharmacological Reviews 55:27–55. doi: 10.1124/pr.55.1.2

Yorke, CD, (1983) Survival of embryos and larvae of the frog *Polypedates leucomystax* in Malaysia. Journal of Herpetology. Vol 17. doi: 10.2307/1563825

Zairi A, Tangy F, Bouassida K, Hani K (2009) Dermaseptins and Magainins: Antimicrobial Peptides from Frogs' Skin—New Sources for a Promising Spermicides Microbicides—A Mini Review. Journal of Biomedicine and Biotechnology 2009:452567. doi: 10.1155/2009/452567

Zasloff M (2002) Antimicrobial peptides of multicellular organisms. Nature 415:389–395. doi: 10.1038/415389a

Zhao Y, Brown MB, Jones SA (2010) Pharmaceutical foams: are they the answer to the dilemma of topical nanoparticles? Nanomedicine: Nanotechnology, Biology and Medicine 6:227–236. doi: 10.1016/j.nano.2009.08.002

Zhao Y, Brown MB, Jones SA (2009) Engineering novel topical foams using hydrofluroalkane emulsions stabilised with pluronic surfactants. European Journal of Pharmaceutical Sciences 37:370–377. doi: 10.1016/j.ejps.2009.03.007

Zhao Y, Jones SA, Brown MB (2010) Dynamic foams in topical drug delivery. The Journal of pharmacy and pharmacology 62:678–84. doi: 10.1211/jpp.62.06.0003

Zhao Y, Moddaresi M, Jones SA, Brown MB (2009b) A dynamic topical hydrofluoroalkane foam to induce nanoparticle modification and drug release in situ. European Journal of Pharmaceutics and Biopharmaceutics 72:521–528. doi: 10.1016/j.ejpb.2009.03.002

Zuidema JM, Rivet CJ, Gilbert RJ, Morrison FA (2014) A protocol for rheological characterization of hydrogels for tissue engineering strategies. Journal of Biomedical Materials Research Part B: Applied Biomaterials 102:1063–1073. doi: 10.1002/jbm.b.33088